HYDRODYNAMIC EFFECTS ON ANIMAL CELLS

IN MICROCARRIER BIOREACTORS

BY

MATTHEW SHANE CROUGHAN

B.S. Chemical Engineering
University of California at Berkeley
(June, 1983)

Submitted to the Department of Chemical Engineering
in Partial Fulfillment of the Requirements for the Degree of

DOCTOR OF PHILOSOPHY IN CHEMICAL ENGINEERING

at the

MASSACHUSETTS INSTITUTE OF TECHNOLOGY

June, 1988

Signature of Author: _____
Department of Chemical Engineering
February 23, 1988

Certified by: _____
Daniel I.C. Wang
Professor of Chemical and Biochemical Engineering
Thesis Supervisor

Accepted by: _____
Robert C. Armstrong
Professor of Chemical Engineering
Chairman of the Committee for Graduate Students

HYDRODYNAMIC EFFECTS ON ANIMAL CELLS
IN
MICROCARRIER BIOREACTORS

BY
MATTHEW SHANE CROUGHAN

Submitted to the Department of Chemical Engineering
Massachusetts Institute of Technology
on February 23, 1988
in partial fulfillment of the requirements for the Degree of
Doctor of Philosophy in Chemical Engineering

ABSTRACT

In this thesis, a fundamental approach was initiated toward the design of microcarrier bioreactors for industrial animal cell culture. Cell damage from hydrodynamic forces was considered along with the agitation requirements for mass transfer. Hydrodynamic effects on the growth and death of FS-4 cells on microcarriers were studied in small stirred-tank bioreactors. With mild agitation, growth was not affected by changes in fluid viscosity, microcarrier concentration, or level of agitation, and thus appeared to unaffected by the hydrodynamic environment. With high agitation, a reduction in net growth was observed and was found to be entirely due to cell death and removal and not growth inhibition.

The mechanisms of hydrodynamic death were investigated through experiments on the effects of fluid viscosity, microcarrier concentration, and agitation power. Cell death in microcarrier bioreactors was found to occur through microcarrier-eddy interactions, microcarrier collisions, and, in unusual circumstances, time-average flow fields. Microcarrier-eddy interactions led to cell death when the turbulence generated eddies which were smaller than the microcarriers. For dilute cultures, the specific death rate was found to be proportional to the concentration of eddies in the viscous dissipation regime. For both dilute and concentrated cultures, cell death was found to increase with agitation power and decrease with fluid viscosity.

A quantitative expression was derived which related the cell population kinetics to the microcarrier concentration, kinematic viscosity, and agitation power. The expression included the contributions from cell growth, which was not a function of hydrodynamic environment, and cell death from both microcarrier-eddy interactions and microcarrier collisions. The expression was used to quantify the trade-off between hydrodynamic cell death and oxygen transfer upon scale-up. An illustration was presented to show how bioreactor design can be approached as an optimization problem involving quantitative rate expressions.

Thesis supervisor: Dr. Daniel I.C. Wang
Title: Professor of Chemical and Biochemical Engineering

TABLE OF CONTENTS

ACKNOWLEDGEMENTS

The author wishes to acknowledge the following organizations for financial support:

National Science Foundation of the United States of America

for supporting much of this research through the Engineering Research Center Initiative to the M.I.T. Biotechnology Process Engineering Center under the cooperative agreement CDR 8500003

Biogen, Inc.

for supporting the initial phases of this research

Exxon Corporation and E.I. Dupont Denemours Corporation

for fellowship support during my coursework

The author also wishes to acknowledge the following individuals and greater beings who have contributed to this thesis:

God

for creating the earth, the universe, and M.I.T., and for serving as the ultimate reviewer of this research

Claire Malloy Croughan and Mabel Wilson Croughan

for creating me, and for their continuous support of my education

Kathryn Colleen Kidd, soon to be Kathryn Kidd Croughan

for her joy when the experiments were successful and her support when they were unsuccessful

Professors C.K. Colton, T.A. Hatton, C.L. Cooney, and A.J. Sinskey

for serving as members of my thesis committee, for their review of this research, and for their insightful comments

Jean-Francois Hamel, Elizabeth Sayre, Jeff Bigler, and Bruce Woodson

for their participation in this research

Don Giard and the staff of the Cell Culture Center at M.I.T.

for sharing their knowledge of animal cell culture, for their services and help, and for Don's advice regarding my golf swing

Professor Preetinder S. Virk

for his useful and stimulating suggestions, and for his good wit

John Aunins, Steve Perry, Jono Goldstein, Mark Applegate, Brian Kell, Steve Lee, Marc Davidson, Dave Robbins, Linda Cima, Mike Glacken, Enno Adema, Chris Hwang, Dawn Orton, Shiping Wang, and many others

for their suggestions and help, and for the good times in the lab

Professors Harvey Blanch and Frances Arnold, and Robert Lesch

for spawning my interest in biotechnology at U.C. Berkeley

Ruth Ayers, Diana Kenney, Marguerite Walsh, and Lynne Comeau

for their services and good humor

Professor Daniel I.C. Wang (last but not least)

Professor Wang has been an outstanding research advisor. He exhibits a tremendous commitment to the training of his students and to the advance of scientific knowledge. For Professor Wang, who reminds me of a wise and dexterous owl, the following poem was written:

An owl can see in the dark

and find lost coins

An owl can soar above the trees

and view the entire forest

An owl can build a nest

and raise more owls

LIST OF FIGURES

LIST OF TABLES

INTRODUCTION

Large-scale animal cell culture is currently being developed for the industrial production of many valuable proteins. For the culture of cells that will adhere to surfaces, growth on the surface of microcarriers appears promising for industrial operations. First developed by van Wezel (1967), the microcarrier technique can provide a homogeneous culture environment with high cell densities and simple medium/cell separation (Nahapetian, 1986).

Many researchers have employed the microcarrier technique and have noted its advantages. Nonetheless, improvements of the technique have been primarily limited to the development of new and improved microcarriers, media formulations, and inoculation procedures. Although reactors have been developed and successfully used for microcarrier cultures, no thorough study has been published which compares and determines the best reactor designs and agitation procedures.

It is widely accepted but not well documented that animal cells on microcarriers are especially susceptible to damage from fluid-mechanical forces. This susceptibility results from the lack of a protective cell wall, the relatively large size of animal cells, and the lack of individual cell mobility. Anchored cells can not freely rotate or translate; they therefore can not reduce the net forces and torques experienced upon exposure to fluid-mechanical forces.

In microcarrier cultures, agitation is required for cell-liquid mass transport, gas-liquid mass transport (oxygenation), and liquid-phase mixing. For maximum cell growth, adequate mass transfer must be achieved with little or no detrimental effects from hydrodynamic forces. Although this condition can be readily attained in low-density laboratory cultures, it becomes more difficult to attain as cell densities or culture volumes are increased. Successful scale-up to high-density, large-volume cultures will require a thorough understanding of the hydrodynamic and mass transport phenomena.

Accordingly, the overall objective of this work is to formulate a fundamental approach to the design, operation, and scale-up of microcarrier bioreactors. The general approach will be to:

1) determine the effects of momentum transfer on cell growth, independent of the effects of heat and mass transfer,
2) perform experimental investigations on the mechanisms of cell damage from fluid-mechanical forces,
3) develop theoretical models to describe the mechanisms of cell damage,
4) use the verified models of hydrodynamic damage, along with published models of mass transport, to develop a quantitative engineering approach to the design of microcarrier bioreactors.

The knowledge generated by this research will be useful in the design of microcarrier bioreactors and will add to the general understanding of hydrodynamic phenomena.

Hydrodynamic Effects on Cell Growth

The effects of well-defined hydrodynamic forces on cell growth have not been thoroughly investigated. No investigations have been performed with regard to normal forces and only a few have been performed with regard to shear stresses.

Under flow conditions which do not lead to substantial removal of cells from their growth surface, cell growth appears to be unaffected by fluid shear stresses. For endothelial cells growing on glass coverslips, Dewey et al (1981) found that cell growth was not affected by fluid shear stresses up to 8 dyne/cm^2. In more recent experiments with endothelial cells growing on plastic coverslips, Sprague et al (1987) found that cell growth was not affected by shear stresses up to 30 dyne/cm^2.

For moderate to high levels of shear stresses, a few quantitative studies have been performed regarding removal of cells from their growth surface. In experiments with endothelial cells on glass coverslips, Viggers et al (1986) observed extensive cell removal from the growth surface for shear stresses of 128 dyne/cm^2. In experiments with BHK, Vero, and MRC-5 cells grown on plastic or glass slides, Crouch et al (1985) observed extensive cell removal for shear stresses in the range of 30 dyne/cm^2 or higher. In experiments with kidney cells on glass slides, Stathopoulos and Hellums (1985) observed cell removal for shear

stresses of 6.5 dyne/cm^2 or greater.

Under flow conditions which result in substantial removal of cells from their growth surface, the viability of the cells which remain attached is generally reported to be greater than 90% (Crouch et al, 1985; Stathopoulos and Hellums, 1985). However, these viabilities are measured in terms of trypan blue exclusion and not in terms of the ability to reproduce and grow. The hydrodynamic effects on cell growth are unknown for flow conditions which can cause extensive cell removal or death.

When animal cells are grown in an agitated vessel, a reduction in net growth is frequently observed with an increase in the level of agitation. The biological basis behind this reduction in net growth has not been investigated. The reduction could be due to growth inhibition, cell death, or a combination of death and growth inhibition. One objective of this thesis is to investigate whether cell growth is inhibited, unchanged, or enhanced by the hydrodynamic forces in microcarrier cultures. The primary thrust will be to determine whether growth inhibition and/or cell death account for the reduced net growth in overagitated microcarrier cultures.

The Cell Cycle and DNA Replication

To understand the potential hydrodynamic effects on cell growth, one must first understand the growth cycle of animal cells. To replicate their DNA and pass it on to their progeny, cells pass through a cycle

with four sequential phases: G_1, S, G_2, and M (Alberts et al, 1983). General biosynthesis occurs during the G_1 phase, DNA synthesis during the S phase, preparation for mitosis during the G_2 phase, and actual mitosis during the M phase. For almost all animal cells growing in culture, the duration of the S, G_2, and M phase is roughly constant at 7 hours, 3 hours, and 1-2 hours, respectively (Darnell et al, 1986; Alberts et al, 1983). A change in the average doubling time of a cell population will occur because of a change in the duration of G_1, and/or because some fraction of the cell population enters or exits an out-of-cycle, non-growing state termed G_o.

There is some debate whether a G_o state actually exists or whether all differences in doubling time are due to differences in the duration of the G_1 phase (Pardee et al, 1978; Darnell et al, 1986). Clearly, however, a restriction point for cell growth exists at some point late in G_1 or at the passage between G_o and G_1. At the restriction point, the decision is made whether a given cell will replicate. The basis behind this decision is not fully understood, although it clearly depends on several environmental factors (Darnell et al, 1986). Independent of the basis behind the decision, a cell stimulated to divide will pass through the S, G_2, and M phases essentially irrespective of the "post-decision" environment. Non-growing cells are almost always held up in the G_1 or G_o phase.

There are at least two ways in which high levels of agitation may inhibit cell growth. The hydrodynamic environment may affect the

biosynthetic capability required for cell growth, or it may affect the cell's decision whether to replicate. These effects would be uncoupled with changes in cell metabolism which are not involved with growth.

If hydrodynamic stresses actual kill cells rather than just inhibit growth, it would be interesting to know if cells are killed at random or only at certain positions in the cell cycle. When anchorage-dependent animal cells grow on a surface, cells in mitosis generally round-up and assume a less flattened morphology than the interphase cells (Alberts et al, 1983). For some cell lines, mitotic cells can be selectively and viably removed by applying mild shear stresses to the growth surface (Prescott, 1976; Pardee, 1978; Terasima, 1962). This procedure does not work for many cell lines and growth surfaces (Freshney, 1983). Cell removal is frequently not selective for mitotic cells if the agitation is excessive (Terasima, 1962) or if the cells are grown on microcarriers and have not been pretreated with colcemid (Ng et al, 1980; Mitchell and Wray, 1979).

If anchored cells are killed by hydrodynamic forces, it is unclear whether death occurs before, during, or after removal of the cells from the microcarriers. It is also unclear whether death will eventually result in cell lysis and disintegration. If removal, lysis, and disintegration occur, counting whole cells in suspension will not fully account for the number of cells killed. Accordingly, one may wish to analyze for a stable intracellular component which is released by the disintegrated cells. It is then important to know how much of this

component was originally contained by each cell.

Assessment of Cell Death through DNA Release Measurements

To quantitatively assess cell death and lysis from hydrodynamic forces, one could analyze for DNA release into the culture fluid. For normal diploid cells, the DNA content of each cell is solely a function of the cell's position in the growth cycle and should not depend on the hydrodynamic environment per se. The specific DNA content of cell populations is well-defined and thus DNA release can be directly correlated to the number of cells killed.

The amount of DNA release will depend upon what type of cells are lysed. If cells in G_o or G_1 are lysed, the DNA release will be one diploid equivalent per cell. If cells in G_2 or M are lysed, the DNA release will be two diploid equivalents per cells. If cells are removed randomly throughout the cell cycle, the average DNA release will depend upon the distribution of the cell population among the phases of the growth cycle. For a cell population growing exponentially through binary fission, the distribution function, f(t), of cell ages is given by (Johnson, 1961)

$$f(t) = \frac{(\ln 2)\ 2^{(1 - t/T_d)}}{t_d} \qquad \text{(Eq. 1)}$$

where t is the time since mitosis, T_d is the doubling time, and f(t) times dt is the fraction of the cell population with an age between t and t + dt.

There are at least two reasonable approaches to determine the average DNA content of a cell population. For the first approach, one can assume that a distinct G_o phase does not exist and that all cells are going through the cell cycle. All changes in growth rate are therefore due to changes in the duration of G_1. The average DNA content per cell, S_a, is then given by

$$S_a = \int_0^{T_d} f(t)\ S(t)\ dt \qquad \text{(Eq. 2)}$$

where S(t) is the DNA content per cell in diploid equivalents at a given time t since mitosis. If one assumes that the rate of DNA synthesis is constant throughout the S period, the integral above can be solved to yield

$$S_a = \frac{2^{(T_M + T_{G2} + T_S)/T_d} + 2^{(T_M + T_{G2})/T_d}}{2} \qquad \text{(Eq. 3)}$$

where T_S, T_{G2}, and T_M are the respective durations of the S, G_2, and M phases.

For a second approach to determine the average DNA content of cell populations, one can assume that a separate, out-of-cycle G_o phase does exist and that the duration of the G_1 phase is actually constant. The specific growth rate will then depend upon the fraction of the population, I_{Go}, which resides in G_o. The average DNA content of the

population is then given by

$$S_a = \frac{T_d - T_c(1 - 0.5(2^{(T_M + T_{G2} + T_S)/T_c} + 2^{(T_M + T_{G2})/T_c}))}{T_d} \qquad \text{(Eq. 4)}$$

where T_d is the observed doubling time and T_c is the total cycle time ($T_{G1} + T_S + T_{G2} + T_M$).

In this thesis, cell death is quantitatively assessed through measurements of the DNA content of culture fluids. The DNA measurements are related to cell numbers through the models presented above. For conditions of excessive agitation, the amount of cell death is compared to the net reduction in growth. The comparisons are used to determine whether cell growth is affected by hydrodynamic forces under conditions of excessive agitation.

The effects of hydrodynamic forces on cell growth could also be assessed through monitoring the incorporation of radioactive DNA precursors, such as thymidine, at different levels of agitation. However, when there is extensive cell lysis, such as that which occurs with excessive agitation, the radioactive precursor technique has unresolved complications and difficulties (Aherne et al, 1977). The radioactive precursor technique is therefore not used in this thesis.

Hydrodynamic Effects on Cell Metabolism

Hydrodynamic forces may not only lead to cell death and lysis but could also lead to significant changes in cell metabolism. Many of the

metabolic events that occur in animal cells are not directly related to cell growth. Whether or not cell growth is inhibited by hydrodynamic forces, metabolic events which are not growth associated could be influenced by agitation.

For endothelial cells, several studies have shown that cell shape, metabolism, and endocytotic activity can be strongly affected by fluid flow. The results are summarized as follows:

1) the cells align and elongate in the direction of flow over 1-2 days exposure to shear stresses above 5 dyne/cm^2 (Dewey et al, 1981; Levesque and Nerem, 1985)
2) the histadine decarboxylase activity of the cells increases linearly with shear stress for 1-2 hour exposures to shear stresses above 2.8 dyne/cm^2 (DeForrest and Hollis, 1980; Hollis and Ferrone, 1974; Rosen et al, 1974)
3) cell permeability to proteins increases for 1-hour or longer exposures to shear stresses above 7 dyne/cm^2 (Fry, 1968; DeForrest and Hollis, 1980)
4) prostacyclin production increases 6-fold upon exposure to a mean shear stress of 10 dyne/cm^2 and increases 16-fold upon a pulsed exposure at 1 Hz between 8 and 12 dyne/cm^2 (Frangos et al, 1985)
5) exposure to a shear stress of 30 dyne/cm^2 significantly enhances receptor-mediated binding, internalization, and degradation of low-density lipoproteins (Sprague et al, 1987)

These results are due, at least in part, to the natural adaptation of endothelial cells to fluid flow in blood vessels.

For cell lines other than endothelial, there has been a very limited number of direct studies on how cell metabolism is affected by the hydrodynamic environment. For hybridoma cells, Dodge and Hu (1986) found that net cell growth was slightly reduced, but volumetric glucose consumption was unchanged, by high levels of agitation. This result may be due, in part, to conversion of glucose to lactic acid by dead or lysed cells. It may also indicate that the specific glucose uptake rate of the cells was slightly increased by agitation.

For epithelial kidney cells on glass slides, Stathopoulos and Hellums (1985) found that post-shear urokinase release was increased by exposure to shear stress levels between 6.5 and 13 dyne/cm^2. For recombinant mouse-L cells on microcarriers, Schulz et al (1986) found no effects of agitation on specific β-interferon productivity. Besides these direct studies, there are reports of differences in cell metabolism between agitated and stagnant (or nearly stagnant) cultures (Bryant, 1969; Giard et al, 1979). It is unclear, however, whether these differences are due to mass or momentum transfer.

In this thesis, a thorough investigation is made into the hydrodynamic effects on cell growth, while only a very limited investigation is made into the hydrodynamic effects on cell metabolism. Before any reactor design can be fully optimized, hydrodynamic effects on both cell growth and metabolism will have to be fully understood.

Microscopic Flow Fields and Cell Deformation Mechanics

When shear flow occurs over a cell anchored to a surface, the microscopic flow field is affected by the protusion of the cell. The cell experiences a net torque created by the flow around its circumference. This torque is countered by the adhesive force between the substrate and the front of the cell.

Hyman (1972a) attempted to solve for the microscopic flow field around a cell protuding into a linear shear field. He later admitted that his published solution was incorrect (1972b). From a literature survey, the problem appears to remain unsolved. The relevant Reynold's number is given by

$$Re = Y h^2/\nu \qquad \text{(Eq. 5)}$$

where Y is the undisturbed shear rate, h is the cell height (hemispherical shape assumed), and ν is the kinematic fluid viscosity. For the range of parameters which are of interest in cell culture, the flow around the cell will be creeping with a Reynold's number below 0.5. Because currently available flow visualization techniques can not resolve to better than 20-30 microns, any theoretical solution to the microscopic flow field can not be experimentally verified with actual cells.

Because there is no available solution to the microscopic flow field around a cell protuding into a shear field, all shear effects on anchored cells have been correlated with the undisturbed wall shear stress. This approach is taken not only because very little is known

about the detailed fluid mechanics, but also because the microscopic flow field is coupled to the cell shape and cell deformation mechanics. The cell shape will be determined, at least in part, by the local flow field and hydrodynamic forces. To determine the cell shape and the local flow field, one must simultaneously solve for both the fluid motion and the cell deformation mechanics.

The deformation mechanics of red blood cells have been successfully described from purely physical models (Hochmuth et al, 1972, 1973; Evans, 1983). The deformation mechanics of nucleated cells are only currently being elucidated (Sato et al, 1987; Cheng, 1987). In contrast to a red blood cell, a nucleated cell with dynamic internal structures can not be modelled as a Newtonian solution surrounded by an elastic membrane. Furthermore, in response to fluid shear stresses, nucleated cells will actively adjust their shape by lengthening and shortening cytoskeleton fibers. Purely physical models for nucleated cells would be successful only for time scales which are shorter than the response time of the cell. It will clearly be a challenging problem to solve for the deformation mechanics of nucleated cells.

In most microcarrier cultures, the flow field is turbulent. The cells are exposed not only to shear forces, but also to normal forces. The effects of normal forces on animal cells have, to my knowledge, never been quantitatively investigated. The undiscovered role of normal forces may account for the typically poor agreement between shear effects in laminar flow fields and global hydrodynamic effects in

stirred tanks, such as reported by Rosenberg et al (1987). The poor agreement may also arise due to the limited understanding of turbulence. For microcarrier cultures in turbulent bioreactors, one can only roughly estimate the magnitude and direction of the hydrodynamic forces on the cells.

To investigate the mechanisms of hydrodynamic damage in turbulent reactors, information should be obtained both through direct experiments with turbulent reactors and through translation of results from experiments with well-defined hydrodynamic forces. In this thesis, the mechanisms of cell damage in turbulent reactors are directly investigated through experiments with turbulent reactors. A reasonable attempt is made to present results in terms of normal forces and shear forces. Further elucidation of the effects of well-defined forces, including the incorporation of cell deformation mechanics and the solution of microscopic flow fields, are left for future research.

Effects of Microcarrier and Cell Concentration

For industrial cell culture, high cell concentrations can potentially reduce production costs through four different means:

1) increased volumetric productivities and thus reduced capital and overhead costs,
2) decreased labor required per cell and thus reduced labor costs,
3) increased concentrations of the desired product and thus reduced purification costs, and
4) increased concentration of other cell-derived products (growth

factors, etc..) which may result in accelerated growth, accelerated product formation, or reduced serum requirements.

For a specific cell line, the maximum number of cells per microcarrier is approximately constant. Accordingly, if one wishes to obtain high cell densities, microcarrier concentrations must be increased. It is therefore important to understand how an increase in microcarrier concentration will affect the hydrodynamic environment near the cells.

Currently-available data on the effects of microcarrier concentration is limited and frequently contradictory. In small spinner flasks, Hu et al (1985) found no decrease in growth rate when bare microcarriers were added to cultures, or when cultures with 5 g/l microcarriers were concentrated to 15 g/l. In contrast, however, Feder and Tolbert (1983) report that cell damage occurs when microcarrier concentrations are increased above 12 g/l. Furthermore, Mered et al (1980) observed decreased growth rates as microcarrier concentrations were increased from 1 to 5 g/l.

If there is no detrimental effect of microcarrier concentration, and if similar chemical environments can be maintained, an increase in microcarrier concentration should lead to a proportional increase in cell concentration. When this proportionality is not observed, it is often attributed, without apparent proof, to a detrimental effect from microcarrier collisions. However, in most studies, the physical effects of microcarrier concentration are not clearly separated from the

chemical effects of cell concentration. The detrimental effects attributed to collisions may actually be due to nutrient limitations or some other effect from high cell concentrations. Furthermore, the previous experiments were conducted with various culture vessels at different levels of agitation. The role of collisions, along with any other hydrodynamic effects of microcarrier concentration, may depend upon the vessel geometry, impeller configuration, and level of agitation.

Accordingly, the bioreactor design engineer now faces the following unanswered questions:

1) What are the physical effects associated with microcarrier concentration?
2) How do these effects vary with the level of agitation?
3) Do collisions between microcarriers lead to cell damage? If so, at what level of agitation, and at what rate of damage?

In this thesis, results are presented which address these questions.

Hydrodynamic Damage in Microcarrier Cultures

Hirtenstein and Clark (1980) have studied the effects of agitation in microcarrier cultures. Their data, shown in Figure 1, indicate that there is an optimal stirring speed near 60 rpm for growth of Vero cells in a 250-ml traditional spinner vessel. The poorer growth at the slow speeds was likely due to transport limitations, probably brought about by either inadequate surface aeration or incomplete suspension of the beads. The poorer growth at the high speeds was likely due to

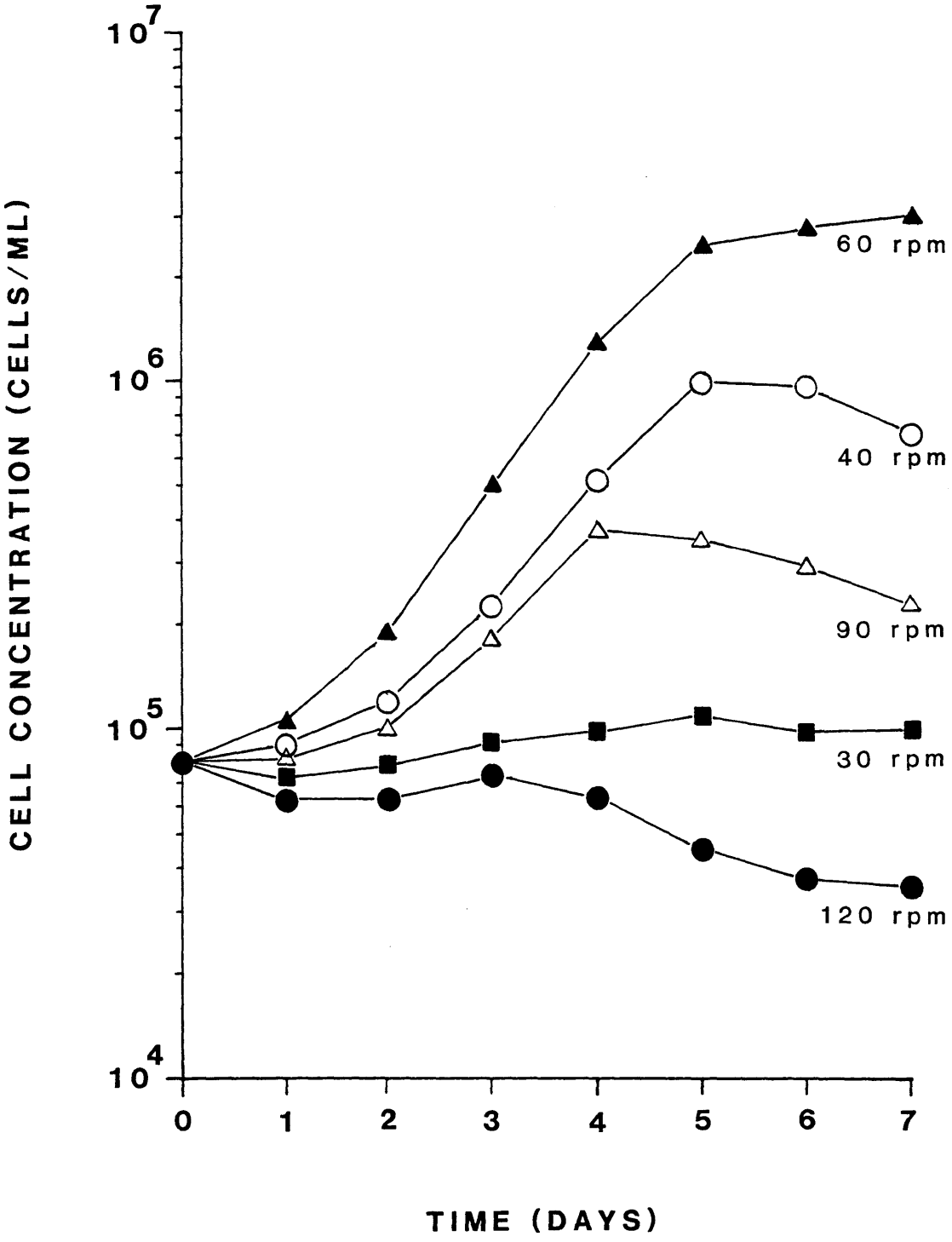

Figure 1. Growth of Vero cells at different stirring speeds (Hirtenstein and Clark, 1980)

detrimental effects from excessive agitation. The results in Figure 1 clearly show the trade-off between mass transport and hydrodynamic damage in microcarrier cultures. Nonetheless, these results can not be readily translated into the design of an industrial-scale reactor.

Sinskey et al (1981) and Hu (1983) have studied the effects of agitation on microcarrier cultures in small stirred vessels. As shown by the data of Hu in Figure 2, relative cell growth can be correlated with an integrated shear factor (ISF), as given by

$$ISF = \frac{2 \pi N D_i}{(D_t - D_i)} \qquad \text{(Eq. 6)}$$

where N is the impeller rotation rate, D_t is the vessel diameter, and D_i is the impeller diameter. The integrated shear factor is a measure of the strength of the shear field between the impeller and vessel wall.

Although the correlation of net growth with integrated shear factor is useful, it is not readily incorporated into a mechanistic model of hydrodynamic effects on cells attached to microcarriers. The problem must be analyzed in terms of the more fundamental parameters of fluid mechanics. The response of the cells to the hydrodynamic environment must be clearly elucidated. The effects of mass transport must be included in a more thorough quantitative analysis.

Cell-liquid Transport in Microcarrier Cultures

When investigating the effects of hydrodynamic forces, or momentum transfer, one must eliminate any other effects due to mass and heat

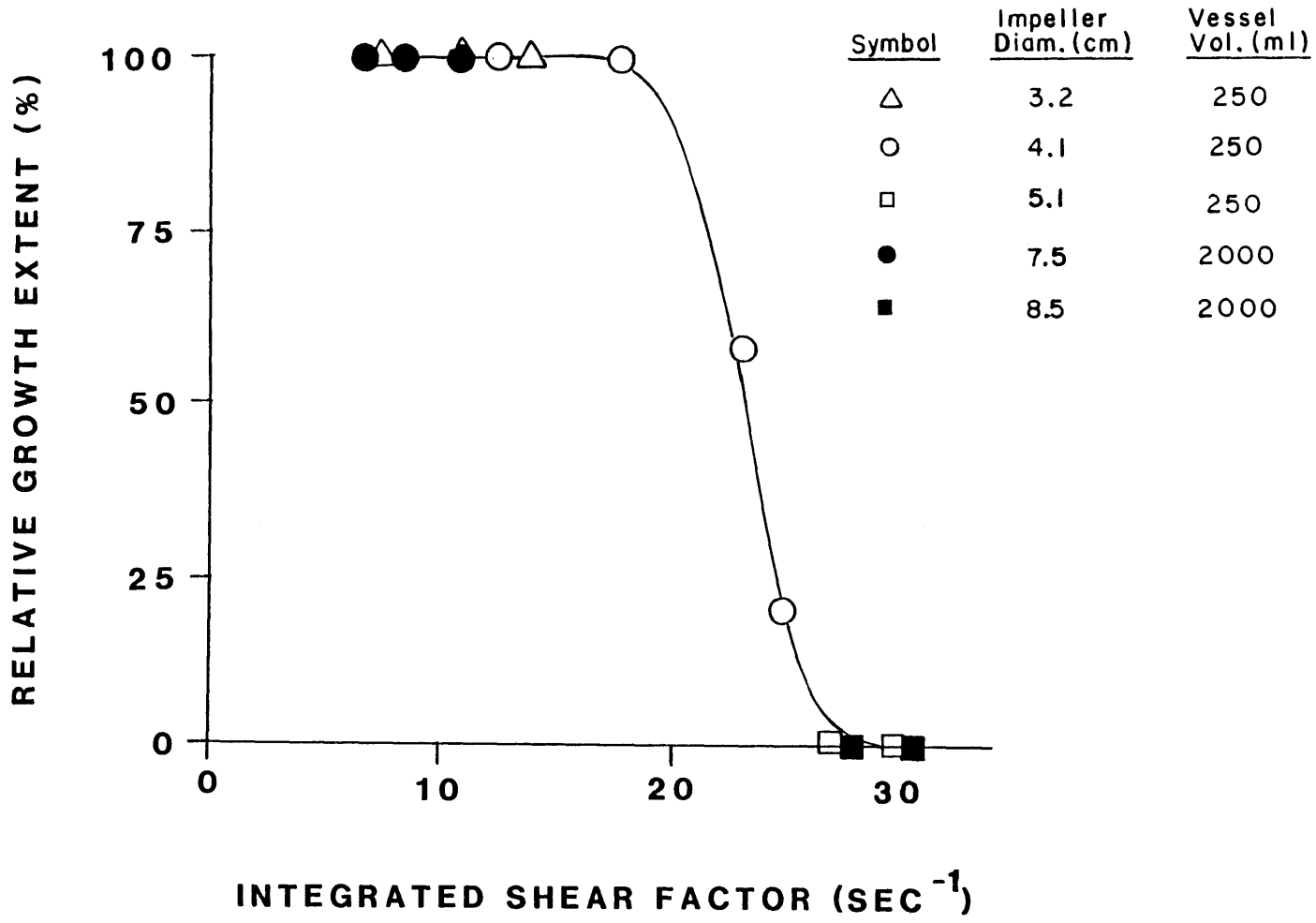

Figure 2. Relative growth extent vs. integrated shear factor (Hu, 1983)

transfer. If a stagnant cell culture is shaken, the subsequent mixing may induce cell growth simply through the elimination of chemical gradients (Stoker, 1973, 1974; Dunn and Ireland, 1984). For microcarrier cultures, it is important to understand whether there are any transport limitations between the cells and medium.

When a sphere, such as a microcarrier, is suspended in a turbulent vessel, mass transport between the sphere surface and bulk medium can be described by (Sano et al, 1974; Chaudhari and Ramachandran, 1980)

$$Sh = 2 + 0.4(\bar{\epsilon}\ d_p^4/D_f\ \nu^2)^{1/3} \qquad \text{(Eq. 7)}$$

where Sh is the Sherwood number, $\bar{\epsilon}$ is the average power dissipation per unit mass, d_p is the sphere diameter, and D_f is the diffusion coefficient for the chemical under consideration. For microcarrier cultures, the Sherwood number given by equation 7 represents the Sherwood number for cell-liquid mass transport, Sh_c. For each chemical species which is consumed or produced by cells on microcarriers, the normalized gradient between the chemical concentration in the bulk medium, X_b, and the concentration at the cell surface, X_c, is given by

$$\frac{X_b - X_c}{X_b} = \frac{\Psi\ R_c\ d_p}{D_f\ X_b\ Sh_c} \qquad \text{(Eq. 8)}$$

where Ψ is the surface coverage in cells per unit area, and R_c is the uptake rate per cell for a given chemical species. For chemicals which are produced by the cells, R_c will be negative.

Substituting typical values for the parameters in equations 7 and 8, one generally finds that the normalized gradients are far less than unity, with values on the order of 0.001 to 0.1. The chemical concentrations at the cell surface are therefore essentially equal to the concentrations in the bulk medium. A Nusselt number analysis shows that a parallel conclusion can be made with regard to temperature gradients. Furthermore, the temperature and chemical gradients are insignificant even if the microcarriers are suspended in a stagnant flow field ($Sh_c = 2$, $Nu_c = 2$).

Thus, it appears that mere suspension of microcarriers provides for adequate mass and heat transport between the cells and medium. This conclusion is supported by the results of Sinskey et al (1981) and Hu (1983); uniform growth is observed over a wide range of nondetrimental levels of agitation that are sufficiently strong to suspend the microcarriers and provide for adequate surface aeration. As long as the microcarriers are suspended, and as long as the bulk chemical concentrations are maintained at suitable levels, the effects of agitation will come solely through momentum transfer.

Fluid-lift, Airlift, and Stirred-tank Bioreactors

The vast majority of microcarrier cultures are conducted in stirred-tank bioreactors. Such vessels provide a relatively homogeneous culture environment which can be readily assessed and controlled. In fact, almost all currently-available microcarriers are designed for use in such equipment. Most microcarriers have a specific density in the range

of 1.03 to 1.04. This allows for complete suspension with relatively mild agitation. Neutrally buoyant microcarriers are generally not used as they could not be separated from the medium through gravity sedimentation.

Fluid-lift reactors have been employed for microcarrier cultures (Clark and Hirtenstein, 1981). When fluid-lift reactors are used with microcarriers that have a specific density of 1.04 and a diameter of 185 microns, the maximum linear velocity through the bed is on the order of 5 cm/min. The cells are exposed only to very weak hydrodynamic forces (less than 1 dyne/cm^2). The cell density and reactor height, however, are limited by the uptake of oxygen from the medium as it flows past the cells. If one wishes to operate a fluidized bed with high cell densities on a industrial scale, microcarriers with a specific density more comparable to glass will have to be used. The energy dissipation rates, and fluid forces, will then be comparable to the values in a stirred-tank reactor with microcarriers of a specific density near 1.04.

Airlift reactors have been used for cultures of freely-suspended animal and insect cells (Tramper et al, 1986; Boraston et al, 1984; Handa et al, 1987). No published reports were found which document their use for microcarrier cultures. It is frequently stated that direct sparging causes damage to cells on microcarriers (Pharmacia, 1981; Spier and Griffiths, 1984). Nonetheless, no published reports were found which document such damage.

One purpose of this thesis is to experimentally investigate and document whether cell damage occurs from direct sparging of microcarrier cultures. Cell damage is known to occur from direct sparging of suspension cultures (Tramper et al, 1986; Handa et al, 1987). It is likely that damage occurs from direct sparging in microcarrier cultures. In fact, the damage may be more extensive in microcarrier cultures, given that the cells are immobilized and are more susceptible to mechanical forces. If foam is generated, transfer of the microcarriers into the foam phase (Fleischaker, 1982) may cause further problems.

Independent of whether microcarriers are suspended in a airlift, fluid-lift, or stirred-tank reactor, there will be a trade-off between mass transfer and hydrodynamic damage upon scale-up. For all three reactor types, the fluid-mechanical environment will be comparable in high-density, large-scale cultures. In this thesis, hydrodynamic phenomena in the stirred-tank design are investigated.

Cell Damage from Turbulence

When a vessel is agitated with a rotating impeller, the Reynold's number for the bulk flow is given by (Nagata, 1975)

$$Re = N D_i^2/\nu_b \qquad \text{(Eq. 9)}$$

where ν_b is the kinematic viscosity of the bulk suspension, N is the impeller rotation rate, and D_i is the impeller diameter. If this Reynold's number exceeds approximately 1000, the flow field becomes turbulent (Nagata, 1975). For complete off-bottom suspension of

microcarriers, virtually all stirred-tank bioreactors must be operated in the turbulent regime.

In the turbulent flow field of a microcarrier culture, short-term hydrodynamic forces arise through the motion of turbulent eddies. In conjunction with the transfer of energy from large to small eddies, there exists a spectrum of eddy sizes down to the viscous dissipation regime. For sufficiently high bulk flow Reynold's numbers, the smallest eddies exist in a state of isotropic, statistical equilibrium and can be described by the Kolmogorov scales for eddy length and viscosity (Hinze, 1975).

In a stirred-tank, the large energy-containing eddies are highly nonisotropic and nonhomogeneous (Nagata, 1975). Nonetheless, isotropic equilibrium at the Kolmogorov scale will exist if the eddies in the viscous dissipation regime are much smaller than the energy-containing eddies (Hinze, 1975). There are several results which indicate isotropic equilibrium exists at the viscous dissipation scale in stirred-tank microcarrier bioreactors:

1) For stirred tanks, Komasawa et al (1974) found that the energy containing eddies, or turbulent macroscales, have sizes roughly given by one-fifth the impeller width. Translating these results to most microcarrier cultures, one can estimate that the energy-containing eddies are more than an order of magnitude larger than eddies in the viscous dissipation regime.
2) For stirred tanks, Nagata (1975) found that the lateral and

longitudinal energy spectra became nearly superimposable at high wave numbers. This indicates that local isotropy exists at the viscous dissipation scale.

3) In analyzing several sets of results, including those of Sato et al (1967) for stirred tanks, Wadia (1975) found that energy spectra in the viscous dissipation regime followed the prediction of Heisenberg (1948) for isotropic turbulence in statistical equilibrium. The observation held for agitation in an unbaffled stirred tank with an impeller Reynold's number of 8400, typical of the conditions in a stirred-tank microcarrier reactor.

4) As shown by the tracer-particle studies of Komasawa et al (1974), the presence of particles in the turbulent flow of a stirred tank does not preclude the existence of isotropic equilibrium. If the bulk-flow Reynold's numbers are high, if the particles are nearly neutrally-buoyant, and if the particles are comparable in size to the Kolmogorov eddy length scale, isotropic equilibrium should exist in the viscous dissipation regime. Microcarriers are nearly neutrally-buoyant and are comparable in size to the Kolmogorov eddy length scale.

In light of the evidence presented, it appears that a condition approaching isotropic equilibrium exists in the viscous dissipation regime for many microcarrier cultures.

With the belief that Kolmogorov's theories of isotropic equilibrium can be applied to microcarrier cultures, one might first consider the

role of eddy size. If a relatively large eddy formed in a region occupied by a microcarrier, the microcarrier would be entrained and would rotate and translate in a manner that would reduce the net torques and forces on its surface. If a relatively small eddy formed adjacent to a microcarrier, the motion of the microcarrier would be more limited, as shown by the results of Kuboi et al (1974), and the cells on the microcarrier would have to experience more of the full force of the eddy. Accordingly, cells on microcarriers will be the most damaged by small intense eddies of a size and velocity large enough to affect individual cells, but too small to readily entrain entire microcarriers.

In microcarrier cultures, turbulent eddies in the viscous dissipation regime are often intermediate in size between the cells and microcarriers. Because these eddies appear to exist in a state of isotropic equilibrium, they are described by the Kolmogorov scales (Tennekes and Lumley, 1985)

$$L = (\nu^3/\epsilon)^{1/4} \qquad \text{(Eq. 10)}$$

$$v = (\nu\epsilon)^{1/4} \qquad \text{(Eq. 11)}$$

$$\theta = (\nu/\epsilon)^{1/2} \qquad \text{(Eq. 12)}$$

where L is the length scale, v is the velocity scale, and θ is the time scale for the eddies. These scales are functions of only the power dissipation per unit mass, ϵ, and the kinematic fluid viscosity, ν.

The size of the smallest eddies decreases with an increase in power

or a decrease in kinematic viscosity. For sufficiently high power inputs at a given viscosity, the turbulence should generate eddies which are smaller than microcarriers. Cell damage from turbulence should then become evident, if the proposed role of eddy length is correct.

In this thesis, the effects of both power input and viscosity are investigated to determine if hydrodynamic damage correlates with the Kolmogorov length scale for the smallest eddies. Experimental investigations are performed with regard to the average power dissipation rates. Although the role of local power dissipation rates is partially investigated and discussed, more thorough investigations are left for future work.

In this thesis, separate experiments are performed for both dilute and concentrated cultures. In dilute cultures, cell damage should occur primarily through microcarrier-eddy interactions. In concentrated cultures, cell damage may occur not only through microcarrier-eddy interactions, but also through microcarrier-microcarrier interactions. To provide clear and unique information with regard to each mechanism, microcarrier-eddy and microcarrier-microcarrier damage mechanisms are studied separately.

Protective Polymers

To eliminate or reduce cell damage from fluid-mechanical forces, many investigators have added polymers to their medium. The most commonly used polymer is methylcellulose (Kuchler et al, 1960; Bryant,

1966, 1969; Holmstrom, 1968; Birch and Pirt, 1969; Tramper et al, 1986). Pluronic polyols have also been used (Swim and Parker, 1960; Runyan and Geyer, 1963; Kilburn and Webb, 1968; Mizrahi, 1984), along with sodium carboxymethylcellulose (Mizrahi, 1984), polysucrose (Pharmacia, 1981), dextran (Schulz et al, 1986), and hydroxyethyl starch (Mizrahi, 1984). In general, metabolic uptake of these polymers is insignificant (Mizrahi, 1984). The polymers appear to have no nutritive value (Bryant, 1966, 1969; Mizrahi, 1984), although they can provide trace metals in deficient medium (Thomas and Johnson, 1967) and can eliminate protein precipitation from medium with poor serum (Swim and Parker, 1960).

It is widely believed that these polymers protect animal cells from mechanical damage. In agitated systems, cell disruption is frequently observed if the medium is not supplemented with either serum or one of these protective polymers (Swim and Parker, 1960; Kuchler et al, 1960; Runyan and Geyer, 1963; Bryant, 1966; Thomas and Johnson, 1967; Holmstrom, 1968; Kilburn and Webb, 1968; Birch and Pirt, 1969; Mizrahi, 1984). Because the known protective polymers and serum can substitute for each other with regard to mechanical protection, it appears that serum contains a protective polymer, although it has not been identified.

The mechanism of the protective effect of these polymers has not been determined. The mechanism may involve a reduction of turbulent damage through an increase in viscosity. Addition of the polymers would

likely increase the medium viscosity and the size of the smallest eddies, and thus reduce cell damage from turbulence. This hypothesis will be investigated in this thesis.

Cell Damage from Time-Average Flow Fields

In a turbulent flow field, there are both time-average and time-flucuating pressure and velocity components. If the time-average velocity components change greatly over small intervals in position, strong hydrodynamic forces could arise and damage cells.

To evaluate the role of time-average velocity components in a thorough fashion, one might determine the position-dependent time-average flow profile around a microcarrier as it circulates through various time-average flow fields in a stirred tank. Because this approach is very difficult, if not currently impossible, one might instead employ a simplified approach and ignore the dynamic effects due to microcarrier circulation. If the time-average flow field is broken down into small regions, and if turbulent velocity flucuations are ignored, the problem can be simplified to the situation depicted in Figure 3. This schematic of a sphere in a shear field represents a small region in the reactor where the gradient in the time-average velocity field is approximately constant. Such gradients will subsequently be referred to as time-average shear rates.

Lin et al (1970) developed an analytical steady-state solution to the flow profile near a neutrally-buoyant sphere, as depicted in Figure

3. The relevant Reynold's number is given by

$$Re = Y\ r_m^2/\nu \qquad \text{(Eq. 13)}$$

where r_m is the microcarrier radius and Y is the undisturbed shear rate. For microcarrier bioreactors, the Reynold's numbers calculated from equation 13 are generally below 1, and the flow can be approximated as creeping. The maximum shear stress, τ, on the sphere surface is then given by

$$\tau = 3\ \eta\ Y \qquad \text{(Eq. 14)}$$

where η is the fluid viscosity.

As shown in equation 14, the maximum shear stress depends upon the time-average shear rate and fluid viscosity. In most vessels, the maximum time-average shear rate is proportional to the impeller tip speed, ITS, and is given, in the reference frame of the rotating impeller, by (Oldshue, 1983):

$$Y = K_1\ ITS = K_1\ \pi\ N\ D_i \qquad \text{(Eq. 15)}$$

and where K_1 is a constant. If a radial flow impeller is used, the maximum shear rate occurs in the radial jet from the impeller. Analyzing the flow profiles developed by Nagata (1975), one can estimate that K_1 takes on a value near 0.4 cm^{-1} for a typical paddle impeller.

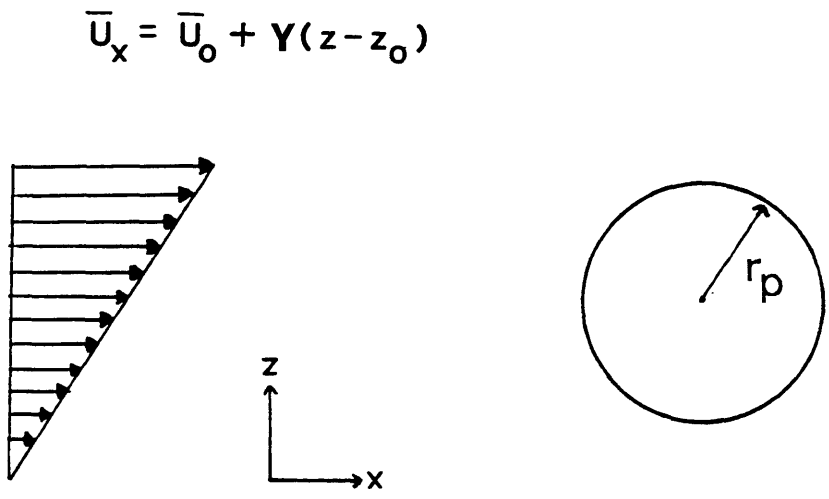

Figure 3. Schematic of a sphere caught in a simple shear field

Both Hu (1983) and Sinskey et al (1981) found that cell growth does not correlate with impeller tip. As shown by the data of Hu (1983) in Figure 4, maximum growth or zero growth can be observed at the same tip speed, depending on the size of the vessel. As originally concluded by Hu, the impeller tip speed, or the maximum time-average shear rate, does not appear to play a fundamental role in determining whether there are detrimental hydrodynamic effects.

In the experiments of Hu (1983), the maximum time-average shear rate was approximately 16 sec^{-1}, as calculated from equation 15. The maximum shear stress was approximately 0.4 $dyne/cm^2$, as calculated from equation 14. This maximum shear stress is much less than 7 $dyne/cm^2$, the minimum value reported to cause cell damage or removal (Stathopoulos and Hellums, 1985). Thus, it appears that cell damage from time-average shear fields was not occurring in the experiments performed by Hu (1983). This probably accounts for the lack of correlation between cell damage and maximum time-average shear rate.

To determine whether cell damage from time-average shear fields can occur, one can not only calculate and compare shear stresses, but one can also investigate the effects of viscosity. If cell damage from time-average flow fields is occurring, an increase in viscosity should increase the amount of damage, since this will lead to higher shear stresses. If cell damage from turbulence is occurring, an increase in viscosity will reduce the amount of damage, as it will dampen the turbulence. Viscosity can be used to distinguish between damage from

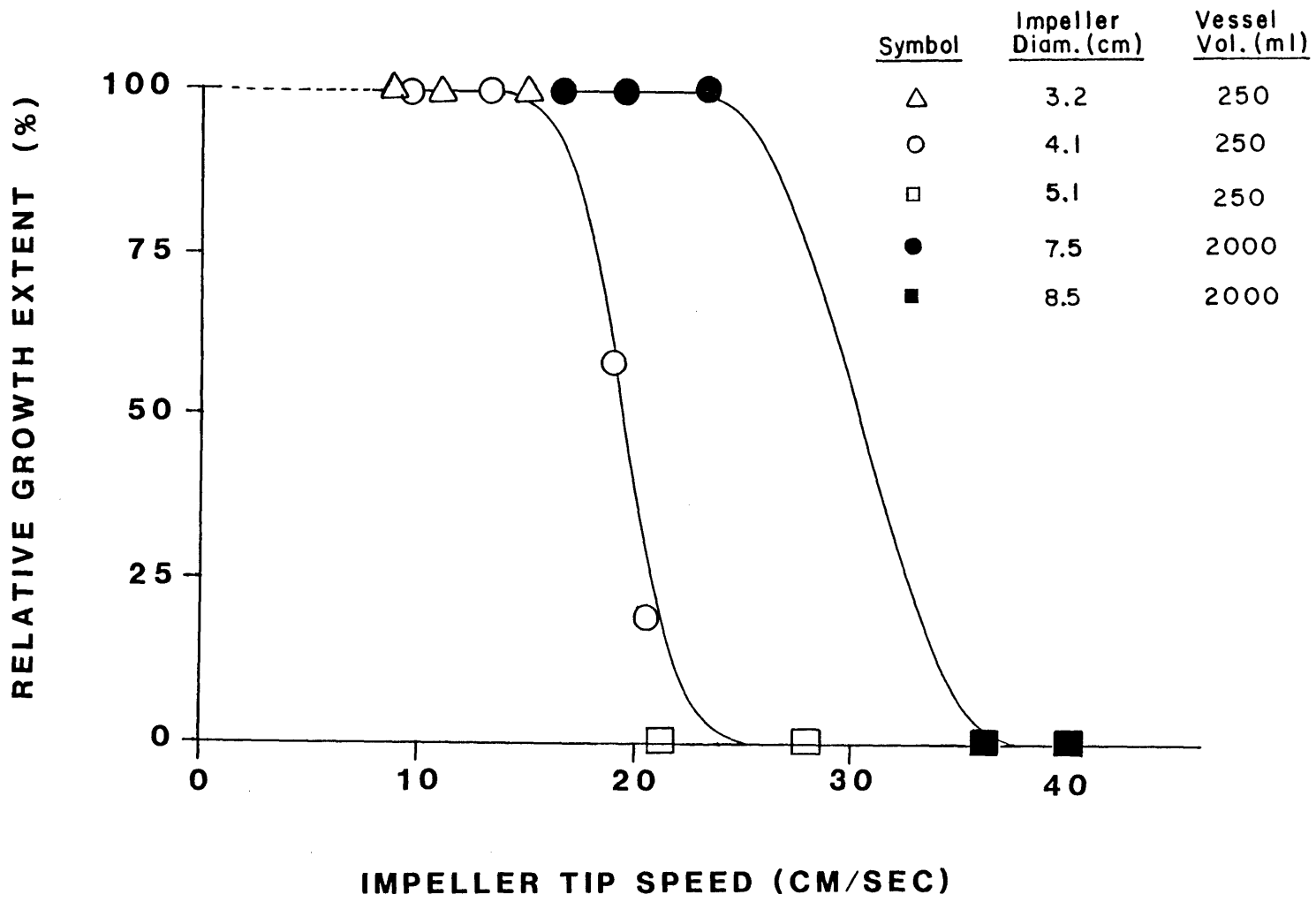

Figure 4. Relative growth extent vs. impeller tip speed (Hu, 1983)

turbulence and damage from time-average flow fields.

An increase in viscosity will cause cell damage only if a reactor has sufficiently high time-average shear rates. As was mentioned, the maximum time-average shear rate for most reactors occurs in the jet off the impeller. In some reactors, the maximum time-average shear rate may occur in a region of close clearance between the rotating impeller and a stationary vessel component. For instance, if there is a close clearance between the impeller and vessel wall, the tangential flow profile in this region may periodically assume a character similar to the flow between concentric rotating cylinders. The maximum tangential shear rate may then be estimated from the solution of Lee (1966) for the flow profile between concentric rotating cylinders, and is thus given by

$$Y = \frac{4 \pi N D_t^2}{D_t^2 - D_i^2} \qquad \text{(Eq. 16)}$$

where D_t is the vessel diameter, N is the impeller rotation rate, and D_i is the impeller diameter.

In this thesis, a vessel with a close clearance between the impeller and vessel wall is used to investigate the onset of cell damage from time-average flow fields. The effects of viscosity are investigated for shear stresses below and above 7 dyne/cm^2, as calculated from equations 14-16. Criteria are developed to predict the onset of cell damage from time-average flow fields. These criteria are used to purposefully avoid

cell damage from time-average flow fields during the experiments on turbulence.

MATERIALS AND METHODS

Cell Types

Two types of representative cells were used in this thesis: human foreskin fibroblasts (FS-4) and recombinant Chinese hamster ovary cells engineered to produce γ-interferon (γ-CHO). The FS-4 cells are diploid and fully anchorage-dependent. The γ-CHO cells are aneuploid and, although not fully anchorage-dependent, are difficult to grow in suspension (Perry, 1987). The γ-CHO cells were obtained from Biogen Research Corporation, Cambridge, MA. The FS-4 cells were obtained from Dr. Jan Vilcek, New York University School of Medicine. Prior to experimental use, the FS-4 cells were propagated to doubling 14-22 in 850-cm^2 roller bottles (Corning Science Products, Corning, NY). No deterioration of the cell line was detected prior to doubling 32.

Cell Culture Reagents and Procedures

In nearly all experiments, cultures were grown on Cytodex 1 microcarriers (Pharmacia Inc., Uppsala, Sweden) or in polystyrene T-flasks or roller bottles (Corning). A few experiments were conducted with cells grown on Cytodex 2 and 3 microcarriers (Pharmacia) or in glass petri dishes (Corning). Unless otherwise noted, the term "microcarrier" refers to Cytodex 1 microcarriers.

All cultures were grown in Dulbecco's Modification of Eagle's Medium (DMEM; Gibco, Grand Island, NY) supplemented with 50 U/ml penicillin (Gibco), 50 mg/l streptomycin (Gibco), and either 5 or 10% (v/v) fetal

calf serum. For the FS-4 cultures, a single lot of fetal calf serum (Hazelton Dutchland Inc., Denver, PA) was used for all experiments. For the γ-CHO cultures, a single lot of dialyzed fetal calf serum (Flow Laboratories, McLean, VA) was used for all experiments, and the medium was additionally supplemented with 0.25 μM methotrexate (L- + amethopterin, Aldrich Chemical Co., Milwaukee, WI). All serum was screened for viral and mycoplasma contamination. The serum lots used in these experiments were originally tested against several other lots; they were chosen for their ability to promote superior cell growth and attachment.

The microcarrier cultures were grown in 125 or 500-ml Corning Slow-Speed spinner vessels (Corning Science Products, Corning, NY). These vessels are specially designed for gentle agitation and can suspend up to 30 g/l of microcarriers at 35 RPM. The 125-ml vessels have an impeller diameter of 5.3 cm, an impeller width of 1.9 cm, and an internal vessel diameter of 6.3 cm. The 500-ml vessels have an impeller diameter of 7.8 cm, an impeller width of 2.5 cm, and an internal vessel diameter of 9.6 cm. In nearly all of the experiments, the middle of each impeller was positioned at approximately half the liquid height. When the 5.3 cm impeller was used in the 500-ml vessels, the middle of the impeller was positioned at one-third of the liquid height. Prior to use, the glass components of the vessel were siliconized with Prosil 28 (SCM Specialty Chemicals, Gainesville, Florida) to prevent adherence of the microcarriers.

For each experiment, all cultures were grown at the same time from a single inoculum. This was achieved for the microcarrier cultures through the use of numerous spinner vessels (Corning) and magnetic stirrers (Bellco Biotechnology, Vineland, NJ). The stirring speed for all cultures was determined with a stroboscope (Pioneer Model DS303, Cole Parmer, Chicago, IL) and was verified, if possible, through direct visual observations with a stopwatch. The stirring speeds were found to vary less than 5% from setpoint.

All cultures were inoculated from roller bottles according to the procedures developed by Giard et al (1979) and Hu et al (1985). They were grown at 37°C in a humidified incubator with 10% carbon dioxide in air. The cultures were fed by replacing 60-80% of the culture medium with fresh medium at predetermined intervals. For each culture, the interval length between medium exchanges, I_L, was determined in hours from the equations

$$I_L = \frac{180}{C_m} \qquad \text{(for FS-4 cultures)} \qquad \text{(Eq. 17)}$$

$$I_L = \frac{44}{C_m} \qquad \text{(for } \gamma\text{-CHO cultures)} \qquad \text{(Eq. 18)}$$

where C_m is the microcarrier concentration in dry grams per liter. These interval feeding schedules maintained glucose levels between 1.0 and 4.5 g/l. They also limited lactic acid build-up, maintained pH values between 7.2 and 7.45, and hopefully eliminated nutrient limitations.

Culture Aeration and Effect of Dissolved Oxygen on Cell Growth

Oxygen was supplied to all cultures through surface aeration. In a preliminary control experiment, the effect of dissolved oxygen on cell growth in microcarrier cultures was investigated. Two FS-4 cultures were grown at different levels of dissolved oxygen in the 125-ml vessels at 35 RPM. In one culture, the dissolved oxygen level was maintained between 85 and 90% of saturation with respect to air. In the other culture, the dissolved oxygen level was maintained between 60 and 85% saturation with respect to air.

Figure 5 shows the growth of the FS-4 cells in the two cultures. Growth at 60-85% dissolved oxygen was nearly identical to growth at 85-90% dissolved oxygen. Thus, it appears that growth of FS-4 cells is essentially uniform over a dissolved oxygen range of 60-90% saturation with respect to air. Accordingly, all FS-4 cultures were grown within this dissolved oxygen range. Because similar effects of dissolved oxygen were expected for the γ-CHO cultures, all γ-CHO cultures were also grown in this dissolved oxygen range.

For nearly all cultures, the headspace gas was equilibrated with the 90:10 air-CO_2 incubator atmosphere through loosened caps on the vessel sidearms. This maintained adequate oxygen levels in the headspace and provided for sufficient culture oxygenation through surface aeration. For the high density cultures, however, oxygen transfer from surface aeration required elevated levels of oxygen in the headspace. Thus, for the high density cultures, the headspace was continuously exchanged with

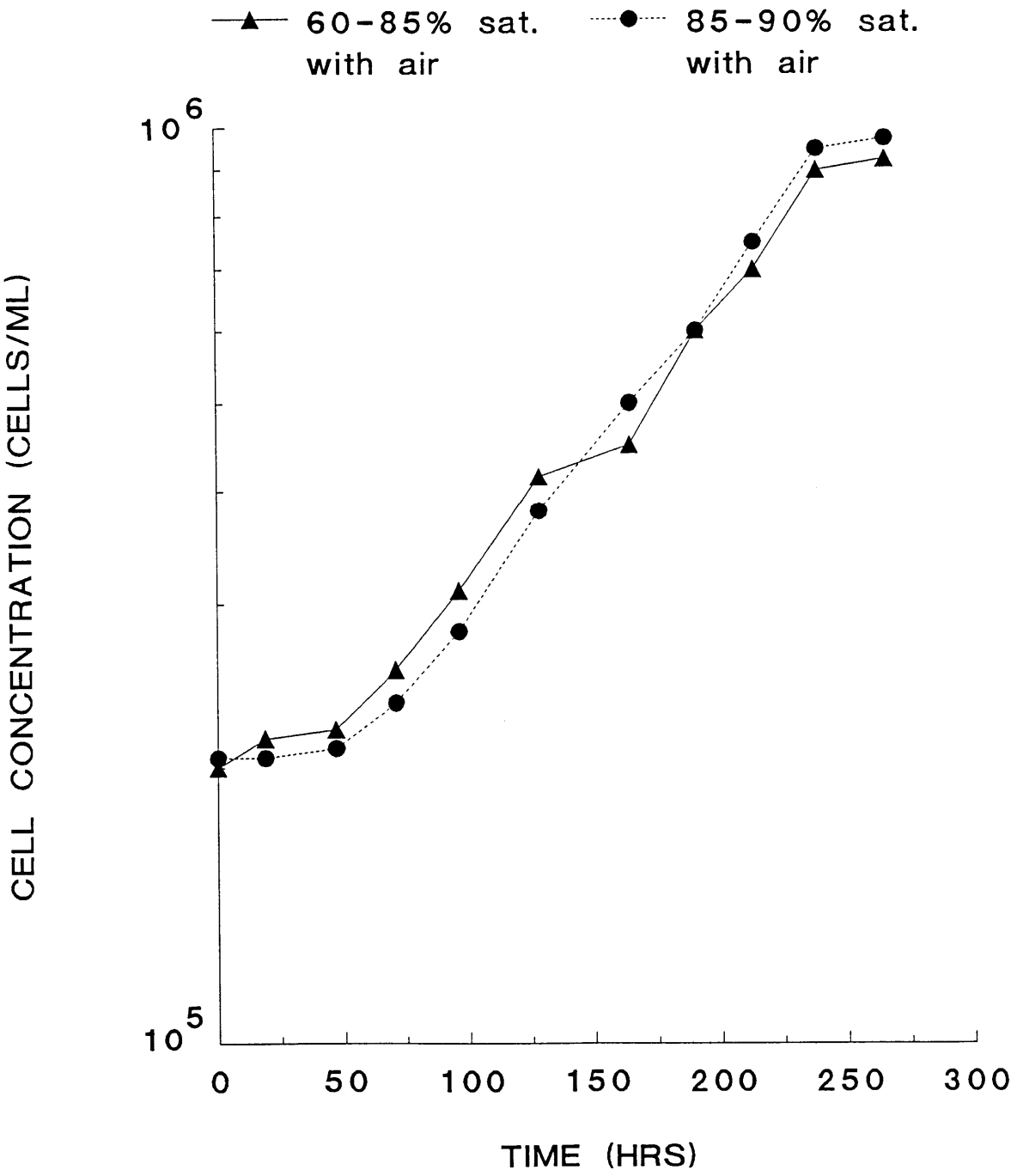

Figure 5. Effect of dissolved oxygen on growth of FS-4 cells

a humidified mixture of air, carbon dioxide, and oxygen. The flow rates of the three gases were controlled with variable-area flowmeters (Models FM042-07, FM042-15, and FM062-01, Aalborg Instruments, Monsey, NY). The oxygen content of the headspace was adjusted so as to control the oxygen level in the culture between 60-90% of saturation with air. The carbon dioxide content of the headspace was maintained at 10% so as to control the culture pH between 7.2 and 7.45.

Agitation Power Determinations

For each microcarrier culture, the average power input per unit mass, $\bar{\epsilon}$, was determined from the standard power-number correlation:

$$\bar{\epsilon} = N_p N^3 D_i^5 / V_c \qquad \text{(Eq. 19)}$$

where N_p is the power number, N is the impeller rotation rate, D_i is the impeller diameter, and V_c is the average culture volume. Power numbers were determined from the correlations presented in Nagata (1975) for flat-blade paddles in unbaffled vessels. These correlations are described by the following equations:

$$N_p = \frac{A}{Re} + \frac{B\,(10^3 + 1.2\,Re^{0.66})^p}{(10^3 + 3.2\,Re^{0.66})^p} \qquad \text{(Eq. 20)}$$

where A, B, and p are empirical constants given by the equations:

$$A = 14 + (w/D_t)[670(Di/Dt - 0.6)^2 + 185] \qquad \text{(Eq. 21)}$$

$$B = 10^{[1.3 - 4(w/D_t - 0.5)^2 - 1.14(D_i/D_t)]} \qquad \text{(Eq. 22)}$$

$$p = 1.1 + 4(w/D_t) - 2.5(D_i/D_t - 0.5)^2 - 7(D_i/D_t)^4 \qquad \text{(Eq. 23)}$$

where w is the impeller width, D_i is the impeller diameter, D_t is the tank diameter, and Re is the impeller Reynold's number given by equation 9. The bulk kinematic viscosity, ν_b, of a microcarier suspension was estimated by the ratio of suspension viscosity (Hiemenz, 1977) to volume-average density:

$$\nu_b = \frac{\eta(1 + 2.5\phi + 10\phi^2)}{\rho_f (1 - \phi) + \rho_m \phi} \qquad \text{(Eq. 24)}$$

where η is the fluid viscosity, ρ_f is the fluid density, ρ_m is the hydrated microcarrier density, and ϕ is the volume fraction of solids.

Cell Concentration Determinations

For all microcarrier cultures, supernatant and microcarrier samples were taken at least once a day. Glucose concentrations were determined through the hexokinase method (Sigma Chemical Co., St. Louis, MO). The concentration of cells attached to microcarriers was measured in duplicate with a modification of the nuclei counting technique described by Hu et al (1985). Samples from 1 to 15-ml were withdrawn from the well-mixed spinner vessels and placed in polystyrene centrifuge tubes. As soon as the microcarriers settled to the bottom of the tube, the supernatant was removed and the microcarriers were resuspended in 0.15 M citric acid with 0.5 g/l crystal violet. After incubation for 2 hours at 37°C, the samples were sheared with a Pasteur pipette. The released nuclei were then counted in a hemacytometer under 120-200 fold magnification with phase-contrast or Hoffmann modulation microscopy. Complete nuclei release was always verified through microscopic examination of the microcarriers. For the samples with high concentra-

tions of inert microcarriers, which will be susequently described, the citric acid concentration was increased to 0.3 M so as to overcome the dilution effect from the extra bead volume.

In this thesis, results for microcarrier cultures will frequently be expressed in terms of cell concentration, or the number of cells per ml of culture volume, including solids. Because the nuclei counts are performed on a liquid volume basis, it is necessary to correct for the solids volume, especially for cultures with high concentrations of microcarriers. Accordingly, cell concentrations were determined from the equation

$$C = \frac{10^4 \, (\xi/E)}{F \, (1 + F \, \phi)} \qquad \text{(Eq. 25)}$$

where C is the cell concentration in cells/ml, ξ is the number of nuclei counted, E is the number of hemacytometer squares scored, ϕ is the volume fraction of solids in the culture, and F is the initial sample volume divided by the final sample volume. To minimize any bias associated with the frequency of nuclei observation in the hemacytometer field, samples were concentrated or diluted such that the ξ/E was generally in the range of 30 to 80. To provide an adequate volume for sampling, the cultures with only 0.05 g/l microcarriers were grown in 500-ml vessels.

Samples from all cultures were frequently observed under a microscope after being fixed with crystal violet. The morphology of the

cells was qualitatively recorded along with the approximate average number of cells per microcarrier. These direct microscopic counts were used, along with glucose and oxygen uptake data, as a redundant check on the nuclei counts. No discrepancies were found in the results presented in this thesis.

For the T-flask cultures, cell concentrations were also determined by counting the number of nuclei released after treatment with crystal violet and citric acid (0.3 M). In order to obtain complete nuclei release, the cells were first washed twice with PBS and then incubated in the counting solution for 48 hours at 37°C. After the flasks were vigorously slapped and shaken, the released nuclei were counted.

DNA Assay

The DNA content of the culture fluid was determined with a fluorometric technique (Brunk et al, 1979) employing Hoechst 33258 dye (Hoefer Scientic Instruments, San Francisco, CA). Samples of culture fluid, complete with suspended cells but void of microcarriers, were taken before and after each interval feeding. The samples were placed in 15-ml polystyrene centrifuge tubes and stored at -20°C. The samples were later thawed, mixed for 10 seconds on a vibromixer, sonicated for two minutes in a sonication bath (Model 8850, Cole-Parmer Inst. Co., Chicago, IL) with intermitant mixing, and then centrifuged for 5 minutes at 300g. From the sample supernatant, 0.8 mls were taken and then added to a UV-fluorometric cuvette (Spectrocell Inc., Oreland, PA) containing 2.7 mls of phosphate buffered saline (PBS) with 1 μg/ml Hoechst dye and

no calcium or magnesium. The content of each cuvette was mixed and the pH was adjusted to 7.60 ± 0.01 with 10 μl aliquots of dilute NaOH. The fluorescence was then measured with a fluorimeter (Model LS-5, Perkin-Elmer, Norwalk, CT). The excitation wavelength was 365 nm, the emission wavelength was 458 nm, and the band widths were 3 nm.

Several control experiments were performed to validate the procedures listed above for the DNA assay. The response of the assay to DNA concentration was determined through the use of calf thymus DNA (Sigma Chemical Co., St. Louis, MO) dissolved in DMEM with 5% FCS and antibiotics. Figure 6 shows the increase in fluorescence versus the calf-thymus DNA concentration. The increase in fluorescence represents the fluorescence of the sample minus the fluorescence of a control with no calf thymus DNA. As shown in Figure 6, the fluorescence was found to plateau when the ratio of DNA to dye concentration (w/w) exceeded approximately 20. Similar behavior has been observed for by Brunk et al (1979) for the fluorescent DNA assay with DAPI dye. In Figure 6, the regressed lines through the data in the non-plateau regions have slopes of 1.04 and 0.96, respectively, on log-log coordinates. This indicates a good linear correlation over a wide dynamic range, as also found by Brunk et al (1979). For DNA concentrations below 2 μg/ml, the standard deviation of the assay was 0.06 μg DNA/ml.

For a given DNA concentration in the cuvettes, the fluorescence was found to increase with pH and decrease with the relative proportion of DMEM to PBS. The pH of all samples was adjusted using small aliquots

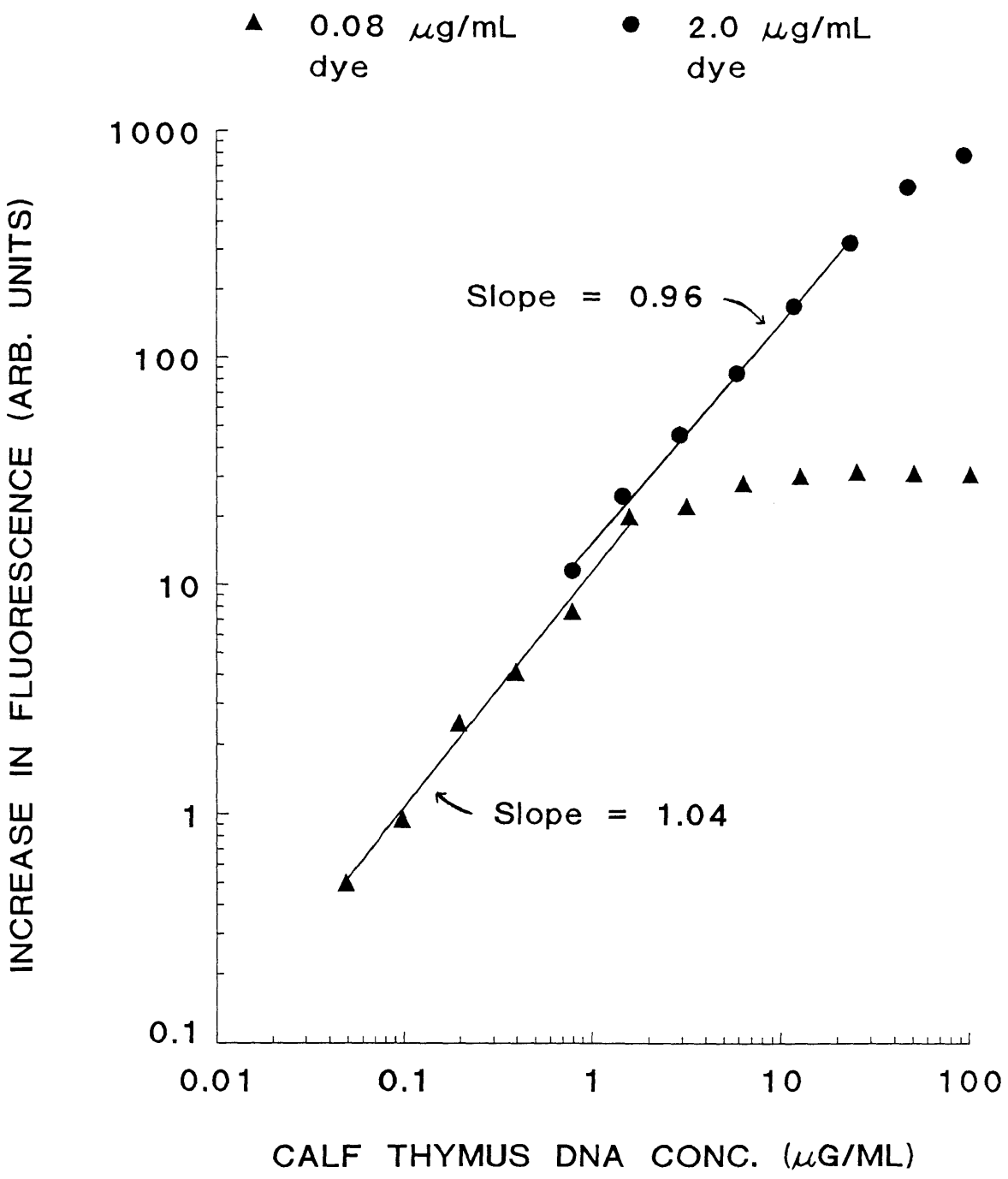

Figure 6. Increase in fluorescence vs. calf thymus DNA concentration

of dilute NaOH as described above. Minor corrections then had to be made for sample dilution and the change in the proportion of DMEM.

The fluorescence of a cell suspension, subsequent to freezing and thawing, was found to only be a weak function of sonication time with a maximum at approximately 2 minutes. The fluorescence of the calf thymus standards was not effected by 2 minutes of sonication or any of the other sample processing procedures.

The fluorescence of medium with serum was unexpectedly high. The DNA content of serum was subsequently measured and found to be approximately 20 μg/ml. The source of this DNA was not determined; the serum was not contaminated with viable microorganisms. The DNA content, however, does correspond to a lysed cell concentration of approximately 10^7 cells/ml, a typical white blood cell count. Thus, the DNA in serum could have come from white blood cell lysis during blood centrifugation or processing. It could also have come from contamination with psychrophilic microbes during serum storage prior to sterilization, as observed by Shiigi and Mishell (1975).

Specific Fluorescence of FS-4 Cellular DNA

The specific fluorescence of the DNA from FS-4 cells was determined through the use of T-flask cultures. Thirty identical cultures were started in 75-cm^2 T-flasks containing 12.5 mls of medium and an initial attached cell concentration of 2.2×10^3 cells/cm^2. At daily intervals, flasks were sacrificed in duplicate and the concentration of attached

cells was measured. The growth curve is shown in Figure 7. The growth curve was used, in part, to determine the growth rate of the cells taken for the DNA assay calibration.

To obtain cells for the DNA assay calibration, two flasks were sacrificed at 60 hours after inoculation. The cells were in exponential growth at a specific growth rate of 0.023 hr^{-1}. The culture fluid was discarded and the attached cells were washed with PBS, removed through trypsinization, centrifuged for 5 minutes at 150 x g, and resuspended in 3 mls of medium containing 5% (v/v) FCS and antibiotics. One-third of this standard cell suspension was removed and diluted 1:6.25 in the same medium. Both the normal and diluted cell samples were stored and processed as previously described for the DNA assay.

Figure 8 shows fluorescence versus cell concentration for the FS-4 cell samples. As found by other researchers (Brunk et al, 1979), the fluorescence increases linearly with cell concentration. The intercept is high due to the DNA from the serum supplement. For these cells, T_d = 30 hours, and one can reasonably assume that T_S is 7 hours, T_{G2} is 4 hours, and T_M is 1.5 hours (Baserga, 1976; Darnell et al, 1986; Alberts et al, 1983). An average DNA content of 1.24 diploid equivalents can then be calculated from equation 3. The value of 1.25 diploid equivalents is obtained if the calculation is performed with equation 4, and if one assumes a G_1 duration of 6 hours, typical for human diploid fibroblasts (Defendi and Mason, 1963; Macieira-Coelho et al, 1966; Baserga, 1976).

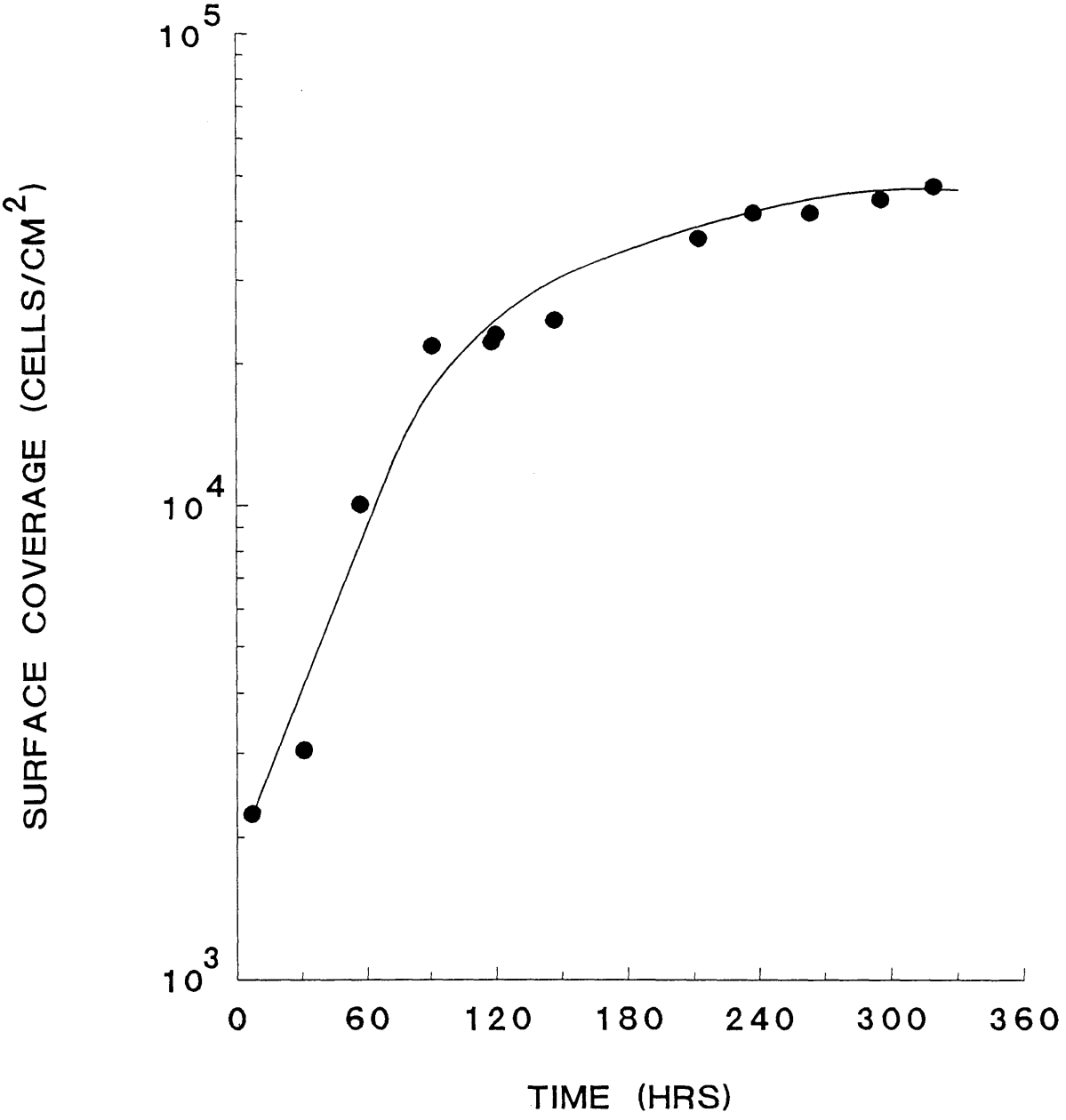

Figure 7. Growth of FS-4 cells in stagnant T-flasks

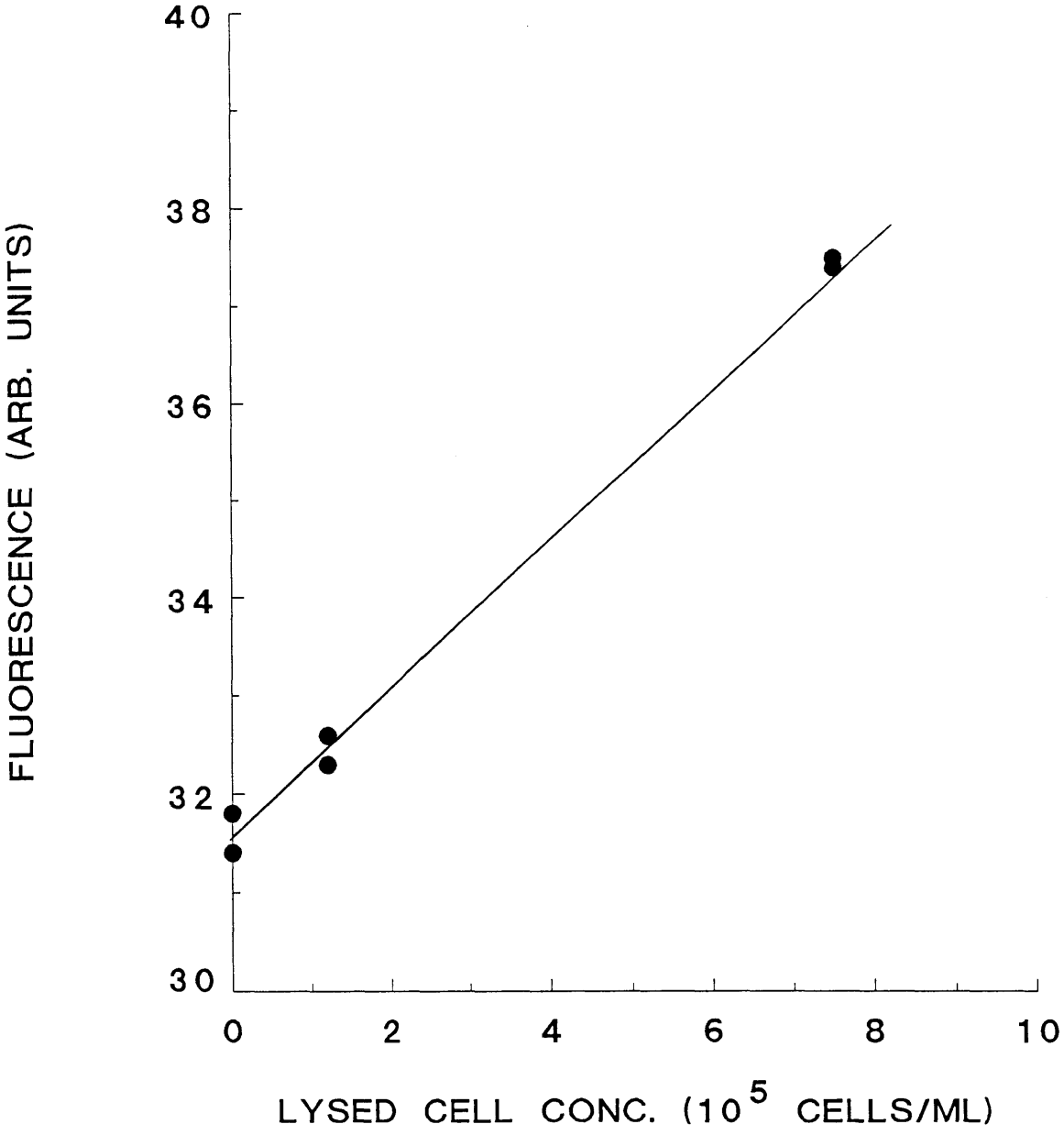

Figure 8. Specific fluorescence of FS-4 cells

There is little difference between the results obtained with equation 3 or 4. For the purposes of this paper, equation 3 will always be used. The DNA assay calibration is thus 6.3 fluorescence units/(million FS-4 diploid equivalents/ml). The average DNA content of an FS-4 cell population is therefore estimated by

$$S_a = 0.5 \left(2^{18.04\mu} + 2^{7.94\mu} \right) \qquad \text{(Eq. 26)}$$

where μ is given in hr^{-1}.

Effect of Cell Concentration in T-flasks

For FS-4 microcarrier cultures under mild agitation, the growth rate was found to decrease with the microcarrier and cell concentration. One could not clearly distinguish, however, whether the observed effect was due to high cell concentrations or high microcarrier concentrations. New experiments had to be designed so that the effects of microcarrier concentration and cell concentration could be studied separately.

Experiments in T-flasks were performed to independently determine the effects of cell concentration separate from the effects of microcarrier concentration. Various volumes of media were added to 75-cm^2 and 25-cm^2 T-flasks. This procedure allows one to vary the ratio of growth surface to medium volume (S/V), or cell concentration, in a stagnant environment free of microcarriers. To insure that the oxygen level was at least 60% of saturation with air at the cell surface, the maximum medium depth used was 2.0 cm. This depth was calculated from a stagnant diffusion model with a specific oxygen uptake rate of 5×10^{-11} mmole/cell-hr (Fleischaker, 1981, 1982) and a maximum surface coverage

of 5 x 10^4 cell/cm^2 (Hu et al, 1985). To insure that the culture surface was completely wetted, the minimum medium depth used was 0.16 cm. All T-flasks contained DMEM with 5% serum and were inoculated at 850 cells/cm^2. The cultures were sacrificed after 250 hours. Growth was measured using triplicate flasks for each surface/volume ratio.

Selection, Use, and Characterization of Inert Microcarriers

Cell growth in microcarrier and T-flask cultures was found to be strongly affected by cell concentration. Thus, to investigate the effects of microcarrier concentration, one would ideally want to use an "inert microcarrier". An inert microcarrier would have the same size and density as a normal microcarrier, but would be chemically inert and incapable of supporting cell growth or attachment. Inert microcarriers could be used to change the solids concentration, even during inoculation, without affecting the chemical environment or the number of cells inoculated per "active" microcarrier.

Sephadex G-50 beads (Pharmacia) were found to fulfill the requirements of an inert microcarrier. These beads have negligible charge and ion exchange capacity. Control experiments showed that they do not support cell growth or attachment. The beads with dry diameters between 90-106 microns have a size distribution, upon hydration, close to that of Cytodex 1 microcarriers. In subsequent paragraphs, the term "inert microcarrier" will refer to this size fraction of Sephadex beads.

A microscopic reticule was used to determine the size of both Cytodex 1 and inert microcarriers. Hydrated in DMEM with 5% serum, Cytodex 1 microcarriers have a diameter of 178 $\pm$ 23 micrometers; inert microcarriers have a diameter of 162 $\pm$ 18 micrometers. Direct microscopic counts were used to determine the number of microcarriers per gram. There are 3.8 million microcarriers per gram of dry Cytodex 1; there are 3.3 million microcarriers per gram of dry inert microcarriers.

To determine the density and specific volume of hydrated microcarriers, microcarrier suspensions were vacuum filtered for 2 minutes to remove unbound medium. The filtered beads were then added to a graduated cylinder containing medium. The change in weight and volume were used to calculate the specific volume and density. For hydrated Cytodex 1 microcarriers, the density is 1.03 g/ml, the hydrated bead volume is 10.2 ml/g, and the gravity-settled bed volume (including void space) is 18 ml/g. In the Pharmacia literature (1981), the bed volume appears to have been accidently substituted for the bead volume, and thus the specific surface area, bead volume, and number per gram are all in error by a factor of 1.76. For example, the specific surface area is 3440 cm^2/g, not 6000 cm^2/g. For the inert microcarriers, the hydrated density is 1.03 g/ml, and the hydrated bead volume is 7.6 ml/g.

Inert microcarriers were used to independently determine the effect of bead concentration in the microcarrier cultures. In one experiment, inert microcarriers were added to four identical vessels at different

concentrations: 0, 8.5, 18.5, and 28.5 g/l. All four cultures had 1.5 g/l Cytodex 1 microcarriers, contained medium with 5% serum, and were agitated at 35 RPM. To determine how the results of this experiment would vary with the level of agitation, it was repeated at a stirring speed of 150 RPM. At the higher speed, the inert microcarriers were added to levels of 0, 5, 10, 15, 20, 25, and 30 g/l. Eventually, the effect of adding inert microcarriers was investigated for a number of stirring speeds and fluid viscosities.

Viscosity and Density Measurements

The density of various medium solutions was measured at 37°C with a balance and volumetric flasks. Viscosities were measured at 37°C with a concentric-cylinder viscometer (Model LVT with UL adaptor, Brookfield, Stoughton, MA) for shear rates between 7 sec^{-1} and 74 sec^{-1}. The shear rate at the surface of the inner cylinder, Γ, was calculated from the equation (Lee, 1966)

$$\Gamma = \frac{4\pi N r_o^2}{r_o^2 - r_i^2} \qquad \text{(Eq. 27)}$$

where N is the rotation rate (sec^{-1}), r_i is the radius of the inner cylinder (1.258 cm), and r_o is the inner radius of the outer cylinder (1.381 cm).

Figure 9 shows the results of the viscosity measurements. The results are plotted as percent of maximum shear stress versus shear rate. Data is shown for water as the calibration standard. Data is also shown for Dulbecco's Modification of Eagle's Medium (DMEM), fetal

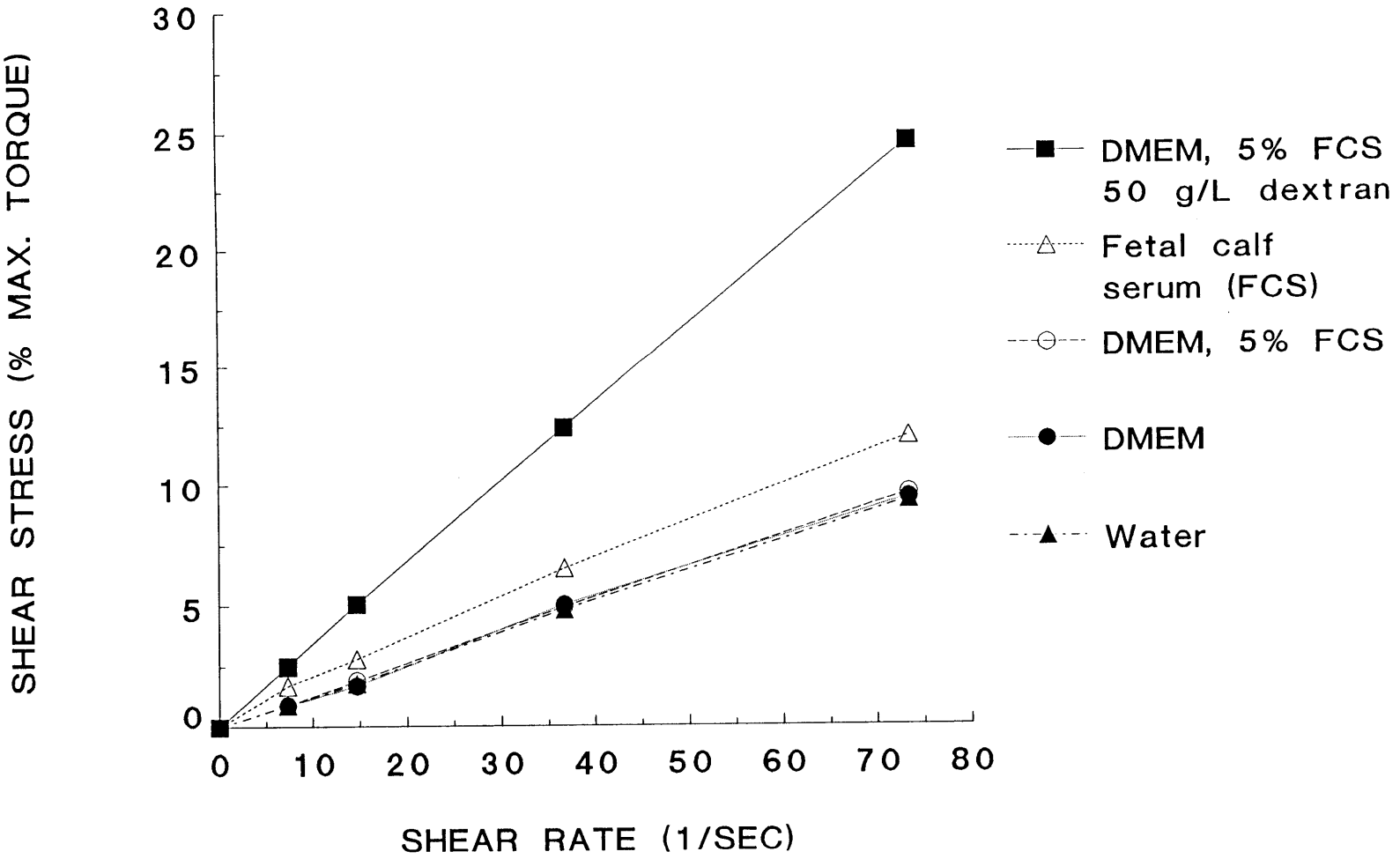

Figure 9. Shear stress vs. shear rate for various medium solutions

calf serum (FCS), DMEM with 5% (v/v) FCS, and DMEM with 5% (v/v) FCS and 50 g/L dextran of 78,500 average molecular weight. The viscosities of the various solutions, as determined by the regressed slopes, are tabulated in Table 1 along with the measured densities.

All solutions exhibited a constant viscosity except fetal calf serum (FCS), which exhibited a very slight pseudo-plastic behavior. The viscosity and density of DMEM were only scarcely greater than the values for pure water. Supplementation of DMEM with fetal calf serum only slightly increased the viscosity and density. Further supplementation with dextran greatly increased viscosity with only slight increases in density. For a given dextran concentration, supplementation with a higher molecular weight allowed for a similar density increase but a greater viscosity increase. Supplementation of medium with 1 g/l Methocel A15LV raised the viscosity by approximately 18% with no significant change in density.

At the beginning and end of several cultures, the viscosity and density of the culture fluid were measured. No significant changes in culture fluid viscosity or density were observed.

Selection and Use of Thickening agent

The mechanisms of cell damage in microcarrier cultures were investigated, in part, with experiments on the effects of viscosity. Such experiments are best performed with Newtonian solutions, i.e., solutions with constant viscosity and no viscoelastic interactions.

TABLE 1. VISCOSITY AND DENSITY MEASUREMENTS

Solution	Density (g/ml)	Viscosity (g/cm-sec)
DMEM	1.003	0.0071
Fetal Calf Serum	1.015	0.0088
DMEM, 5% (v/v) FCS	1.004	0.0074
DMEM, 25% (v/v) FCS	1.006	0.0078
DMEM, 5% (v/v) FCS, with		
20 g/L Dextran, 78,500 MW	1.008	0.0104
35 g/L Dextran, 78,500 MW	1.013	0.0135
50 g/L Dextran, 78,500 MW	1.018	0.0185
60 g/L Dextran, 78,500 MW	1.022	0.0227
80 g/L Dextran, 39,000 MW	1.030	0.0275
180 g/L Dextran, 9,000 MW	1.069	0.0275

Viscous effects can then be uniquely determined, independent of the effects of viscoelasticity. For Newtonian solutions, the viscosity is a single physical constant that can be easily measured with a viscometer.

A search was therefore conducted for a thickening agent which was completely soluble in cell culture medium, and could significantly increase the viscosity in a Newtonian fashion with little or no toxic effect on the cells. Several thickening agents with very low molecular weights were tested, including sucrose, glycerol, 1,3-butanediol, and 1,7-heptanediol. These substances are known to form Newtonian solutions when dissolved in water. At concentrations sufficiently high to give a 2-fold or higher increase in viscosity, all of these substances either killed the cells or severely inhibited growth.

Methylcellulose (A15-LV, Dow Chemical Co., Midland, MI) and sodium carboxymethylcellulose (LV grade, Sigma Chemical Co., St. Louis, MO) were also investigated as thickening agents. Methylcellulose was found to be essentially nontoxic, but did not readily dissolve into a completely clear solution. Small, clear particles, with diameters on the order of 10-100 microns, would gradually form in the methylcellulose-medium solutions even after filtering through 0.2 micron filters. Sodium carboxymethylcellulose gave similar problems with solubility, and was found to be toxic when positive growth surfaces were used, such as Cytodex 1, 2, and 3 microcarriers. Both methylcellulose and carboxymethycellulose are known to be viscoelastic (Hoyt, 1985; Amari and Nakamura, 1973, 1974) and frequently give solutions with pseudoplastic

rheology (Nicodemo et al, 1974; Dow, 1985), although viscosities relatively independent of shear rate can probably be obtained with the lowest molecular weight methylcellulose (Dow, 1985).

The search for a thickening agent was eventually directed toward finding a low-molecular-weight, nonionic polymer which exhibited Newtonian rheology in aqueous solutions. Dextrans were soon identified as promising candidates. Dextran polymers are nonionic are generally nontoxic. For aqueous solutions of low-molecular-weight dextrans, Newtonian rheology can be expected, as will be subsequently shown.

Low-molecular-weight dextrans (Sigma Chemical Co., St. Louis, MO) were tested for their effects on cell growth with mild agitation. The dextran polymers were dissolved directly in DMEM to give entirely clear solutions. Prior to use in cell cultures, the DMEM-dextran solutions were filter sterilized and supplemented with 5% FCS and antibiotics. Three different average molecular weights were investigated: 9,000, 39,400, and 78,500 daltons (clinical grade). The different molecular weights were tested in order to determine the lowest molecular weight which was suitable as a thickening agent.

Figure 10 shows the effect of various dextran supplements on growth in FS-4 microcarrier cultures at 35 RPM in the 125-ml vessels. Specific growth rate, relative to a control culture with no dextran, is plotted against dextran concentration. Data is included for three different

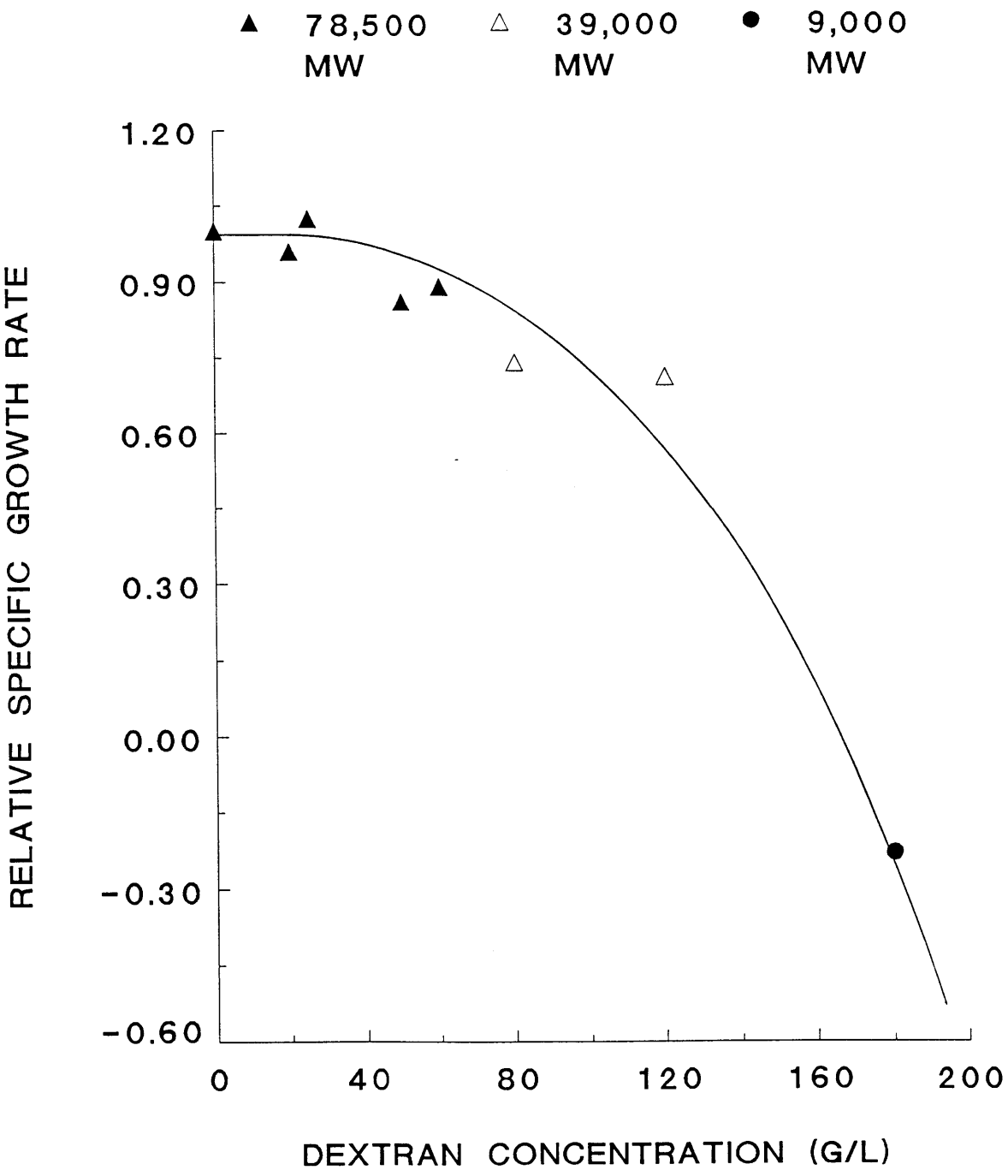

Figure 10. Chemical effects of dextran on cell growth

molecular weights: 78,500, 39,000, and 9,000 daltons. All of the data was collected under conditions of mild agitation. There was no hydrodynamic damage in any of the cultures, as will be shown in the Results and Discussion section.

The data in Figure 10 illustrates the chemical effects of dextran on cell growth. For an average molecular weight of 78,500 daltons, dextran concentrations below 25 g/l have no effect on cell growth, while a concentration of 60 g/l reduces the growth rate by 12%. If one wishes to increase the viscosity by approximately 3-fold, use of 78,500 MW dextran will lead to a 12% reduction in growth rate, 39,000 MW will lead to a 25% reduction, and 9,000 MW will lead to cell death. Dextran of 78,500 MW was acceptably nontoxic within moderate increases in viscosity. This substance was therefore suitable as a thickening agent as long as it exhibited Newtonian rheology.

Rheological Evaluation of Dextran Solutions

In the measurements with the concentric-cylinder viscometer, which covered shear rates between 7 and 74 sec^{-1}, aqueous solutions of low-molecular-weight dextrans were found to have constant viscosities. Typical results were shown in Figure 9 for medium with 50 g/L dextran of 78,500 average molecular weight. In general, for molecular weights up to 176,800, and for concentrations up to 280 g/l, aqueous dextran solutions are known to have constant viscosities for shear rates up to an over 1000 sec^{-1} (Margaritas and Pace, 1985). This is well beyond the range of shear rates observed in agitated microcarrier cultures.

Newtonian rheology can thus be expected as long as the dextran polymers do not exhibit viscoelastic interactions with the turbulence.

Through macromolecular extension, many polymers exhibit viscoelastic interactions with the turbulent bursting process. A viscoelastic interaction occurs when a polymer molecule has a relaxation time which is near the duration time of a turbulent burst (Virk, 1975; Denn, 1980). The relaxation time, Λ, of a polymer molecule can be estimated from the results of Zimm (1956):

$$\Lambda = 0.42\ M_w\ [\eta]\ \eta_s / R\ T \qquad \text{(Eq. 28)}$$

where M_w is the molecular weight of the polymer, $[\eta]$ is the intrinsic viscosity, η_s is the solvent viscosity, R is the ideal gas constant, the T is the temperature. The minimum duration of a turbulent burst, θ_{min}, can be estimated from the Kolmogorov time scale for the highest frequency eddies in the viscous dissipation regime:

$$\theta_{min} = (\nu/\epsilon_{max})^{1/2} \qquad \text{(Eq. 29)}$$

In animal cell culture vessels, typical values of θ_{min} range between 0.01 and 0.001 seconds. If a polymer molecule has a relaxation time which is orders of magnitude less than these values of θ_{min}, there will be no viscoelastic interaction between the polymer molecules and turbulence.

To determine whether such viscoelastic interactions could occur in dextran solutions, the characteristic relaxation time of 72,000 MW

dextran in water at 20°C was calculated from published viscosity data (Wolf et al, 1979). The intrinsic viscosity, $[\eta]$, was calculated through standard methods (Rodriquez, 1982) from the equation:

$$\frac{\eta_{sp}}{x} = [\eta] + k'[\eta]^2 x \qquad \text{(Eq. 30)}$$

where x is the polymer concentration in g/cm^3 and η_{sp} is the specific viscosity. The intrinsic viscosity was thus determined to be 24 cm^3/g. This corresponds to a characteristic relaxation time of 3×10^{-7} seconds, over three orders of magnitude smaller than the minimum turbulent burst durations in microcarrier reactors. Thus, viscoelastic interactions should not occur between the turbulence and dextran polymers of molecular weight near 78,500 daltons. Other researchers have noted that low-molecular-weight dextrans generally do not exhibit viscoelastic behavior in most turbulent flows (Hoyt, 1985).

For a typical commercial mixture of dextran polymers with an average molecular weight near 78,500, such as Dextran T70 (Pharmacia), the ratio of weight-average M_w to number-average M_w is approximately 1.6. This degree of polydispersity should not lead to non-Newtonian behavior.

In summary, dextran polymers of 78,500 average molecular weight exhibit all of the desired properties of a thickening agent: complete solubility, relative nontoxicity, and Newtonian rheology. These polymers were therefore used in the experiments on the effects of viscosity.

Cell Damage from Direct Sparging

The effect of sparging on cell growth was examined for FS-4 microcarrier cultures. Two experimental cultures were grown in 500-ml Bellco spinner flasks (Model 1965-00500, Bellco Biotechnology, Vineland, NJ). The flasks have an internal diameter of 10.2 cm. To eliminate cell damage from time-average flow fields, the Teflon impeller in each flask was cut to a diameter of 5.4 cm and a width of 2.7 cm. A filter stick of porosity C (Ace Glass, Vineland, NJ) was placed through a rubber cork stuck in the sidearm of each flask. The filter sticks were modified such that the solid tubular sections ran down the side of each flask and then curved radially inward near the bottom. The fritted regions layed almost horizontally on the bottom of each flask; this allowed for free bubble rise without interference from the filter stick.

One experimental culture was sparged at a superficial gas velocity of 0.01 cm/sec with a 90:10 air-CO_2 mixture. Foaming was essentially eliminated through the daily addition of 20-40 ppm Medical Emulsion AF antifoam (Dow Corning, Midland, MI). The antifoam was added as a 1% (v/v) solution and was sterilized through 6 hours of exposure to ultraviolet radiation. A second experimental culture was grown with antifoam in an identical vessel, complete with filter stick, but with no sparging. A third experimental culture was grown with no antifoam, no filter stick, and no sparging in a 500-ml Corning vessel with a 7.8 cm impeller. All cultures contained 2.0 g/l microcarriers in DMEM with 5% FCS, were identically inoculated from the same inoculum, and were replenished with nutrients on the normal interval feeding basis. Due to

the low cell concentrations, dissolved oxygen levels were essentially at saturation with 90:10 air-CO_2 gas mixtures. The stirring speeds were set at the minimum levels to provide microcarrier suspension: 50 RPM in the Bellco flasks and 35 RPM in the Corning flask. Net cell growth, or changes in viable cell concentrations, were used to assess the effects of sparging, antifoam addition, and filter stick presence.

RESULTS AND DISCUSSION

As mentioned in the Introduction, the objective of this thesis is to formulate a fundamental approach to the design, operation, and scale-up of microcarrier bioreactors. This objective was fulfilled by a series of experiments on the following topics:

1) hydrodynamic effects on growth of FS-4 cells with mild agitation,
2) hydrodynamic effects on growth of FS-4 cells with high agitation,
3) hydrodynamic phenomena in γ-CHO cultures,
4) mechanisms of hydrodynamic death in dilute cultures,
5) mechanisms of hydrodynamic death in concentrated cultures,
6) cell damage from direct sparging

The topics listed above constitute the first six chapters of the Results and Discussion section. The results from these chapters are used in the seventh chapter to develop a quantitative approach to bioreactor design and optimization.

CHAPTER 1. HYDRODYNAMIC EFFECTS ON FS-4 CELLS WITH MILD AGITATION

1A. Effect of Fluid Viscosity with Mild Agitation

The hydrodynamic effects on growth of FS-4 cells were first investigated under conditions of mild agitation. This established a baseline for the subsequent analysis for conditions of high agitation.

Hydrodynamic effects on growth with mild agitation were investigated with experiments on the effect of fluid viscosity. Figure 11 shows cell growth with and without a 20 g/l dextran supplement (78,500 MW) under mild agitation in the 500-ml vessels. The cultures were agitated with 5.3 cm impellers at 60 RPM, slightly above the minimum speed of 45 RPM for complete microcarrier suspension. The cultures contained only 0.2 g/l microcarriers, or 0.002 volume fraction solids, and were thus very dilute. The cells exhibited the normal growth observed in FS-4 microcarrier cultures with mild agitation. Over 95% of the cells were attached to the microcarriers and excluded trypan blue. The attached cell concentrations were essentially identical with or without 20 g/l dextran. Supplementation with 20 g/l dextran did not lead to toxic chemical effects or mass transfer limitations.

At 60 RPM, or an average power input of approximately 10 cm^2/sec^3, there appeared to be no cell death from time-average shear fields or microcarrier-eddy interactions. If cell death from microcarrier-eddy interactions was occurring, an increase in viscosity should have increased the minimum eddy size, reduced the death rate, and increased

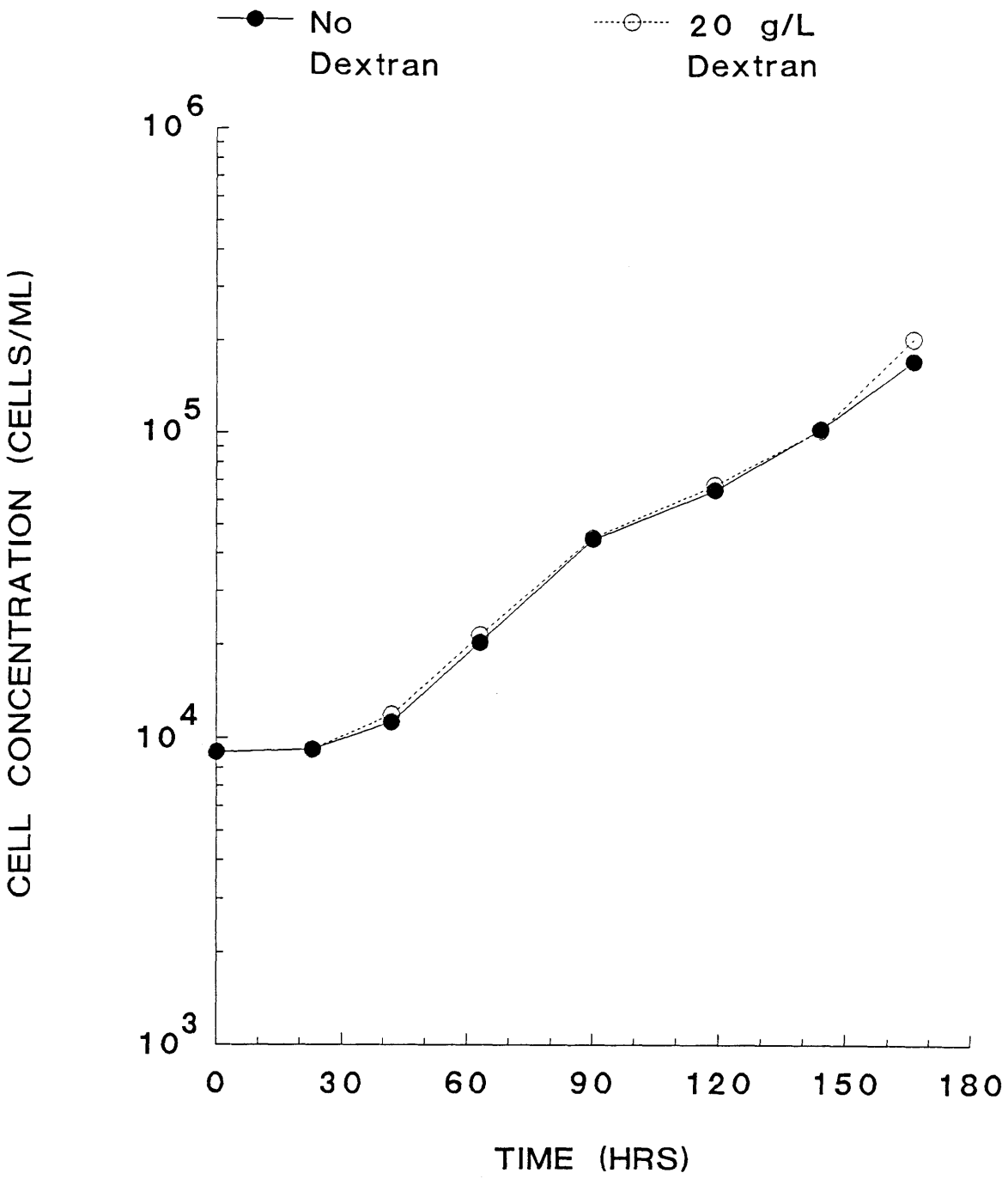

Figure 11. Effect of 20 g/L dextran (78,500 MW) on growth with mild agitation

the viable cell concentrations. If cell death from time-average flow fields was occurring, an increase in viscosity should have increased the maximum shear stress, increased the death rate, and reduced the viable cell concentrations. Because an increase in viscosity had essentially no effect on the viable cell concentrations, there appeared to be no significant cell death from hydrodynamic forces in these dilute cultures.

1B. Growth at Different Microcarrier Concentrations

With mild agitation, microcarrier-eddy interactions and time-average shear fields apparently did not lead to significant cell death. The data for the dilute cultures, however, did not indicate whether cell death can occur through hydrodynamic interactions between microcarriers. These interactions will be subsequently be referred to as collisions, even though the interactions may primarily involve the fluid flow between microcarriers which come in close but not actual contact.

To determine whether cell death occurs through microcarrier collisions with mild agitation, the hydrodynamic effects of microcarrier concentration were investigated. Cultures of FS-4 cells were grown over a range of microcarrier concentrations between 0.05 and 15 g/l. The cultures were fed according to the interval feeding schedules and were inoculated with 17 to 23 cells per microcarrier, clearly above the minimum inoculation requirement of 6 cells per microcarrier, as identified by Hu et al (1985). Through provision of excess defined nutrients, and through prevention of the build-up of toxic metabolites,

it was hoped that the physical effects of microcarrier concentration could be investigated without being strongly influenced by differences in chemical environments. The experiments were first performed with medium supplemented by 5% (v/v) serum. To determine if there were nutrient limitations associated with the 5% serum level, the experiments were repeated with a serum level of 10%.

Figure 12 shows the growth of FS-4 cells at different microcarrier concentrations with 5% serum at 35 RPM. The culture with 0.05 g/l microcarriers was grown in a 500-ml Corning vessel to provide an adequate volume for sampling. All other cultures were grown in 125-ml Corning vessels.

At all microcarrier concentrations, at least a four-fold increase in cell concentration was observed. This represents relatively good performance for microcarrier cultures of FS-4 cells (Hu et al, 1985). Nonetheless, the cultures with high cell or microcarrier concentrations showed very long lag phases, decreased growth rates, and decreased multiplication ratios (final cell concentration over initial cell concentration). The cells in the high density cultures also appeared to be much more "spread out" than the cells in the low density cultures.

Figure 13 shows the maximum surface coverage (cells/cm^2) at each microcarrier concentration. These normalized results clearly indicate that the maximum surface coverage was lower for the high density cultures. However, the detrimental effect of increased microcarrier or

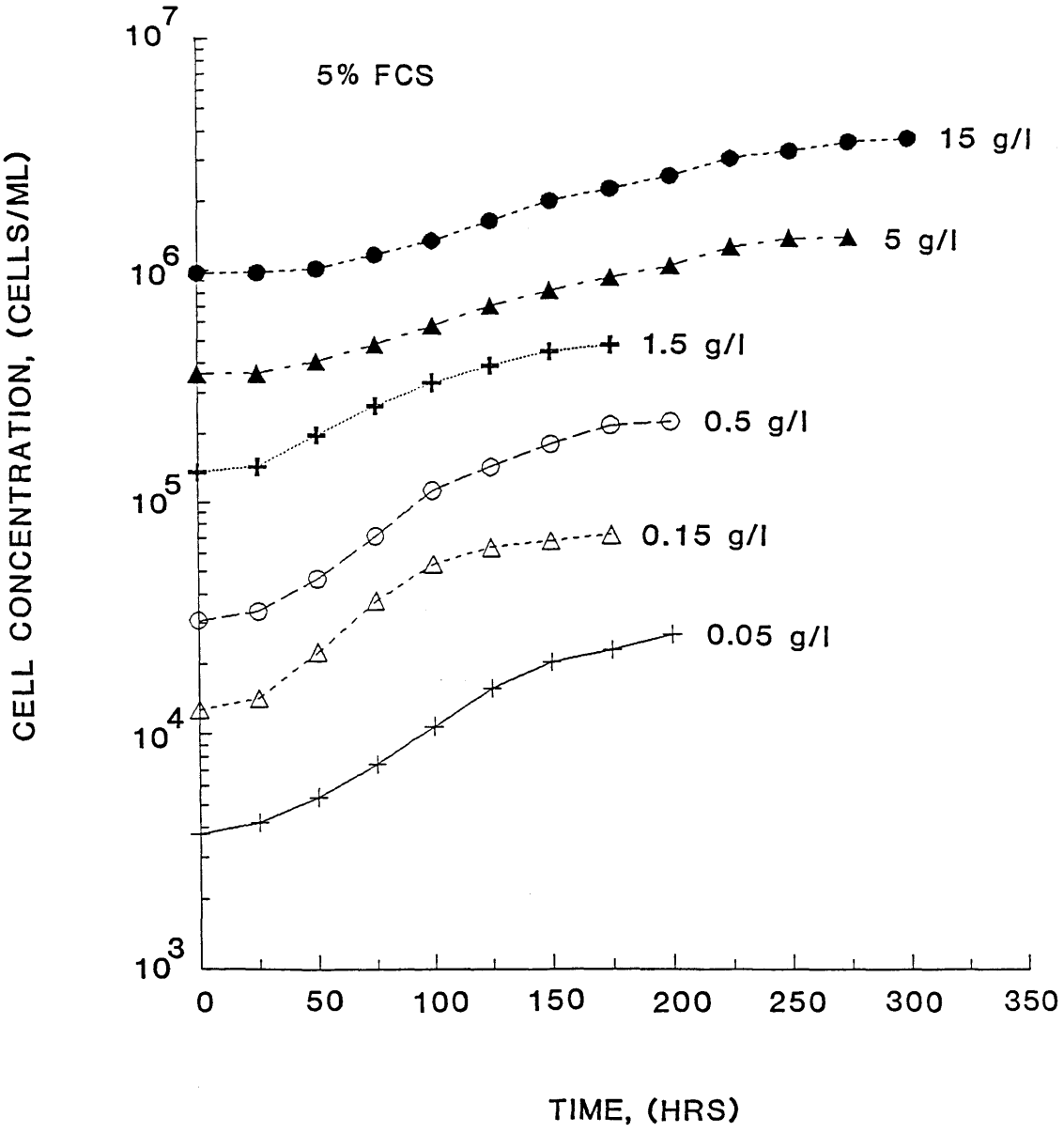

Figure 12. Growth at various microcarrier concentrations with mild agitation

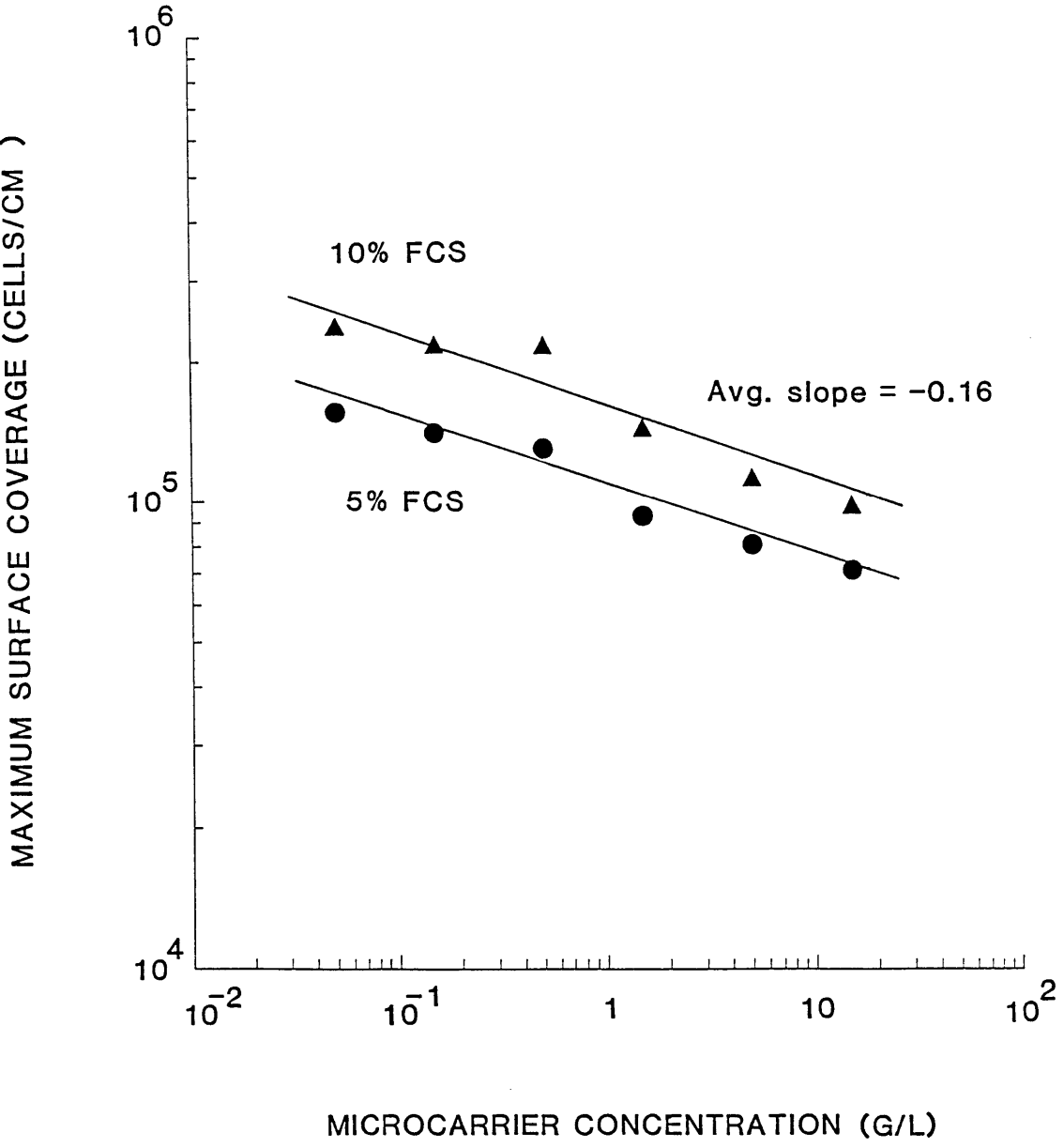

Figure 13. Maximum surface coverage vs. microcarrier concentration

cell concentrations was very weak and had an average exponential dependency on microcarrier concentration of only -0.16. A two-fold increase in microcarrier concentration resulted in only a 10% reduction in maximum surface coverage. Nonetheless, the weak effect was clearly present with both 5 and 10% serum. Furthermore, the slope is approximately the same at both serum levels. Even though the cells in 10% FCS generally grew to 50% higher concentrations than the cells in 5% FCS, the additional serum did not eliminate or even reduce the detrimental effect of higher microcarrier or cell concentrations.

Figure 14 shows the average specific growth rate as a function of microcarrier concentration. With 5% FCS, the growth rate reaches a maximum at approximately 0.2 g/l microcarriers, or an initial cell concentration of 1.5×10^4 cells/ml. With 10% FCS, the growth rate reaches a maximum at approximately 0.15 g/l, or an initial cell concentration of 1.1×10^4 cells/ml. The existence of these maxima indicates that the growth rate was influenced by at least two competing factors. As the microcarrier or cell concentrations were increased, at least one factor exerted a positive influence on the growth rate while at least one other factor exerted a negative influence.

It is well-documented that many animal cells secrete growth-promoting factors (Butler, 1986). As microcarrier or cell concentrations are increased, cell-derived growth factors could exert a positive influence on the growth rate. It is also well-documented that many animal cells secrete growth-inhibiting factors (Stoker and Piggott,

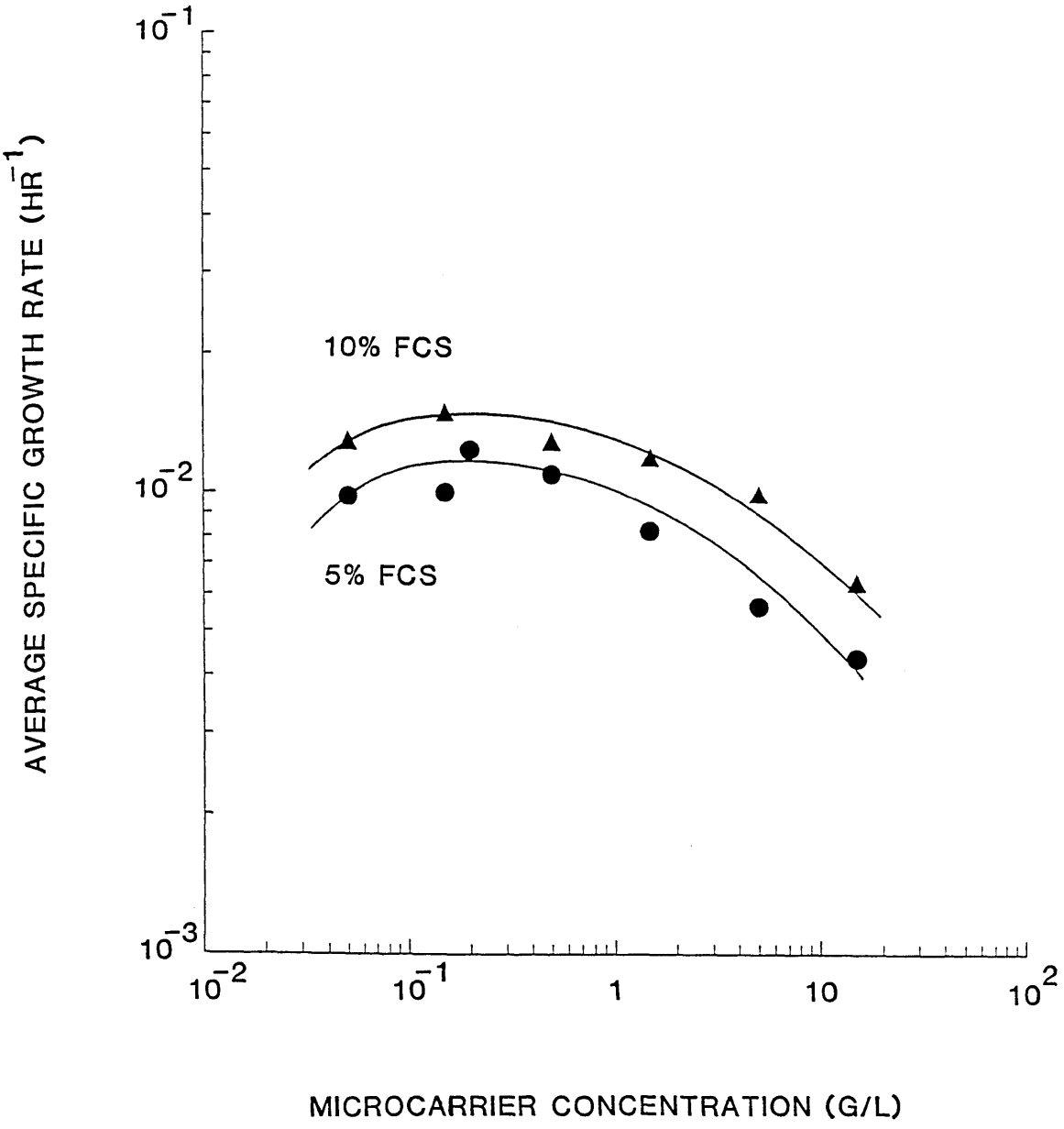

Figure 14. Average specific growth rate vs. microcarrier concentration

1974; McMahon et al, 1982; Bohmer et al, 1985; Hsu and Wang, 1986). As microcarrier or cell concentrations are increased, cell-derived inhibitors could exert a negative influence on the growth rate. The maxima in Figure 14 could result from competition between cell-derived growth promotors and inhibitors.

Cell damage from microcarrier collisions could also exert a negative influence on the observed growth rates. Figure 14 actually presents observed or net growth rates, which represent the difference between growth and death. As will be shown in the section on hydrodynamic damage in concentrated microcarrier cultures, a collision mechanism should decrease the observed growth rate in direct proportion to the microcarrier concentration. For the high-density cultures, however, a two-fold increase in microcarrier concentration resulted in less than a 25% reduction in observed growth rate. The observed growth rates clearly did not decrease in direct proportion to the microcarrier concentration. This is the first indication that the slower growth in the high density cultures was not due to microcarrier collisions.

1C. Growth in Stagnant T-flasks

To further investigate whether cell damage from collisions occurred in the microcarrier cultures at 35 RPM, growth in the microcarrier cultures was compared to growth in stagnant T-flasks. Figure 15 shows the growth curve for FS-4 cells grown in stagnant T-flasks. The data show the concentration of attached cells and was previously presented in Figure 7. The cells exhibited a period of rapid exponential growth

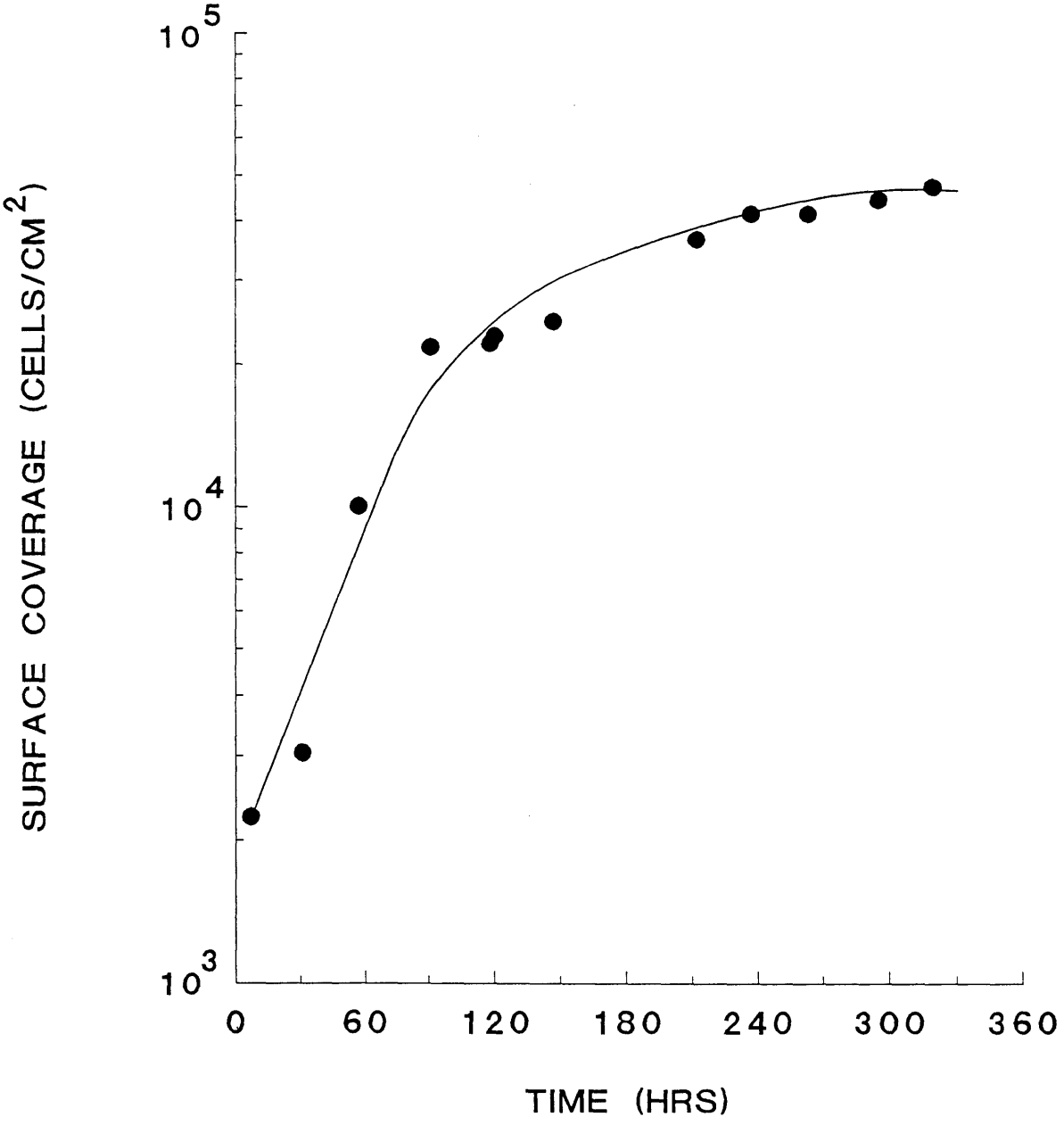

Figure 15. Growth of FS-4 cells in stagnant T-flasks

followed by a period of constantly-decreasing growth rate. In comparison to the microcarrier cultures, the T-flask cultures showed a higher initial growth rate but lower subsequent growth rate. Initial growth in the T-flasks may have been accelerated by the local build-up of cell-derived growth promotors at the cell surface. Subsequent growth may have been inhibited by the build-up of growth inhibitors.

Over the entire growth period, the T-flask cultures had an average growth rate of 0.0085 hr^{-1}. For an FS-4 microcarrier culture at 35 RPM with the same ratio of growth surface area to medium volume (6.0 cm^{-1}), one would expect an average growth rate of 0.009 hr^{-1}. Thus, FS-4 cells in mildly-agitated microcarrier cultures grow just as quickly, on the average, as cells in stagnant T-flasks. Although the average growth rate in the T-flasks may have been somewhat affected by the lack of mixing, it appears that little or no hydrodynamic reduction of cell growth occurred through microcarrier collisions at 35 RPM.

1D. Effect of Cell Concentration on Growth in T-flasks

If the decreased growth rate of the high-density microcarrier cultures was not due to collisions, but was rather due to growth inhibitors or other chemical effects, a similar trend should be observed for cultures grown in T-flasks. The growth rate in T-flasks should decrease with increased surface/volume ratios, or cell concentrations.

Figure 16 shows the effect of surface/volume ratio, or cell concentration, on the average growth rate in stagnant T-flask cultures.

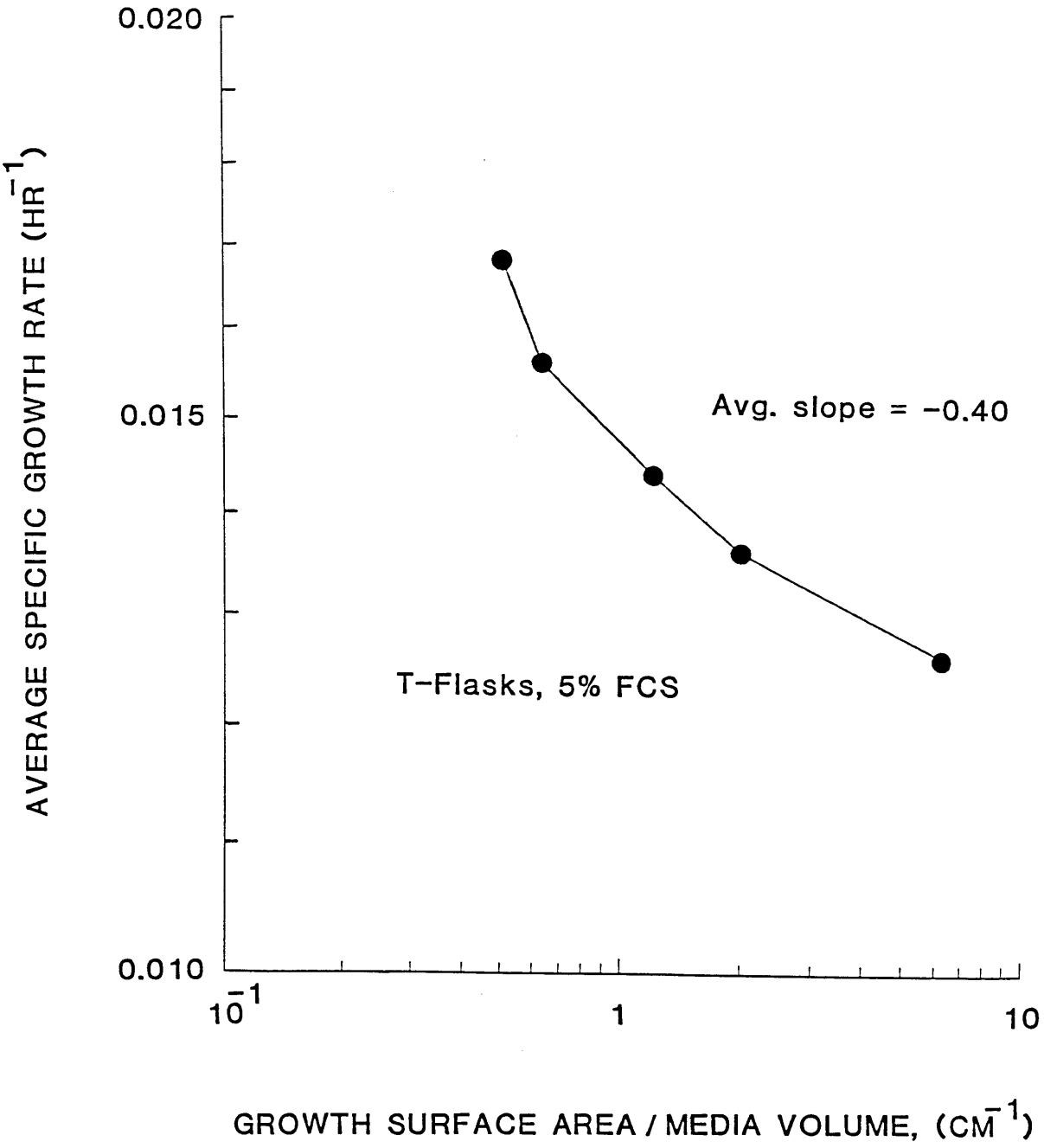

Figure 16. Effect of cell density on growth in stagnant T-flasks

As previously observed with the microcarrier cultures, the average growth rate decreases with an increase in surface/volume ratio. In fact, the average exponential dependency of -0.40 is approximately the same as that observed for the high-density microcarrier cultures. However, for T-flasks cultures, the decrease in growth rate with surface/volume ratio occurs at a lower cell concentration than for microcarrier cultures. This difference may be due to inhibitor build-up at the cell surface in stagnant T-flasks.

Although no conclusive evidence has been shown, it appears that the decreased performance of the high density microcarrier cultures may have been due, at least in part, to growth inhibitors or other chemical effects of cell concentration. There was no indication of significant cell damage from microcarrier collisions. However, the results from the inert microcarrier experiments will further indicate whether microcarrier collisions had any effect.

1E. Effect of Inert Microcarriers with Mild Agitation

To investigate the effects of microcarrier concentration separate from the effects of cell concentration, inert microcarriers were added at various levels to microcarrier cultures in 125-ml vessels. All cultures were agitated at 35 RPM, or average power inputs of approximately 7 cm^2/sec^3, and contained 1.5 g/l microcarriers with 5% (v/v) serum.

Figure 17 shows the attached, or viable, cell concentrations for the

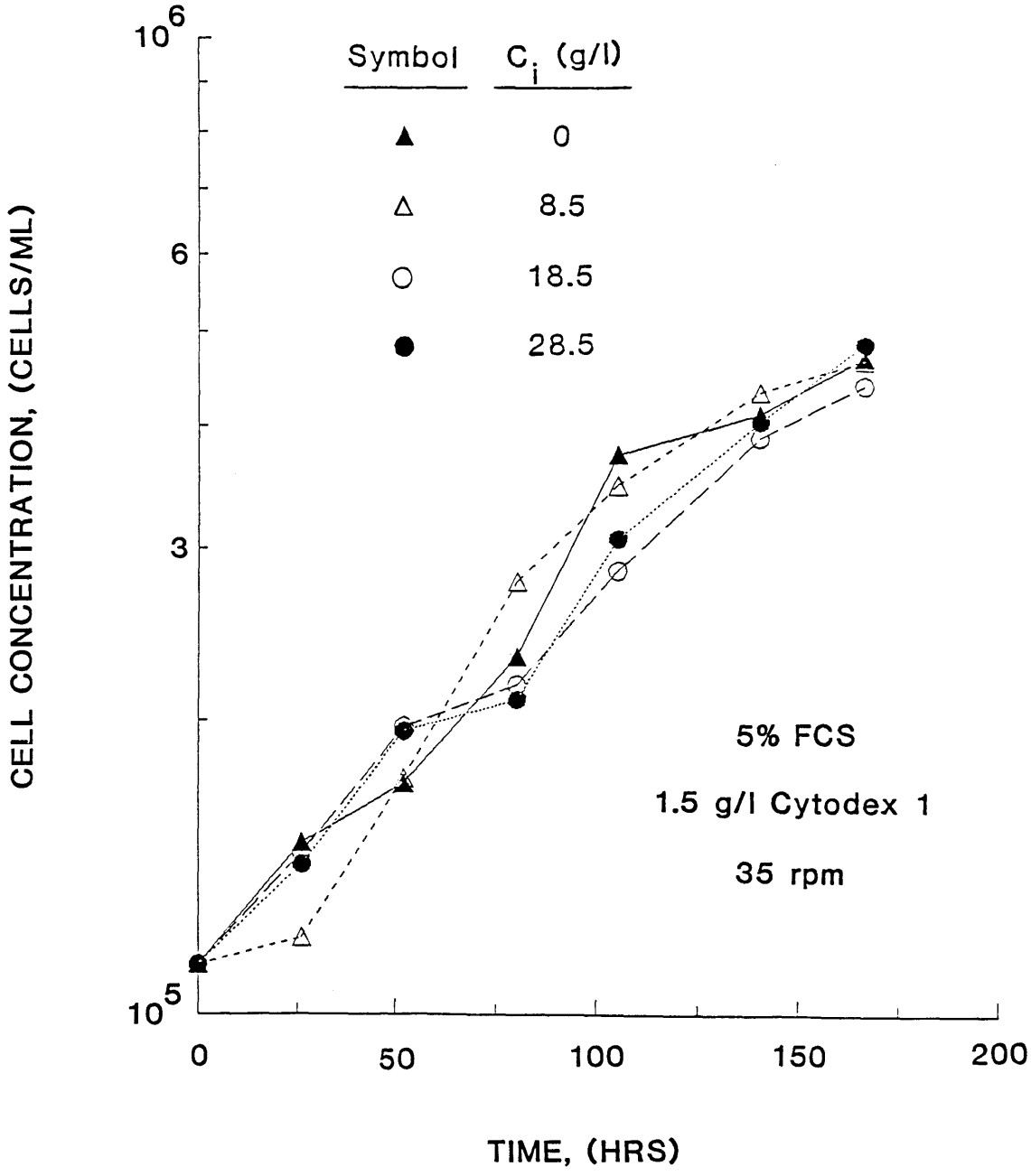

Figure 17. Effect of inert microcarriers on growth with mild agitation

cultures with different inert microcarrier concentrations, C_i. Cell growth was nearly identical in all of the cultures. If cell death from microcarrier collisions was occurring, an increase in inert microcarrier concentration should have increased the collision frequency, increased the death rate, and reduced the viable cell concentrations. However, the viable cell concentrations were clearly not effected from increases in the inert microcarrier concentration even up to 28 g/l. Cell death from microcarrier collisions was therefore not significant in the cultures at 35 RPM. For the cultures grown with high microcarrier concentrations at 35 RPM, the decreases in surface coverage (Figure 13) and observed growth rate (Figure 14) were due to the effects of cell concentration and not microcarrier concentration.

1F. Cell Growth with Mild Agitation

With mild agitation, growth of FS-4 cells was not affected by an increase in viscosity or inert microcarrier concentration. Growth was also not affected by small increases in the level of agitation, as previously observed by Hu (1983). For a given ratio of growth surface area to culture volume, the cells in mildly agitated microcarrier cultures grew just as quickly, on the average, as cells in stagnant T-flasks. All of this evidence indicates that little or no hydrodynamic death occurs in FS-4 microcarrier cultures with mild agitation.

In general, if cell growth or death was influenced from any type of hydrodynamic mechanism, net cell growth should be affected by a change in a fundamental hydrodynamic variable, such as agitation power, fluid

viscosity, or microcarrier concentration. Because changes in these three variables had no effect on net cell growth with mild agitation, it appears that cell growth and death were not significantly influenced by hydrodynamic forces with mild agitation. This conclusion is in line with the published results which show that growth of attached cells is not affected by mild shear stresses (Dewey et al, 1981; Sprague et al, 1987). This conclusion is also in line with the results of Dodge and Hu (1986), which show that growth of freely-suspended animal cells is not affected by moderate increases in the agitation.

CHAPTER 2. HYDRODYNAMIC EFFECTS ON FS-4 CELLS WITH HIGH AGITATION

2A. Growth Reduction and Cell Removal under High Agitation

With mild agitation, there was little or no hydrodynamic damage in microcarrier cultures. Cell growth was apparently not affected by hydrodynamic forces. These conclusions provide a baseline for the analysis of cell growth with high agitation.

Numerous experiments were performed to investigate the effects of high agitation on cell growth and death. Figure 18 shows the attached cell concentrations for FS-4 cultures grown on microcarrriers at different stirring speeds in 125-ml vessels. The data was determined at each speed from duplicate cultures. Net growth of attached cells was highest at 35 RPM and was slightly decreased at 60 RPM. An actual reduction in attached cell concentration was observed at 150 RPM; this indicates there was hydrodynamic removal of the cells from the microcarriers. In general, as the stirring speed was increased, the cells were either removed from the microcarriers and/or inhibited from growing at their maximum rate.

Because FS-4 cells are completely anchorage-dependent, any cells in suspension must have come either through incomplete attachment during inoculation, or through cell removal from the microcarriers subsequent to attachment. Figure 19 shows the removal of whole cells from the microcarriers at different stirring speeds. The results were calculated from measured concentrations of whole cells in suspension. No correction was made for incomplete attachment of the inoculum; such a

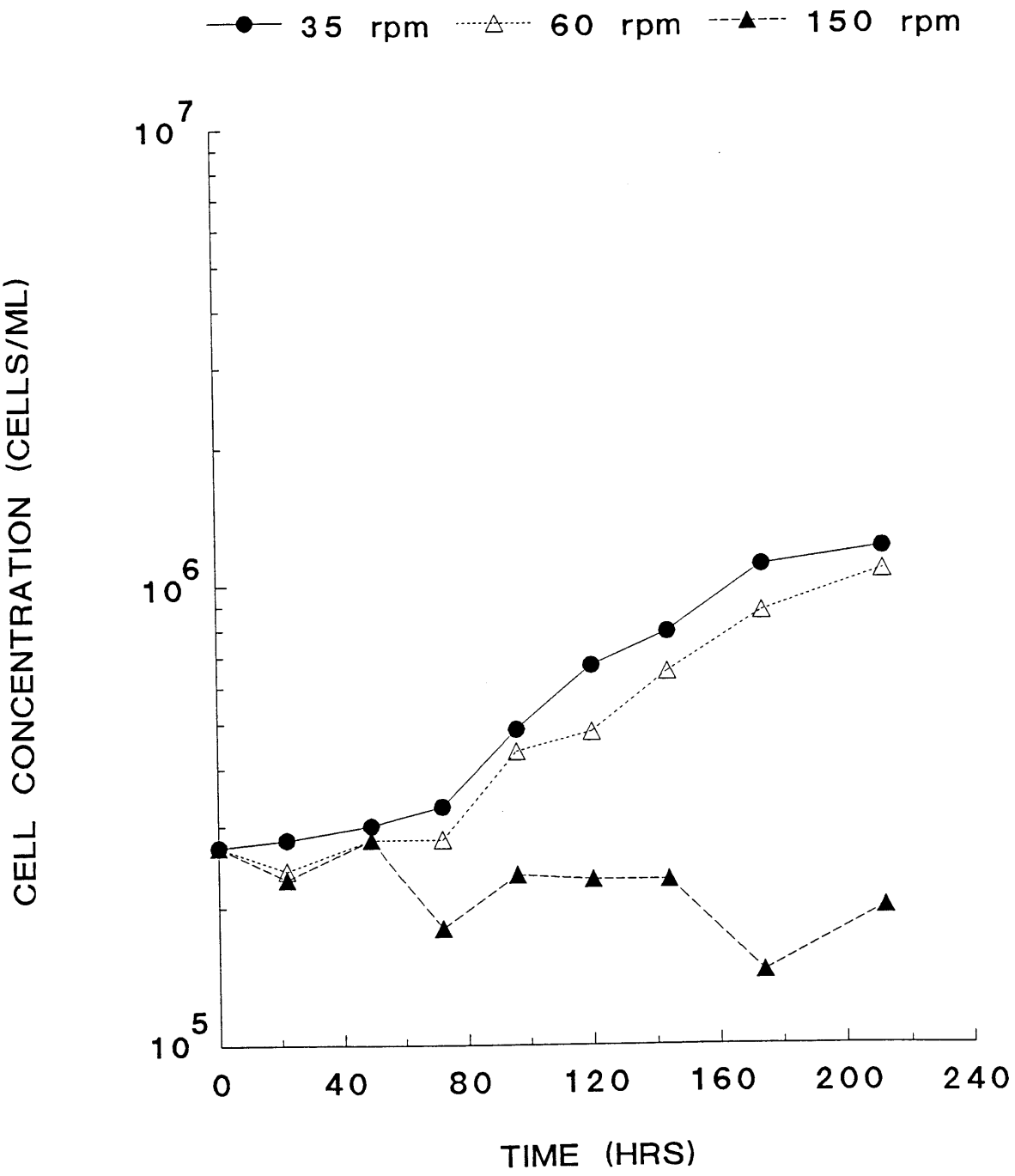

Figure 18. Attached cell concentrations at different stirring speeds

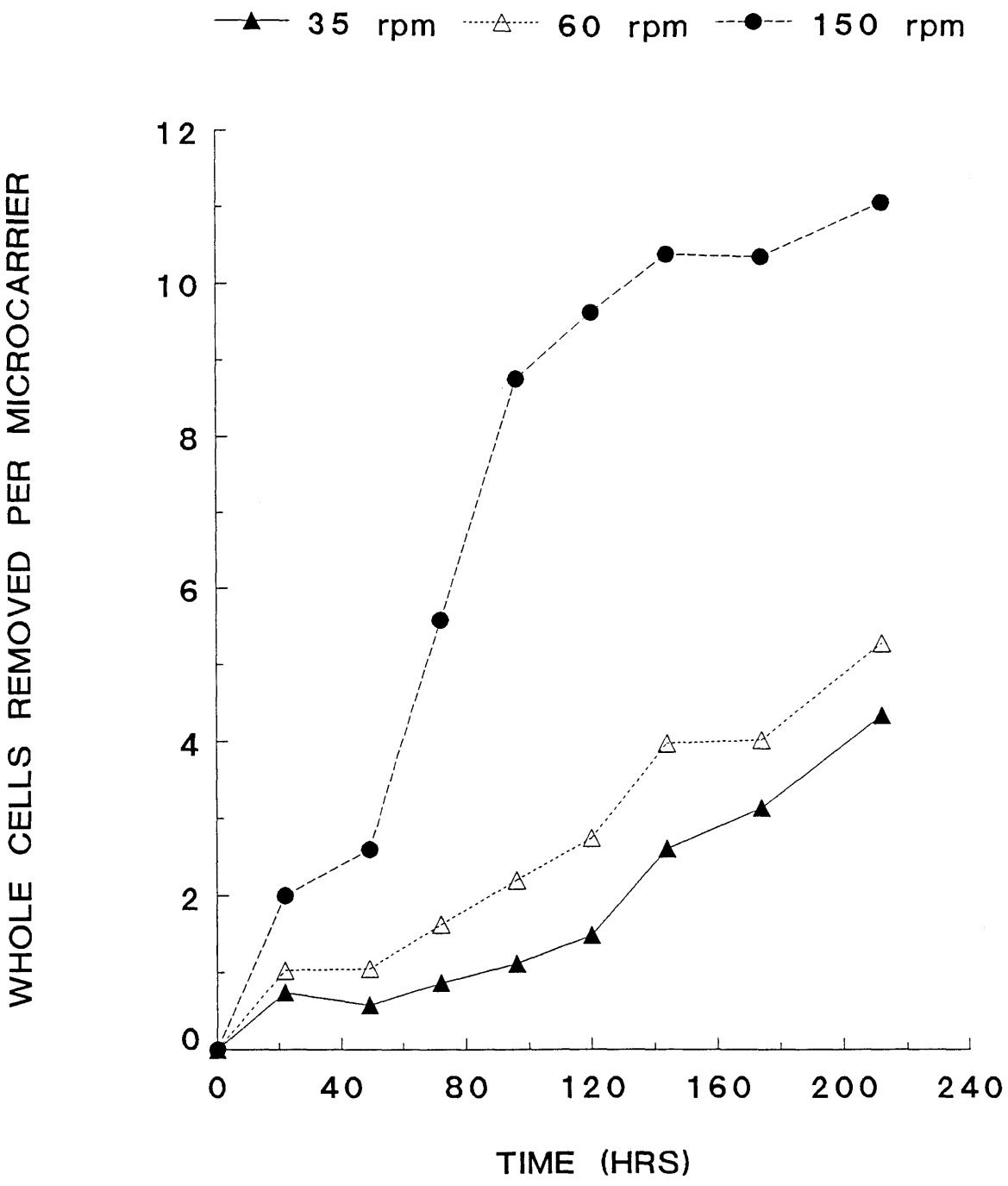

Figure 19. Removal of whole cells from microcarriers

correction would have been minor. Cell fragments were observed in the samples from the cultures at 60 and 150 RPM. However, these fragments could not be accurately counted and were not included in the whole-cell counts.

Figure 19 shows that removal of whole cells from the microcarriers occurred at all stirring speeds, and throughout the duration of all cultures. At 35 RPM, the whole cells removed generally represented less than 5% of the total observable cells (whole cells on microcarriers and in suspension). At 60 RPM, cell removal increased slightly; the whole cells removed generally represented about 9% of the total observable cells. At 150 RPM, cell removal greatly increased; the whole cells removed eventually represented nearly 60% of the total observable cells.

The whole cells in suspension were found to generally lyse and disintegrate over a period between 1-2 days. This lysis reduced the suspension cell counts below the values which would fully account for all of the cells removed. The lysis also resulted in the release of cell fragments into suspension. It was unclear, however, whether the fragments were generated solely through lysis of whole cells in suspension, or whether the fragments were also generated through lysis of attached cells.

Whole animal cells in suspension will generally assume a spherical shape, due to the high surface energy of the cell membrane in aqueous

solutions (Evans, 1983). To maintain a flattened morphology with a high membrane surface area, cells must generally exert mechanical forces with their cytoskeleton. Upon removal from the growth surface, most cells will become spherical. Animal cells exposed to shear, however, can develop mechanical stiffness and may have a non-spherical shape for several hours after removal from the growth surface (Sato et al, 1987). Nonetheless, in the absence of fixing agents, dead animal cells generally do not remain attached and flattened on a growth surface in an agitated environment.

At all stirring speeds, the cells attached to the microcarriers exhibited flattened morphologies and did not uptake trypan blue. Thus, in terms of the ability to exclude trypan blue and remain attached with a flattened morphology, the cells on the microcarriers always appeared to be viable.

In contrast, the cells in suspension always appeared to be nonviable. Generally over 90% took up observable amounts of trypan blue stain. Most of them lysed over a period between 1-2 days. The suspension cells had extensive surface irregularities and roughness. They did not attach and grow upon inoculation into new microcarrier or T-flask cultures. In terms of the ability to reproduce and exclude trypan blue, the cells in suspension were always nonviable. It appears that the cells in suspension were essentially killed upon removal from the microcarriers.

2B. Random Cell Removal Through Normal Forces

The removal of cells from the microcarriers increased with the level of agitation and thus appeared to have been due to the action of hydrodynamic forces. If this removal was selective for mitotic cells, which tend to be more rounded, the specific rates of removal should have increased with mitotic index. To investigate whether cell removal was selective for mitotic cells, the rates of whole cell removal presented in Figure 19 were analyzed on an interval basis.

For the culture at 35 RPM, the agitation was mild. The attached cell concentrations presented in Figure 18 reflect cell growth with insignificant hydrodynamic death. The mitotic index, I_M, during each time interval t_1 to t_2 can thus be determined from the equation presented in Johnson (1961):

$$I_M = \frac{T_M \mu}{\ln 2} = \frac{T_M \ln(C_2/C_1)}{(t_2 - t_1) \ln 2} \qquad \text{(Eq. 31)}$$

where T_M is the duration of mitosis, μ is the specific growth rate in the interval, and C_1 and C_2 are the attached cell concentrations at times t_1 and t_2, respectively. The duration of mitosis can be reasonably estimated as 1.5 hours (Alberts et al, 1983).

In the culture at 35 RPM, there was a small but measurable removal of cells from the microcarriers. For each time interval, the specific

rate of whole cell removal, J_w, can be estimated from the equation:

$$J_w = \frac{W_2 - W_1}{(t_2 - t_1)\ (C_2 + C_1)/2} \qquad \text{(Eq. 32)}$$

where W_1 and W_2 are the suspended whole cell concentrations at times t_1 and t_2, respectively, and C_1 and C_2 are the attached cell concentrations at times t_1 and t_2, respectively.

For the culture at 35 RPM, Figure 20 shows the specific rate of whole cell removal versus the estimated mitotic index. If cell removal was selective for mitotic cells, the specific removal rate should increase linearly with mitotic index. However, the data exhibits random scatter with a linear correlation coefficient of only 0.16. Thus, it appears that cell removal was random and not selective for mitotic cells. The same conclusion can be drawn from a similar analysis for the culture at 60 RPM, although the minor hydrodynamic damage introduces some error in the calculation of the mitotic index from equation 31.

These results are not the first to indicate random cell removal by hydrodynamic forces in microcarrier cultures. When CHO cells are grown on DEAE-dextran microcarriers, cell removal from excessive agitation is apparently random unless the cells are pretreated with colcemid (Ng et al, 1980). These results are surprising if one believes cell removal occurs primarily through shear stresses. In response to a shear field at the growth surface, a rounded mitotic cell will experience a higher distracting torque than a flattened interphase cell. Furthermore, a rounded mitotic cell will probably have fewer attachment sites and a

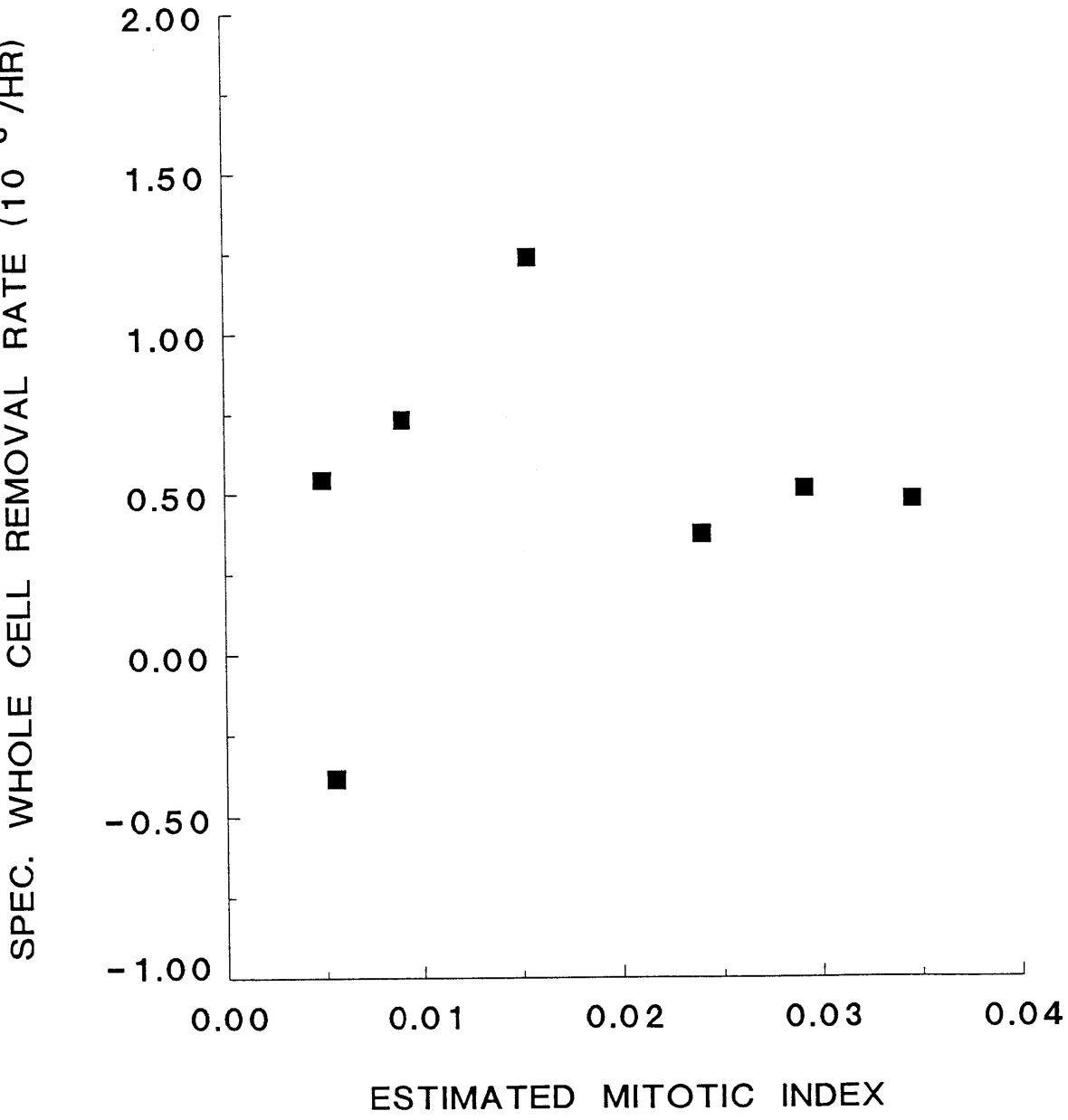

Figure 20. Specific rate of whole cell removal vs. estimated mitotic index

weaker attachment to the growth surface than a flattened interphase cell. If cell removal occurs through the action of shear stresses, rounded cells in mitotis should be more susceptible to removal than flattened cells in interphase.

However, cell removal can occur not only from shear stresses, but also from normal forces. In microcarrier cultures, normal forces can be generated by pressure fluctuations in the turbulent flow fields. In response to a pressure fluctuation near a microrcarrier surface, a cell may be subjected to a distractive normal force. Because the pressure fluctuation will occur on the length scale of a turbulent eddy, which is much larger than a cell, the magnitude of the distractive force will be roughly proportional to cross-sectional area of the cell on the growth surface. If the cell has a constant number of attachment sites per cross-sectional area, the total attachment force will also be proportional to the cross-sectional area. Overall, both the attachment and distractive forces will be proportional to cross-sectional area of the cell. The cross-sectional area, or shape, of the cell will then cancel out as a factor. If cell removal occurs through normal forces, a rounded up cell in mitosis should roughly be no more susceptible to removal than a flattened cell in interphase. For microcarrier cultures, the observed lack of selectivity for removal of mitotic cells may indicate that cell removal occurs primarily through normal forces.

2C. DNA Release Under High Agitation

When FS-4 cultures are exposed to high agitation, there is a net reduction in growth along with random and lethal removal of cells from the microcarriers. The net reductions in growth are due, at least in part, to the cell death and removal from hydrodynamic forces. The question remains, however, whether this was the sole effect of agitation on net cell growth, or whether growth inhibition occurred along with lethal cell removal. To answer this question, one needs a very accurate account of the number of cells killed and removed by hydrodynamic forces, both whole and lysed. This was achieved by monitoring the DNA release into suspension from a high-density microcarrier culture.

To investigate the release of DNA into the culture fluid under high agitation, FS-4 cells were grown on 5 g/l microcarriers in two 500-ml vessels with 7.8 cm impellers. The cultures were operated at 45 RPM to eliminate microcarrier agglomeration. When nearly confluent, the microcarriers were pooled, concentrated to 15 g/l, and transferred to two identical 125-ml vessels. One of these 15 g/l cultures was agitated at 35 RPM while the other was agitated at 150 RPM.

Figure 21 shows the growth of the cells in the cultures with 5 g/l microcarriers. The data show the concentration of cells attached to the microcarriers; it represents typical growth for FS-4 cells under conditions of mild agitation. Figure 21 also shows the subsequent performance of the nearly-confluent cultures with 15 g/l microcarriers. The nearly-confluent culture at 35 RPM showed minor growth with a 25%

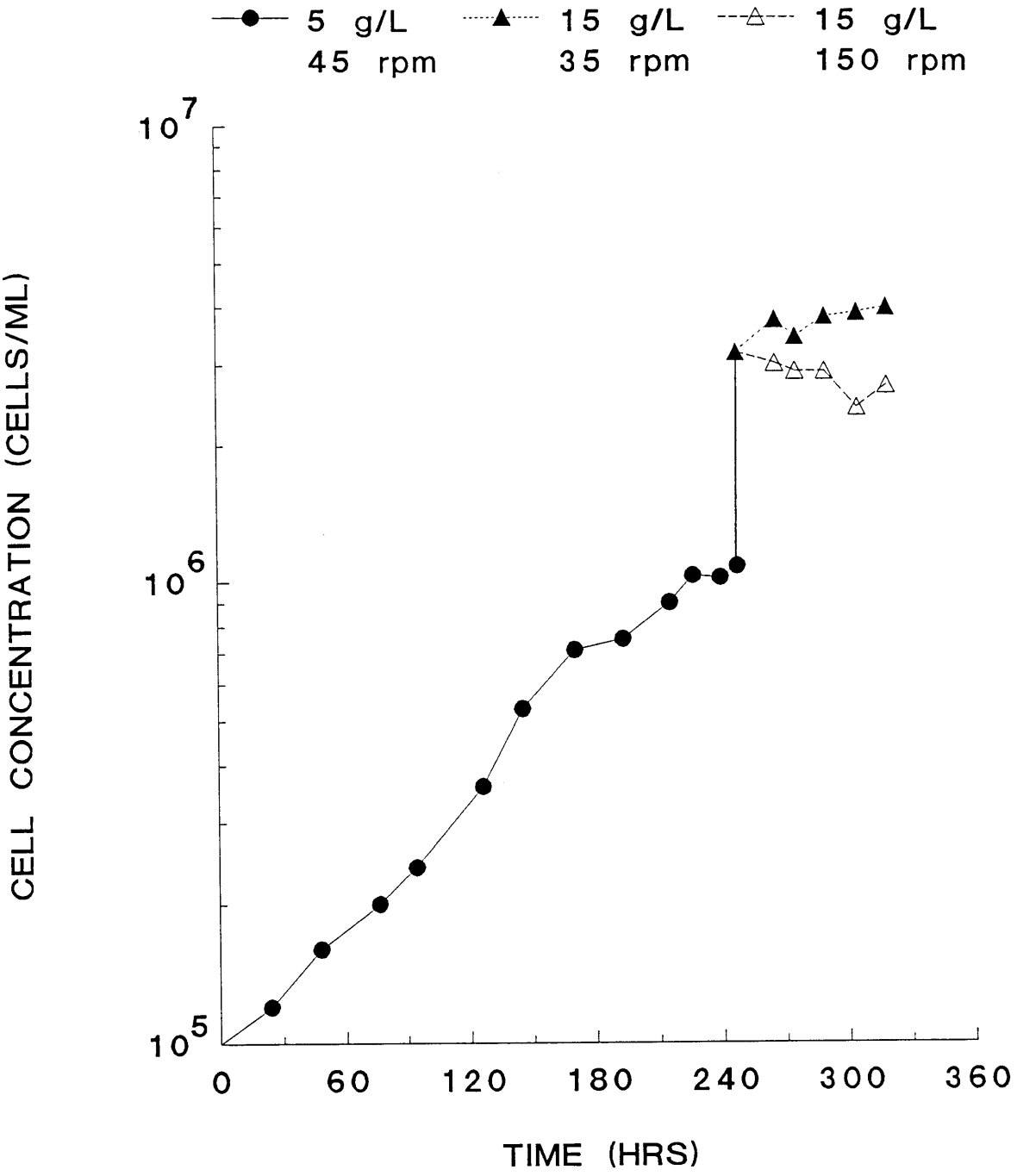

Figure 21. Growth followed by agitation at different speeds after concentration

increase in attached cell concentration. The nearly-confluent culture at 150 RPM exhibited a 15% decrease in attached cell concentration. Cell death and removal clearly occurred in the nearly-confluent culture at 150 RPM.

Figure 22 shows the cumulative release of DNA into suspension from the 15 g/l culture agitated at 150 RPM. The data are plotted in terms of FS-4 diploid equivalents and were calculated relative to the control culture at 35 RPM. The error bars represent the combined uncertainty in both the DNA measurements and in the correction for the control culture, as more thoroughly described in Appendix 1. The data include the DNA from both the lysed and whole cells in suspension. In the culture at 150 RPM, there was extensive release of DNA into the culture fluid. This provides further evidence of significant cell death and removal.

2D. Growth and Death Under High Agitation

In an overagitated microcarrier culture, cell growth must be occurring if the total number of cells, both attached and removed, is increasing. If cell death and removal are occurring at a specific death rate q, the DNA concentration, D, in the culture fluid should increase according to the relation

$$\frac{dD}{dt} = S_r \, q \, C \qquad \text{(Eq. 33)}$$

where C is the cell concentration and S_r is the average DNA content of the cells removed. The DNA concentration, D, includes the DNA for both

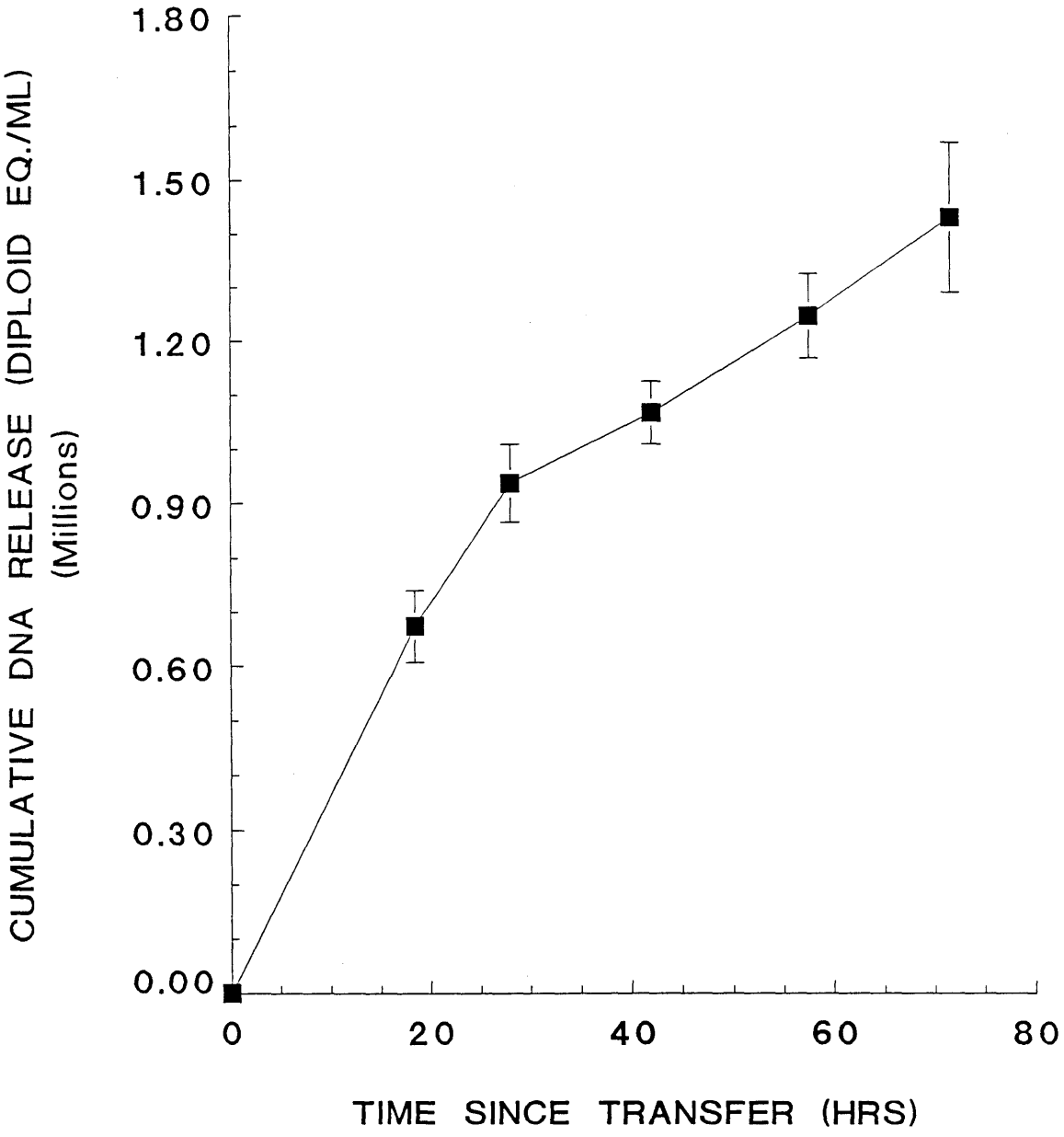

Figure 22. Cumulative release of DNA into suspension for 15 g/L culture at 150 RPM

the lysed and whole cells in suspension, as measured by our assay. If there is random cell removal, such as for FS-4 cells on microcarriers, the average DNA content of the cells removed, S_r, is equal to the average DNA content of the cell population, S_a. This average DNA content is given by equation 26 as presented in the Materials and Methods section.

In FS-4 cultures with high agitation, there is extensive cell death and removal. The specific growth rate will then be strongly dependent on whether secondary growth can occur. Secondary growth, as referred to in this thesis, represents cell growth over areas from which other cells were previously removed through hydrodynamic forces. In a manner analogous to the stimulation of growth through direct mechanical removal of cells, as described in Alberts et al (1983), cell growth in a contact-inhibited culture might be stimulated if areas are opened up through hydrodynamic removal. If secondary growth can occur, a culture at high agitation may actually grow faster than a culture at low agitation which is more confluent and contact-inhibited.

To investigate the nature of cell growth in the 15 g/l cultures at 35 and 150 RPM, the DNA release data were compared to the predictions of three mechanistic models. For the first model, it was assumed that the cells in both cultures were growing at the same rate at any given time since inoculation. Cell growth was neither inhibited by excessive agitation, nor stimulated by cell removal. According to the first model, which represents growth and death with no secondary growth, the

specific growth rate, μ, in each time interval was calculated from the equation:

$$\mu = \frac{\ln(C_{2,35}/C_{1,35})}{(t_2 - t_1)} \qquad \text{(Eq. 34)}$$

where $C_{1,35}$ and $C_{2,35}$ are the attached cell concentrations at 35 RPM for times t_1 and t_2, respectively. The apparent specific death rate, q, at 150 RPM was then calculated from the equation:

$$q = \mu - \frac{\ln(C_{2,150}/C_{1,150})}{(t_2 - t_1)} \qquad \text{(Eq. 35)}$$

where μ is given by equation 34, and $C_{1,150}$ and $C_{2,150}$ are the attached cell concentrations for the 150 RPM culture at times t_1 and t_2, respectively. Assuming there was only cell death and removal with no growth inhibition or secondary growth at 150 RPM, one can calculate the expected change in DNA concentration from the equations:

$$D_2 - D_1 = \frac{S_a\, q\, (C_{2,150} - C_{1,150})}{\mu - q} \qquad \text{for } C_1 \neq C_2 \qquad \text{(Eq. 36)}$$

$$D_2 - D_1 = S_a\, q\, C_{1,150}\, (t_2 - t_1) \qquad \text{for } C_1 = C_2 \qquad \text{(Eq. 37)}$$

where μ and q are given by equations 34 and 35, respectively, S_a is the average DNA content per cell and is given by equation 26, and D_1 and D_2 represent the DNA for both the lysed and whole cells in suspension at 150 RPM, as measured by our assay, for times t_1 and t_2, respectively.

For the second model, it was assumed that secondary growth occurred, and that growth in the overagitated cultures was fully corrected for the

reduced contact inhibition due to cell removal. For areas where cells had been removed, secondary growth was assumed to occur at the same rate as the normal initial growth, with all growth regulated through contact inhibition. The effect of contact inhibition on growth was incorporated with the following empirical equations which fit the data presented in Hu et al (1985) for FS-4 cells:

$$\mu = \mu_{max} (100 - Z)/60 \qquad \text{for } Z > 40 \qquad \text{(Eq. 38)}$$

$$\mu = \mu_{max} \qquad \text{for } Z \leqslant 40 \qquad \text{(Eq. 39)}$$

where Z is the percent confluence. For the culture with 15 g/l microcarriers at 35 RPM, the best fit to equation 38 is given with μ_{max} 0.024 hr^{-1} and full confluence at 4.0 x 10^6 cells/ml.

For the second model, which represents growth and death with secondary growth, the specific growth rate for the culture with high agitation was calculated in each time interval from equation 38. The average percent confluence was used along with the estimated μ_{max} of 0.024 hr^{-1} and full confluence at 4 x 10^6 cells/ml. The specific death rate, and expected change in DNA concentration, were calculated from equations 35-37.

For the third model, it was assumed the reduced net growth at high agitation arose solely through growth inhibition and not cell death and removal. Although this model is clearly not realistic in light of the data presented in this thesis, the predictions of the model are included for the sake of comparison and completeness. For the third model, the

DNA in the culture fluid should not increase at 150 RPM relative to the control at 35 RPM.

Figure 23 shows the predictions of the three mechanistic models along with the measured cumulative release of DNA. The predictions of the two growth and death models scatter because the data was analyzed on an interval basis and because the predictions rely on nuclei counts which are somewhat imprecise (±10%). The measured DNA release clearly does not match the expected release for growth inhibition without cell death and removal, or for growth and death with secondary growth. The measured release data does, however, match the expected release for growth and death without secondary growth.

To the degree that cell removal was random, as indicated for FS-4 cells on microcarriers, the data in Figure 23 demonstrates that the cells in the 150 RPM culture were essentially growing at the same rate as the cells in the 35 RPM culture. If the growth rate at 150 RPM was different than the growth rate at 35 RPM, the amount of DNA release would not have matched the expectation for growth and death without secondary growth.

Thus, the data strongly indicate that there is a situation of growth and death with no secondary growth. The reduction in net growth at 150 RPM appears to have been due entirely to cell death and removal, and not growth inhibition. Even though there was extensive cell removal and death, growth appears to have been unaffected by hydrodynamic forces.

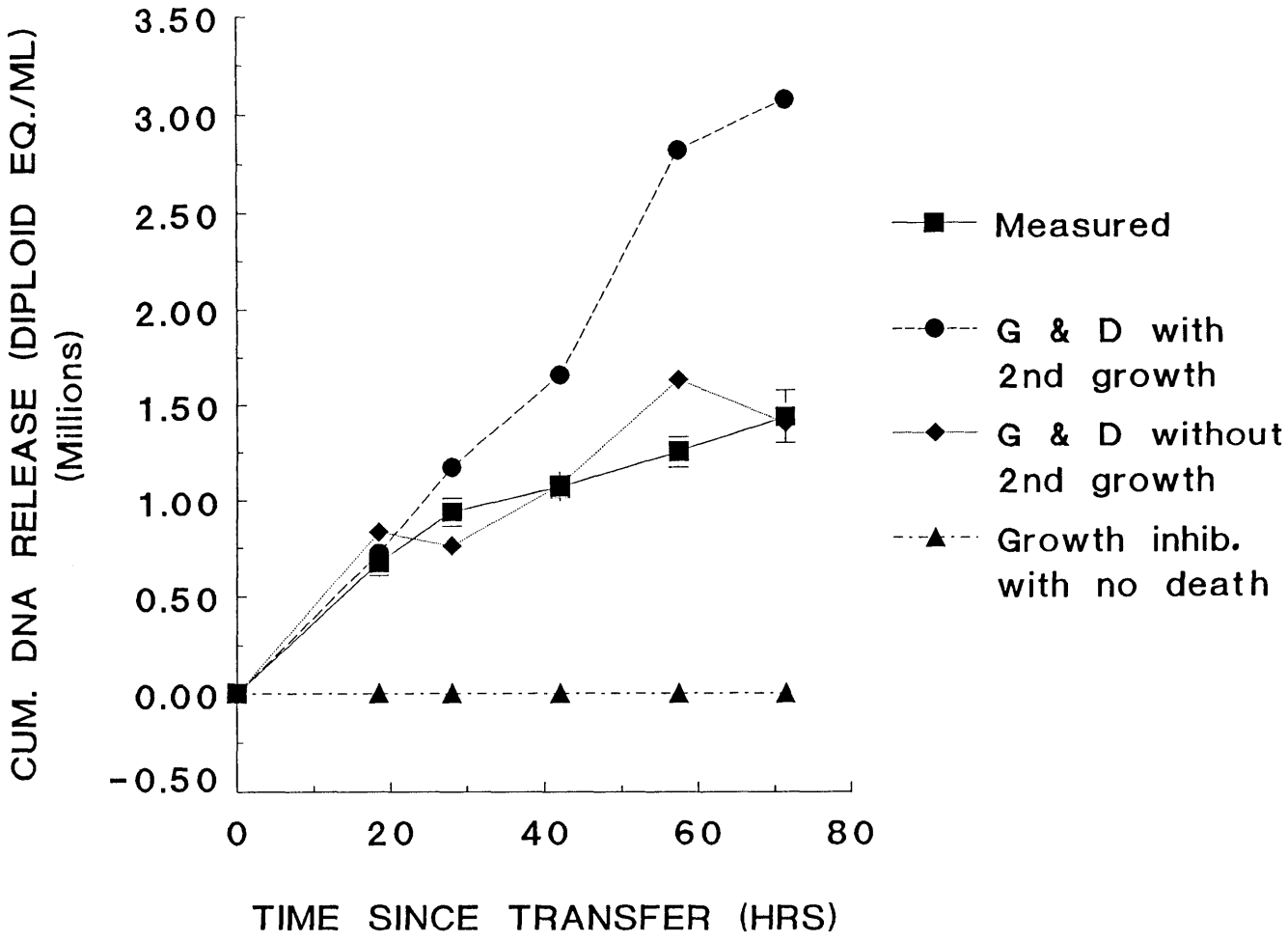

Figure 23. Measured DNA release vs. release expected under three different scenarios

At both 35 and 150 RPM, the attached cells exhibited the normal ability to reproduce, and thus appear to have been truly viable. These findings are the first published results which document a growth and death response of cells under high agitation. A growth and death response was originally proposed in 1984 as published in Croughan et al (1987).

2E. Hydrodynamic Regulation of Cell Growth

For FS-4 cultures exposed to mild agitation, growth is unaffected by hydrodynamic forces. For endothelial cells exposed to mild fluid flow, growth is unaffected by hydrodynamic shear forces (Dewey et al, 1981; Sprague et al, 1987). For FS-4 cells under high agitation, growth appears to also be unaffected by hydrodynamic forces.

The apparent lack of growth regulation from hydrodynamic forces is not surprising. The decision to replicate depends on the cell's genetically-programmed response to environmental factors. For normal cells, such as FS-4, this genetic programming has come through years of evolution and adaptation. It primarily depends upon the cell's role in the original animal donor. If a particular cell type was not normally exposed to fluid flow in vivo, it will have no genetically-programmed response to hydrodynamic forces. Unless fluid flow can influence the normal growth regulation processes, the decision to replicate should not depend on the hydrodynamic environment. For FS-4 cells, and probably for most animal cells, the decision to replicate does not appear to depend on the hydrodynamic environment, and fluid flow does not appear to influence normal growth regulation.

2F. Lack of Secondary Growth After Cell Removal

The data in Figure 23 indicates that there is no secondary growth in FS-4 cultures exposed to high agitation. To further investigate this observation, FS-4 cultures were grown at different stirring speeds from the point of inoculation. The cultures were held at their respective stirring speeds as the culture under mild agitation reached confluence and stopped growing. If there was secondary growth in the overagitated cultures, a clear and very strong trend should have been observed. The observed growth rate at high agitation should have increased relative the observed growth rate at low agitation as the culture at low agitation became confluent and stopped growing. The difference in observed growth rates, or the observed specific death rate, should not have been constant throughout the duration of all cultures, but should been greatly reduced as the culture under low agitation became confluent.

Figure 24 shows the results of experiment. Attached cell concentrations are shown throughout the duration of the experiment. The cultures contained 3 g/l microcarriers and were grown in 100-ml spinner vessels with 3.8 cm impellers, as described in Croughan et al, 1987. The straight lines through the data represent the best fit to a model which assumes that all cultures were growing at the same rate at any given time since inoculation, and that the specific death rates were constant in each culture throughout all time periods. The data follows these assumptions, which represent growth and death with no secondary growth. Furthermore, the data clearly indicates that the specific death

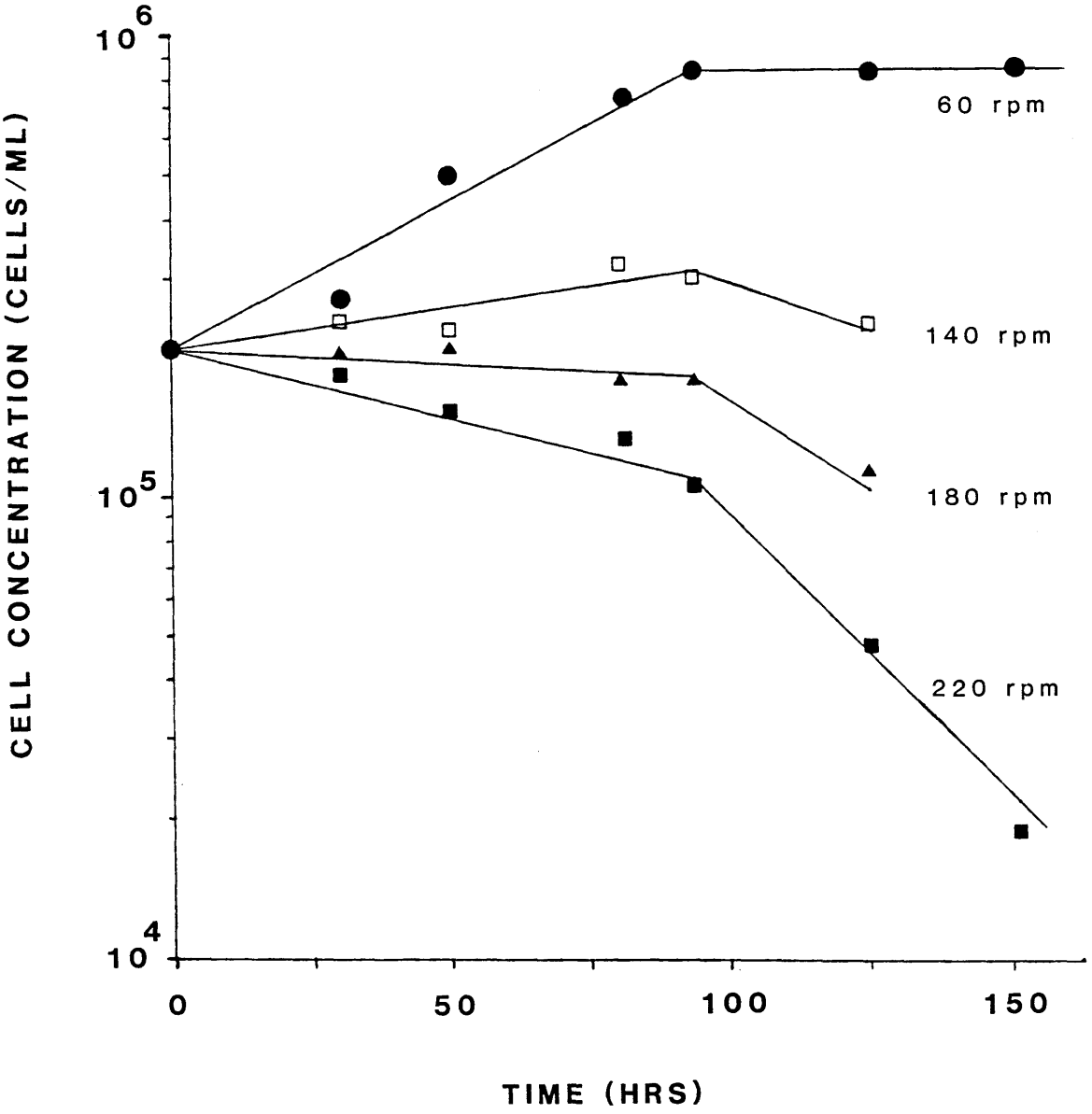

Figure 24. Attached cell concentrations for cultures grown at different stirring speeds

2G. Hydrodynamic Effects on Glucose Consumption

Growth of FS-4 cells appears to be neither inhibited nor enhanced by hydrodynamic forces. The metabolic events required for growth are therefore not significantly altered by agitation. Nonetheless, all metabolic events which are not growth associated could be strongly influenced by agitation.

For the cultures with 15 g/l microcarriers shown in Figure 21, the glucose concentration profiles are given in Figure 25. Samples were taken just before and just after each medium exchange. Analyzing the data in each time interval t_1 to t_2, one can calculate the specific glucose uptake rate, R_g, from the equation

$$R_g = \frac{(G_2 - G_1)\ \ln(C_2/C_1)}{(t_2 - t_1)(C_2 - C_1)} \qquad \text{(Eq. 40)}$$

where G_1 and G_2 represent the glucose concentrations at times t_1 and t_2, respectively, and C_1 and C_2 represent the attached, or viable, cell concentration at times t_1 and t_2, respectively.

For each time interval, Table 2 gives the specific glucose uptake rates. It also gives the specific growth rates for the culture at 35 RPM. There is no correlation between specific growth rate and specific glucose uptake rate (correlation coefficient = 0.18). In all of our experiments with FS-4 cells, no correlation has ever been found between specific growth rate and specific glucose uptake rate. It appears that glucose uptake is not growth associated for FS-4 cells.

rates did not significantly decrease when the culture at low agitation became confluent. This is further indication that there is no secondary growth in FS-4 microcarrier cultures exposed to high agitation.

The apparent lack of secondary growth may be due to the nature of cell removal by hydrodynamic forces. For FS-4 cells, which are strongly adherent, hydrodynamic forces may not generally remove complete cells. Cell remnants may remain which might leave the area unsuitable for secondary growth. The previous attachment and removal of a cell from a given position may preclude future growth over that position. There is a clear analogy between lack of secondary growth and lack of growth through contact inhibition, wherein cells can grow over areas already occupied by other cells.

If cells can not grow over areas previously occupied by other cells, growth would not be stimulated as areas were opened up by hydrodynamic cell removal. The cultures with signficant cell removal would exhibit growth regulation as if they contained a greater number of attached cells, as if they were more contact inhibited. This effect may account, in part, for the similarity in growth rates between cultures at high agitation and more confluent cultures at low agitation. The similarity may also arise through an unidentified mechanism of growth regulation. Cell growth is controlled not only by contact inhibition, but also by many other poorly-understood mechanisms (Darnell et al, 1986).

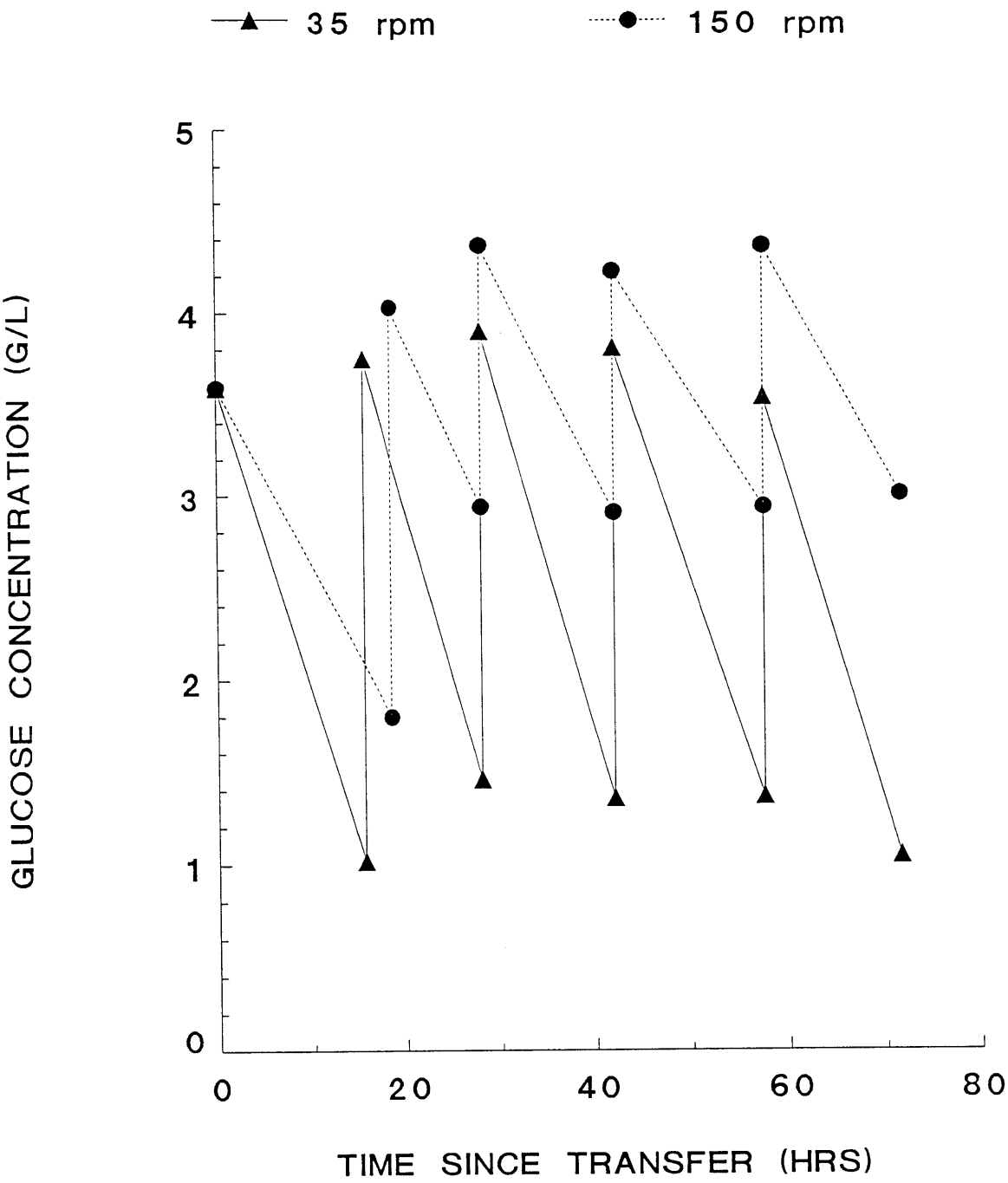

Figure 25. Glucose concentration profiles for the 15 g/L cultures

TABLE 2. GLUCOSE UPTAKE BY FS-4 CELLS IN MICROCARRIER CULTURES

	Specific glucose uptake rate (10^{-12} gm/cell-hr)		Specific growth rate (1/hr)
Interval	35 RPM	150 RPM	35 RPM
1	46	33	0.0106
2	48	38	-0.0069
3	52	38	0.0073
4	40	30	0.0013
5	44	36	0.0018
Avg.	46	35	0.0028

The data in Table 2 show that glucose consumption is dependent on the hydrodynamic environment. For the culture at 35 RPM, the average uptake rate was 46 x 10^{-12} gm/cell-hr. At 150 RPM, the average uptake rate was 35 x 10^{-12} gm/cell-hr, or only 76% of the value at 35 RPM. Within a 99% confidence limit, the difference in average uptake rates was statistically significant. If one accounted for glucose uptake by the whole or lysed cells in suspension, the difference in average rates would be even greater. It appears that high agitation reduces the glucose uptake rate of FS-4 cells.

For FS-4 cells, glucose uptake is not growth associated and is significantly reduced by high levels of agitation. For hybridoma cells, Dodge and Hu (1986) found that net cell growth was slightly reduced, but volumetric glucose consumption was unchanged, by high levels of agitation. This result may have been due, in part, to conversion of glucose to lactic acid by dead or lysed cells. It may also indicate that the specific glucose uptake rate of the hybridoma cells was slightly increased by agitation.

In this thesis, the effects of hydrodynamic forces on cell growth have been extensively investigated. As discussed in the Literature Review section, there are limited but interesting results regarding hydrodynamic effects on cell metabolism. Before any reactor design can be fully optimized, hydrodynamic effects on both cell growth and metabolism will have to be fully understood.

CHAPTER 3. HYDRODYNAMIC PHENOMENA IN γ-CHO CULTURES

3A. Growth, Reversible Cell Removal, and Secondary Growth

Nearly all of the results for this thesis were derived from experiments with FS-4 cells. However, for the purposes of comparison, a few experiments were performed with γ-CHO cells.

Figure 26 presents limited results on the effects of agitation in γ-CHO microcarrier cultures. Both attached and suspended cell concentrations are shown for two cultures grown with 1.0 g/l microcarriers and 5% dialyzed FCS in the 125-ml Corning vessels. One culture was agitated at 35 RPM; the other at 100 RPM.

In contrast with the FS-4 cells, the γ-CHO cells grew to more than a monolayer. However, cell growth still appeared to be regulated by surface coverage. Growth plateaued after the cells were 2-3 layers thick on the microcarriers.

In parallel with FS-4 cells on microcarriers, the γ-CHO cells on the microcarriers excluded trypan blue and appeared healthy at both levels of agitation. However, in somewhat of a contrast with the results from the FS-4 cultures, the γ-CHO culture at 100 RPM exhibited essentially identical attached cell concentrations as the γ-CHO culture at 35 RPM. For an FS-4 culture, the same increase in agitation would bring a 50% reduction in average observed growth rate. Microcarrier cultures of γ-CHO cells are less sensitive to agitation than microcarrier cultures of

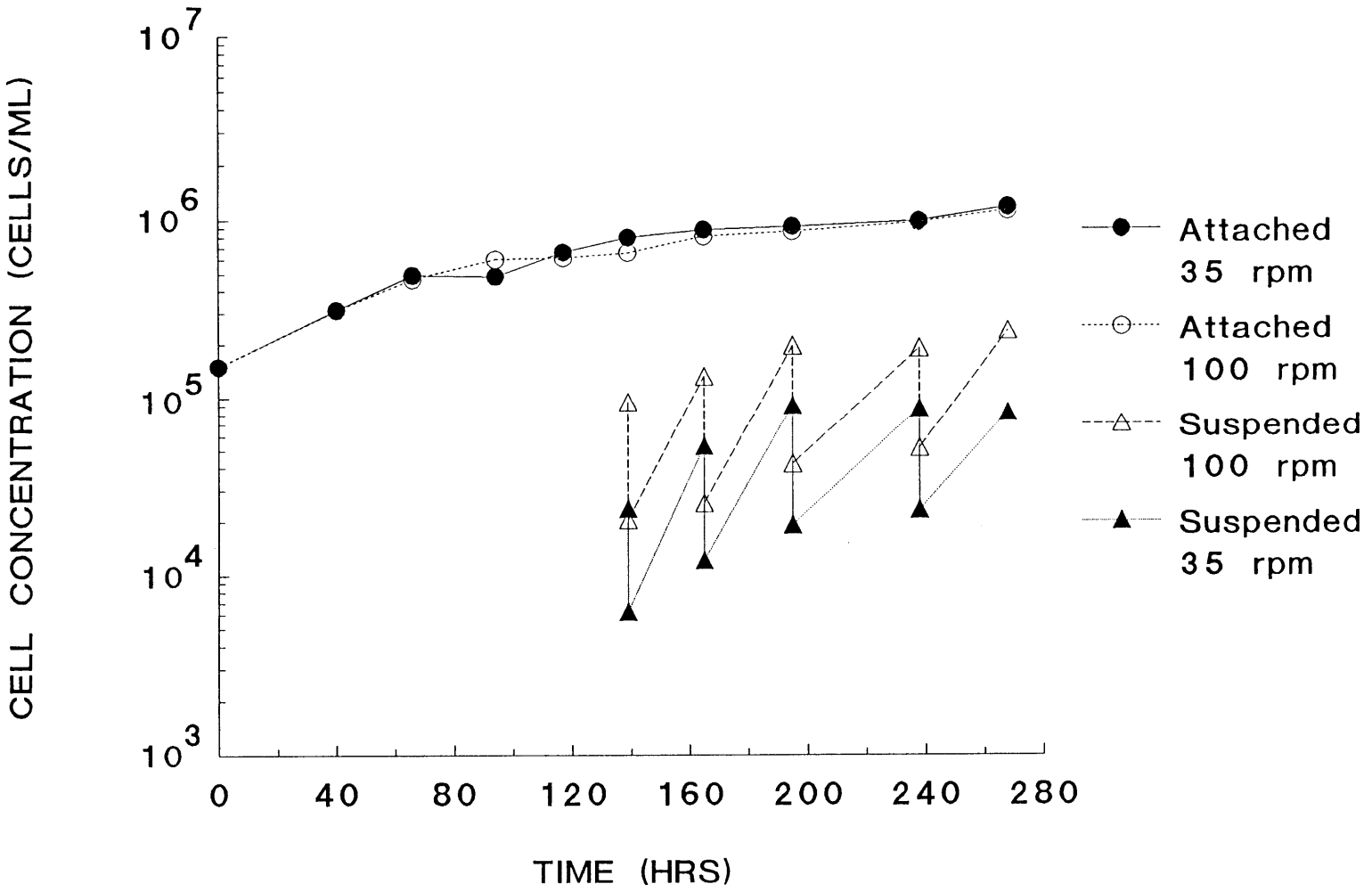

Figure 26. Suspended and attached cell concentrations for γ-CHO cultures

FS-4 cells.

In Figure 26, a vertical drop in suspended cell concentration occurred each time spent medium was exchanged with fresh medium. Subsequent to each medium exchange, the suspended cell concentrations exhibited very rapid recoveries to their pre-exchange values. The specific rates associated with these recoveries were on the order of 0.04 hr^{-1} or greater. These rates are much higher than 0.004 hr^{-1}, the maximum specific growth rate of γ-CHO cells in suspension with comparable medium (Perry, 1987). Thus, the rapid increases in suspended cell concentrations were not due to cell growth, but were rather due to cell removal from the microcarriers.

Prior to each medium exchange, the suspended cell concentrations were essentially independent of the time since the last medium exchange. The suspended cell concentrations were therefore not steadily increasing in each feeding interval, as improperly indicated by the straight lines between the data points in Figure 26. Instead, the suspended cell concentrations were apparently re-established and held relatively constant soon after each medium exchange, as if a sort of equilibrium existed between the cells on the microcarriers and those in suspension.

In Figure 26, the suspended cell concentrations represent the whole cells in suspension, both viable and dead. The γ-CHO culture at the higher level of agitation (100 RPM) exhibited higher suspended cell concentrations than the culture at the lower level of agitation (35

RPM). Thus, for both FS-4 and γ-CHO cells, removal of cell from the microcarriers increased with the level of agitation, and thus appeared to come about, at least in part, through hydrodynamic forces.

The culture at 100 RPM exhibited much more extensive cell removal and yet had essentially the same attached cell concentrations as the culture at 35 RPM. Even though significant cell removal occurred after each medium exchange, the attached cell concentrations recovered to their pre-exchange values or greater by the next medium exchange. This indicates that the γ-CHO cells exhibited secondary growth over areas where cells had been previously removed through hydrodynamic forces.

The γ-CHO cells in suspension appeared much different than FS-4 cells in suspension. In the γ-CHO cultures, 70-90% of the suspended cells appeared healthy and excluded trypan blue. In the FS-4 cultures, none of the suspended cells appeared healthy and less than 10% excluded trypan blue.

To truly measure viability, however, one must determine the ability of the cells to reproduce. For the FS-4 cultures, the cells in suspension did not viably attach and multiply on fresh growth surfaces. To investigate the reproductive capability of γ-CHO cells in suspension, a new microcarrier culture was inoculated from the suspended cells in the γ-CHO culture at 100 RPM. The cells were removed during the medium exchange at 237 hours, centrifuged for 5 minutes at 150 x g, resuspended in fresh medium, and then used to inoculate a new culture with 1.0 g/l

microcarriers at 35 RPM in a 125-ml vessel. In terms of trypan blue exclusion, the cells had a viability of 80%.

The concentration of suspended cells which excluded trypan blue was used to determine the trypan blue viable, or "TPB viable", inoculum concentration. Figure 27 shows the attached cell concentrations and the "TPB viable" inoculum concentration. Given the normal lag phase of microcarrier cultures, it appears that most, if not all, of the suspended cells which excluded trypan blue were actually viable. Within 29 hours, essentially all of "TPB viable" cells attached to the microcarriers and started to multiply. The culture subsequently grew at virtually the same rate as the cultures inoculated from roller bottles shown in Figure 26. Thus, in striking contrast to FS-4 cells, many γ-CHO cells in suspension are viable.

3B. Hydrodynamic Resistance through Secondary Growth

In FS-4 microcarrier cultures, cell removal from excessive agitation is irreversible and lethal. Secondary growth does not occur over areas where removal has occured. The cultures under high agitation exhibit growth regulation as if they were just as contact inhibited as more confluent cultures under low agitation. An FS-4 culture exposed to high agitation will permanently and irreversibly deviate from a control culture with low agitition, as shown by Figure 24 in Chapter 2.

In γ-CHO cultures, cell removal from excessive agitation is frequently reversible and not lethal. Secondary growth will occur over

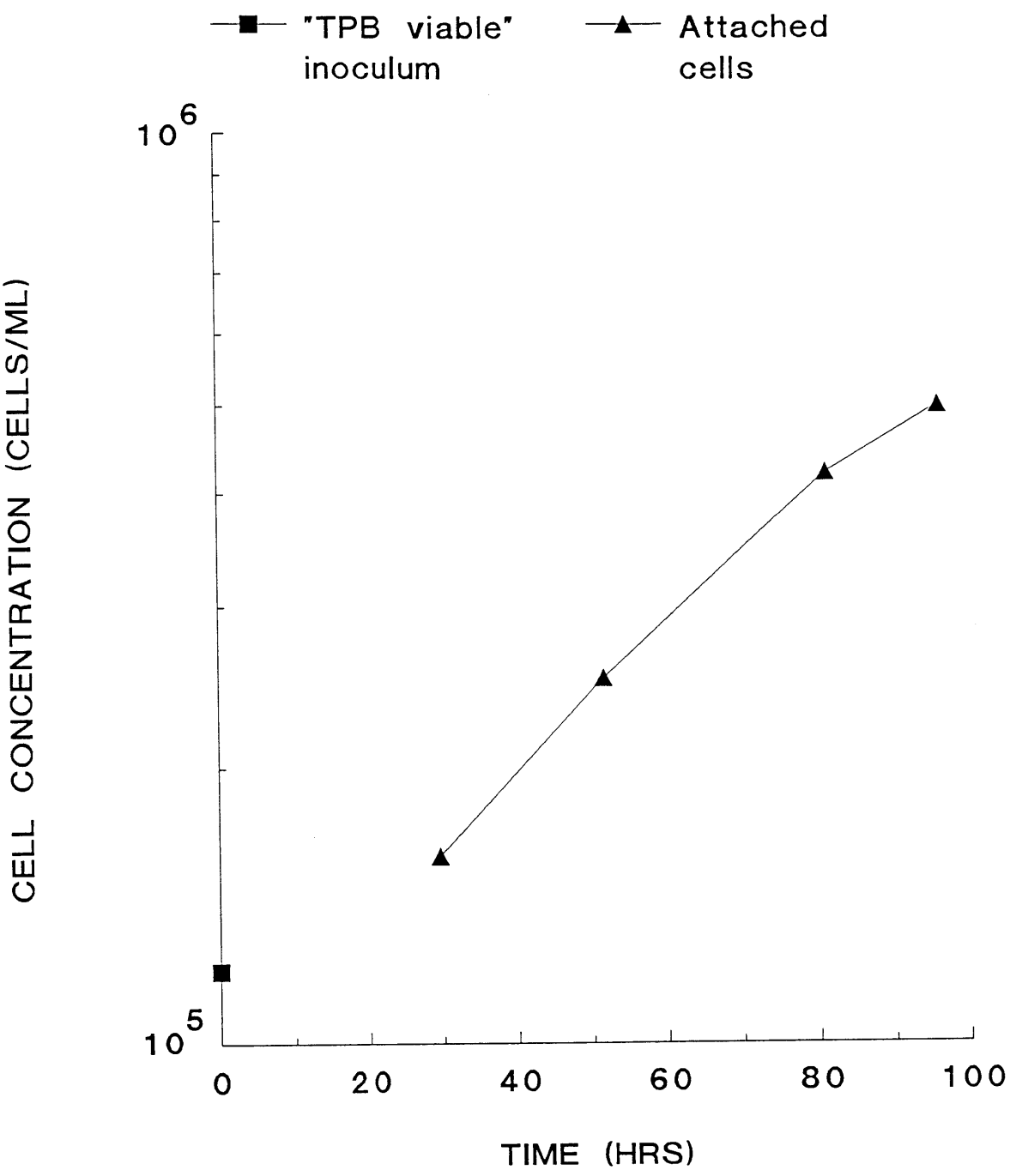

Figure 27. Attachment and growth of γ-CHO cells taken from suspension

areas where removal has occurred. Although the cells grow to more than a monolayer, growth still appears to be regulated by maximum surface coverage. Thus, cell growth should be stimulated if areas are opened up through hydrodynamic cell removal. When cultures are at or near the maximum surface coverage, the cultures with a high degree of removal should exhibit higher total growth rates than cultures with a low degree of removal.

Figure 28 shows the viable cells produced per microcarrier over the time course of the γ-CHO cultures at 35 and 100 RPM. The cells produced per microcarrier represents the cumulative increase in the number of cells subsequent to inoculation. Data are presented for both attached and total viable cells. The number of total viable cells was calculated as the sum of the attached and viable suspended cells, including those removed through medium exchange. As the suspension cell concentrations prior to 117 hours were very low and were not measured, they were not included in the calculations.

The number of attached cells produced per microcarrier was nearly identical at 35 and 100 RPM. However, the total number of viable cells produced per microcarrier was 30% higher at 100 RPM. Total cell growth was clearly higher at 100 RPM.

Cell removal was also higher at 100 RPM. As discussed, the cells in suspension did not primarily arise through growth in suspension, but rather through cell removal from the microcarriers. At 100 RPM, the

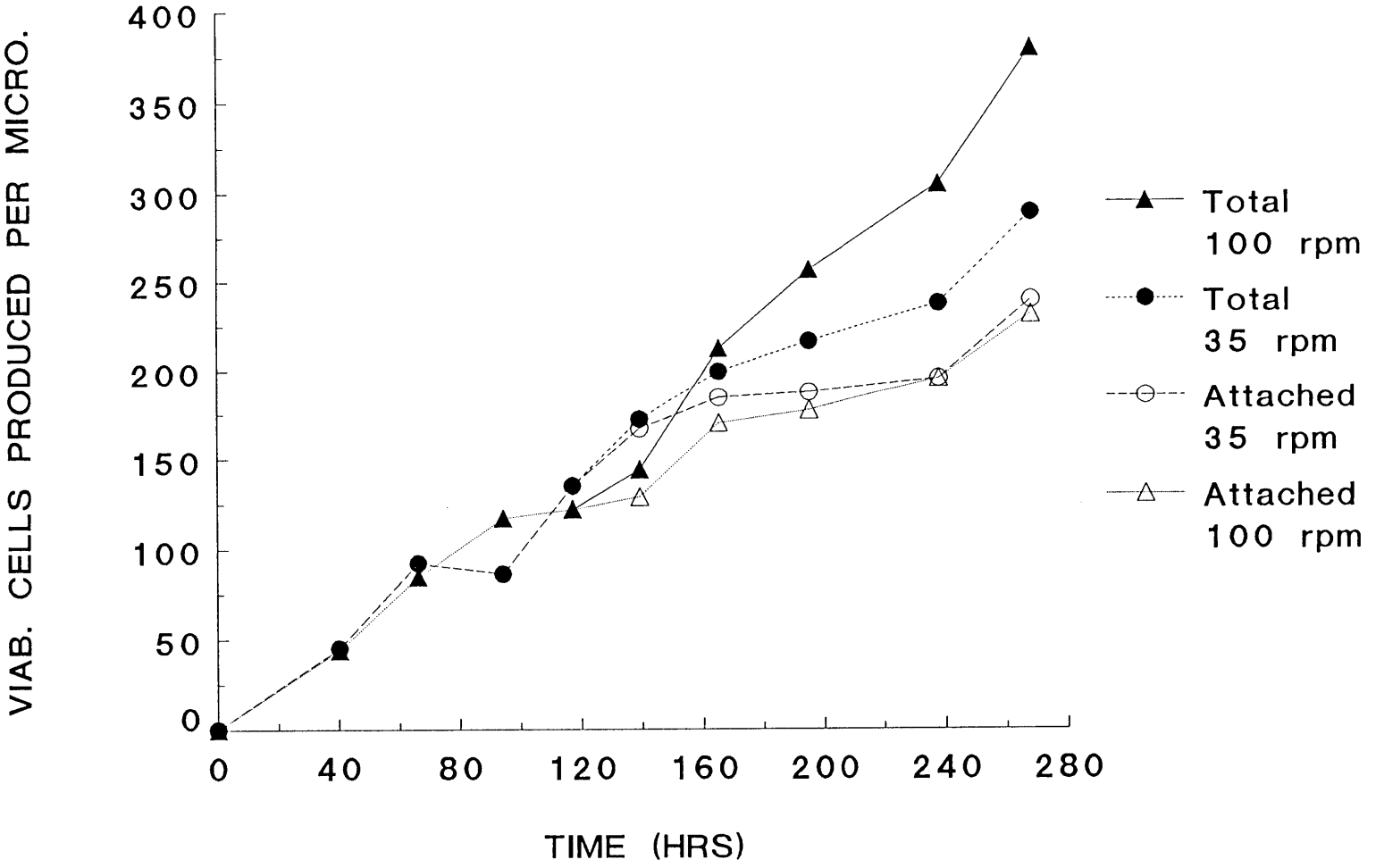

Figure 28. Viable cells produced per microcarrier for γ-CHO cultures

number of viable suspension cells produced per microcarrier, which roughly represents the number of viable cells removed per microcarrier, was 3-fold higher than at 35 RPM.

Thus, as one might expect with secondary growth, increased cell removal went hand-in-hand with increased total growth. Growth was stimulated as areas were left void through hydrodynamic removal. Even though cell removal was much more extensive at 100 RPM, the culture was able to maintain comparable attached cell concentrations to the culture at 35 RPM. Secondary growth was fast enough to overcome any hydrodynamic damage. Secondary growth can clearly lead to reduced hydrodynamic sensitivity.

It is likely that secondary growth accounts for the difference in hydrodynamic sensitivity between FS-4 and γ-CHO microcarrier cultures. It is also likely that secondary growth can occur in γ-CHO cultures because the cells are frequently removed whole and viable. Such reversible removal may leave few remnants to hinder future secondary growth. Such reversible removal may come about because γ-CHO cells are aneuploid and do not exhibit the same attachment properties as diploid cells, such as FS-4 cells. Future research should be performed to more thoroughly elucidate the nature of cell removal and secondary growth.

3C. Selection of Model Cell Line

The viability of γ-CHO cells in suspension greatly complicates the study of hydrodynamic phenomena in these cultures. Because the cells

can reattach after they have been removed from the microcarriers, the rate of removal is not easily measured and does not simply correlate with the rate of death. A form of equilibrium exists between the cells in suspension and those on the microcarriers. The forward rate of removal and the reverse rate of reattachment must be measured simultaneously.

In an FS-4 culture, all of the viable cells are on the microcarriers and all of the dead cells are in suspension. The rate of hydrodynamic removal correlates directly with the rate of death. Hydrodynamic cell removal is not reversible; there is no equilbrium. The forward rate of death and removal can be measured and modelled directly with no required correction for the reverse rate of reattachment. For this reason, FS-4 cultures were chosen as the simpler model system, and nearly all experiments were performed with FS-4 cells. Future work will hopefully extend the analysis based on irreversible removal, suitable for FS-4 cells, to an analysis based on reversible removal, suitable for γ-CHO cells.

CHAPTER 4. MECHANISMS OF HYDRODYNAMIC DEATH IN DILUTE CULTURES

4A. First, Second, and Higher Order Mechanisms of Hydrodynamic Death

Cell death and removal have been identified as the primary response of FS-4 cells to excessive agitation. It is not clear, however, what type of hydrodynamic forces cause this death and removal. For microcarrier cultures with high agitation, cell death may arise through turbulent eddies, time-average flow fields, collisions between microcarriers, or collisions between microcarriers and the solid components of the vessel. From the data currently available, it appears that no significant damage arises through collisions between microcarriers and the solid components of the vessel (Cherry and Papoutsakis, 1986b). Because microcarriers are very small and almost neutrally buoyant, they should not rapidly penetrate the boundary layers surrounding the solid vessel components.

In general, the mechanisms of hydrodynamic death can be grouped into first, second, and higher order mechanisms. The first order mechanisms represent the interaction of a single microcarrier with the surrounding flow field. The second mechanisms represent the simultaneous interaction of two microcarriers with the surrounding flow field. The higher order mechanisms represent the simulateneous interaction of multiple microcarriers with the surrounding flow field.

The first order mechanisms should be predominant in dilute cultures. The second order mechanisms should become more significant as the

microcarrier concentration is increased. The higher order mechanisms should be predominant only in very concentrated cultures. The higher order mechanisms will not be investigated in this thesis.

To provide clear and unique information regarding the first order mechanism, experiments were first performed with dilute cultures. These experiments elucidated the nature of the first-order mechanisms without interference from the second-order mechanisms. Subsequent experiments were performed with concentrated cultures. The higher rates of damage in the concentrated cultures were analyzed to investigate the nature of the second order mechanisms.

4B. Effects of Power and Viscosity in Dilute Cultures

For dilute microcarrier cultures, the mechanisms of cell death from turbulence were investigated through experiments on the effects of power and viscosity. Cell damage from time-average flow fields was avoided through limitations on the maximum time average shear rate and fluid viscosity. The maximum shear stress from time-average flow fields was less than 5 dyne/cm^2. The cultures contained only 0.2 g/l microcarriers, or 0.002 volume fraction solids, and were therefore not subject to significant damage from microcarrier collisions.

Figure 29 shows the effect of 20 g/L dextran supplement (78,500 MW) on cell growth in the dilute cultures at different levels of agitation. The cell concentrations represent the viable, or attached, cell concentrations for the cultures. To eliminate cell damage from time-

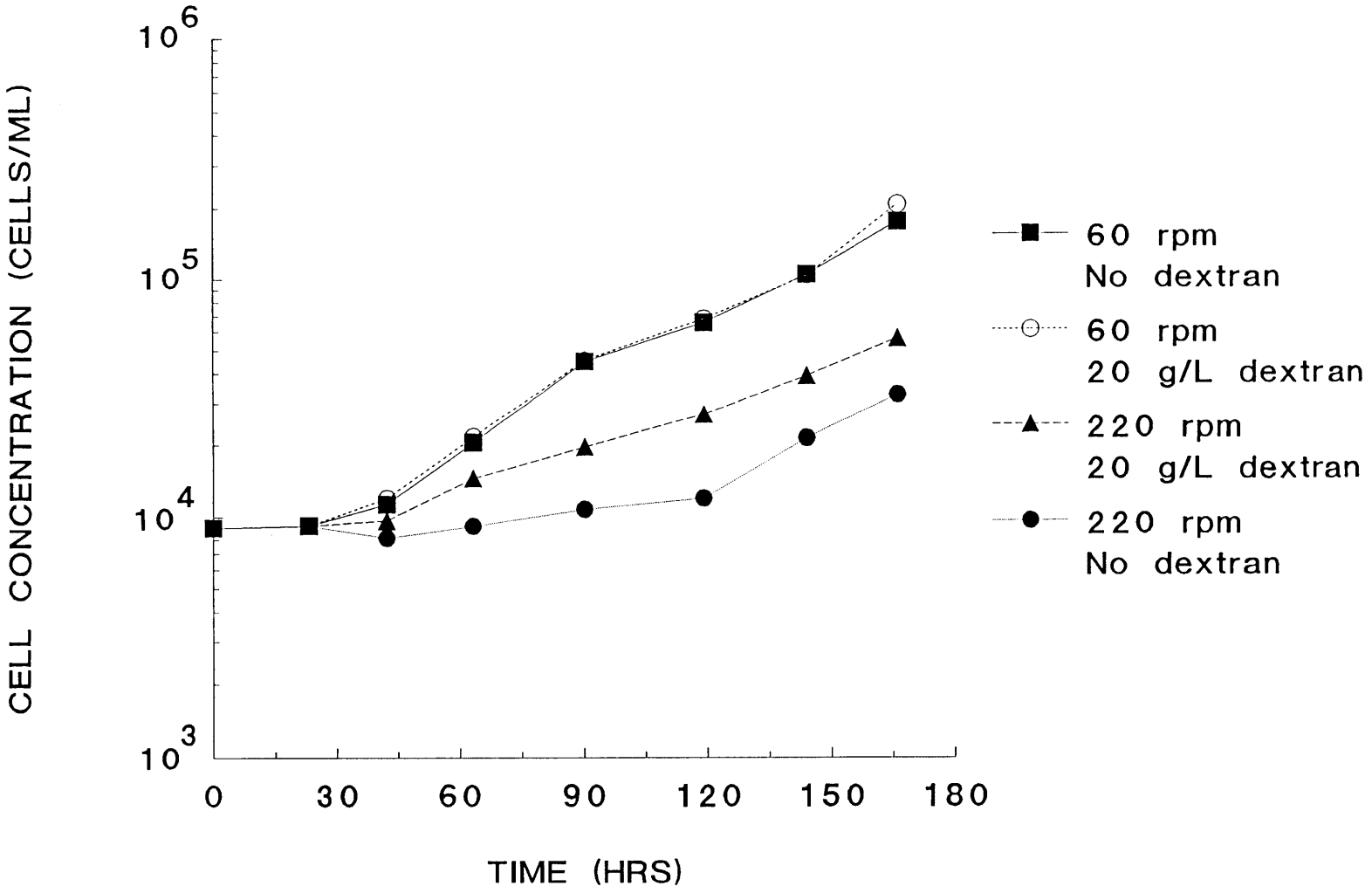

Figure 29. Effect of 20 g/L dextran (78,500 MW) on net growth at different stirring speeds

average flow fields, the cultures were grown in the 500-ml vessels with 5.3 cm impellers. The data for the control cultures at 60 RPM, or a power input of approximately 10 dyne/cm^2, has already been illustrated and discussed in Figure 11 of Chapter 1. It is repeated here for reference.

At 60 RPM, there was no effect from an increase in viscosity and there was no significant hydrodynamic death and removal. At 230 RPM, cell death and removal from hydrodynamic forces were strongly evident. For the cultures with and without dextran at 230 RPM, the viable cell concentrations were lower than in the controls at 60 RPM. The data indicate, however, that hydrodynamic cell death and removal can be reduced with a viscosity increase through dextran supplementation. At 230 RPM, the culture with 20 g/L dextran exhibited much higher viable cell concentrations than the culture with no dextran.

Figure 30 shows the effect of a 50 g/L dextran supplement (78500 MW) on cell growth in the dilute cultures at different levels of agitation. Again, to eliminate cell damage from time-average shear fields, the cultures were grown in the 500-mL vessels with 5.3 cm impellers. At 60 RPM, supplementation with 50 g/L dextan led to a reduction in viable cell concentrations. This reduction was due to the mild toxic effect of 50 g/L dextran on cell growth. At 185 RPM, supplementation with 50 g/l dextran led to an increase in viable cell concentration. This increase was due to viscous reduction of cell death and removal. With 50 g/L dextran, the viable cell concentrations in the culture at 185 RPM were

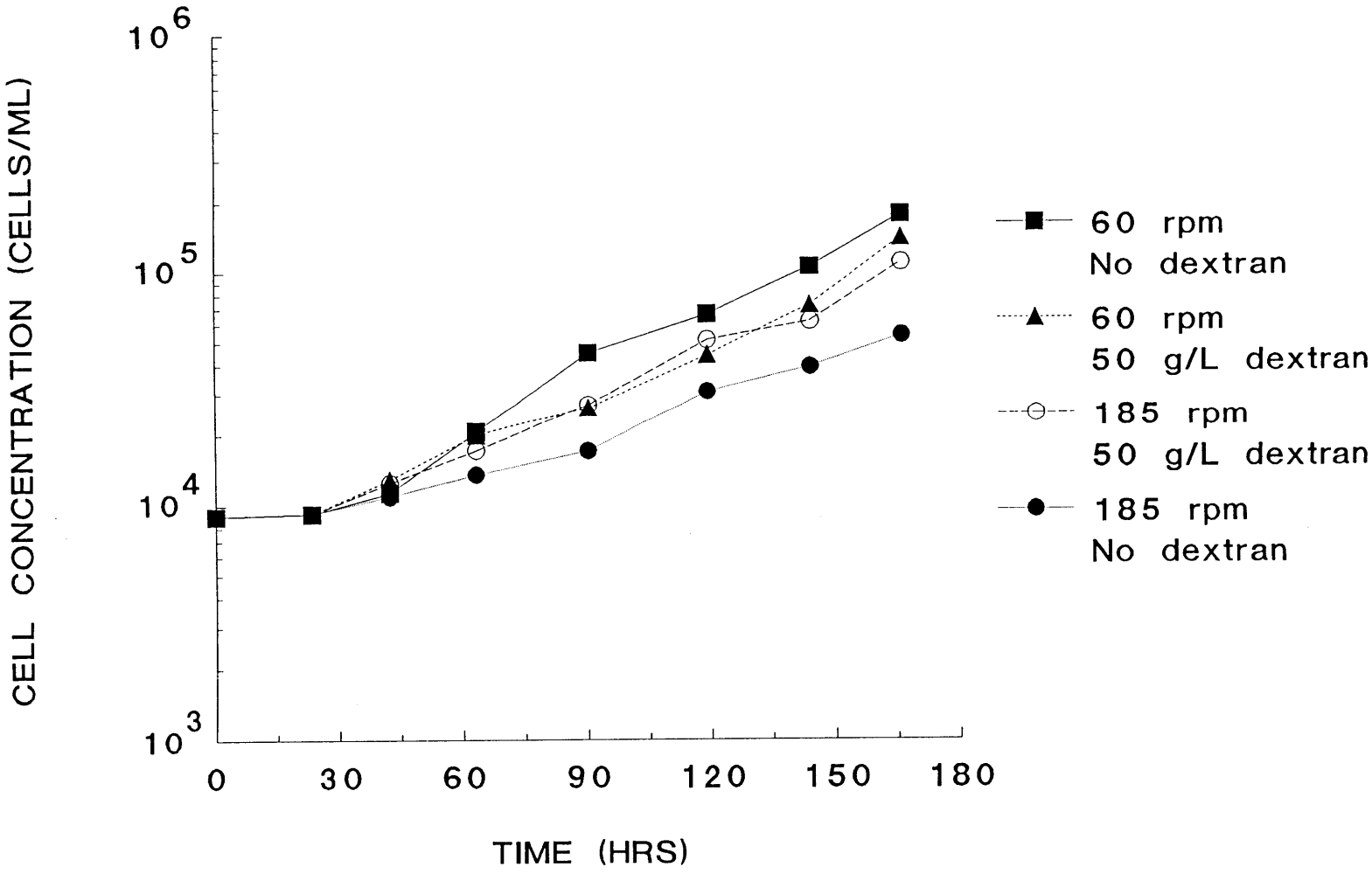

Figure 30. Effect of 50 g/L dextran (78,500 MW) on net growth at different stirring speeds

nearly equal to the concentrations in the culture at 60 RPM. Supplementation with 50 g/L dextran almost completely eliminated hydrodynamic death and removal at 185 RPM.

Numerous other experiments, similar to the one described above, were performed on the effect of various dextran supplements at different levels of agitation. All cultures contained 0.2 g/l microcarriers and were not subject to cell damage from microcarrier collisions or time-average flow fields. The experiments employed dextran supplements between 20 and 50 g/L (78,500 MW) and were performed over a wide range of levels of agitation. The results followed the trends shown in Figures 29 and 30 and are included in the subsequent data analysis.

4C. Cell Death Through Microcarrier-Eddy Interactions

As discussed in the Literature Review and Thesis Formulation section, hydrodynamic death from turbulence should become evident when the turbulence generates eddies which are smaller than the microcarriers. Because isotropic equilbrium appears to exist in the viscous dissipation regime, the average size of the smallest eddies can be estimated by the average Kolmogorov length scale, $\bar{L}$:

$$\bar{L} = (\nu^3/\bar{\epsilon})^{1/4} \qquad \text{(Eq. 41)}$$

where $\bar{\epsilon}$ is the average power input per unit mass and ν is the kinematic fluid viscosity. The size of the smallest eddies decreases with an increase in power or a decrease in kinematic viscosity. For sufficiently high power inputs at a given viscosity, the turbulence should generate eddies which are smaller than microcarriers. Cell damage from

turbulence should then become evident.

To investigate whether the proposed role of eddy length is correct, the experimental data for the dilute cultures was analyzed. For each culture, the relative observed growth rate, μ_r, was calculated from the equation

$$\mu_r = \mu_{obs}/\mu_d \qquad \text{(Eq. 42)}$$

where μ_{obs} was the average observed growth rate of the culture, and μ_d was the average observed growth rate of a control culture grown under mild agitation with the same dextran concentration. The average observed growth rates, which represent the difference between the actual growth rates and death rates, were calculated through linear regressions on the attached cell concentrations. The use of relative observed growth rates corrects for the mild effects of dextran toxicity which were observed with dextran supplements greater than 25 g/l.

Figure 31 shows the plot of relative observed growth rate versus average Kolmogorov eddy length for a number of different fluid viscosities. Cell death through hydrodynamic forces, as indicated by a decrease in relative specific growth rate, becomes apparent when the average Kolmogorov length scale falls below about 130 microns, or about 2/3 of the microcarrier diameter of 185 microns. As expected, hydrodynamic death occurs when the turbulence generates eddies which are smaller than the microcarriers. For a number of different fluid viscosities, hydrodynamic death in dilute cultures correlates well with Kolmogorov length scale. The correlation describes the effect of both

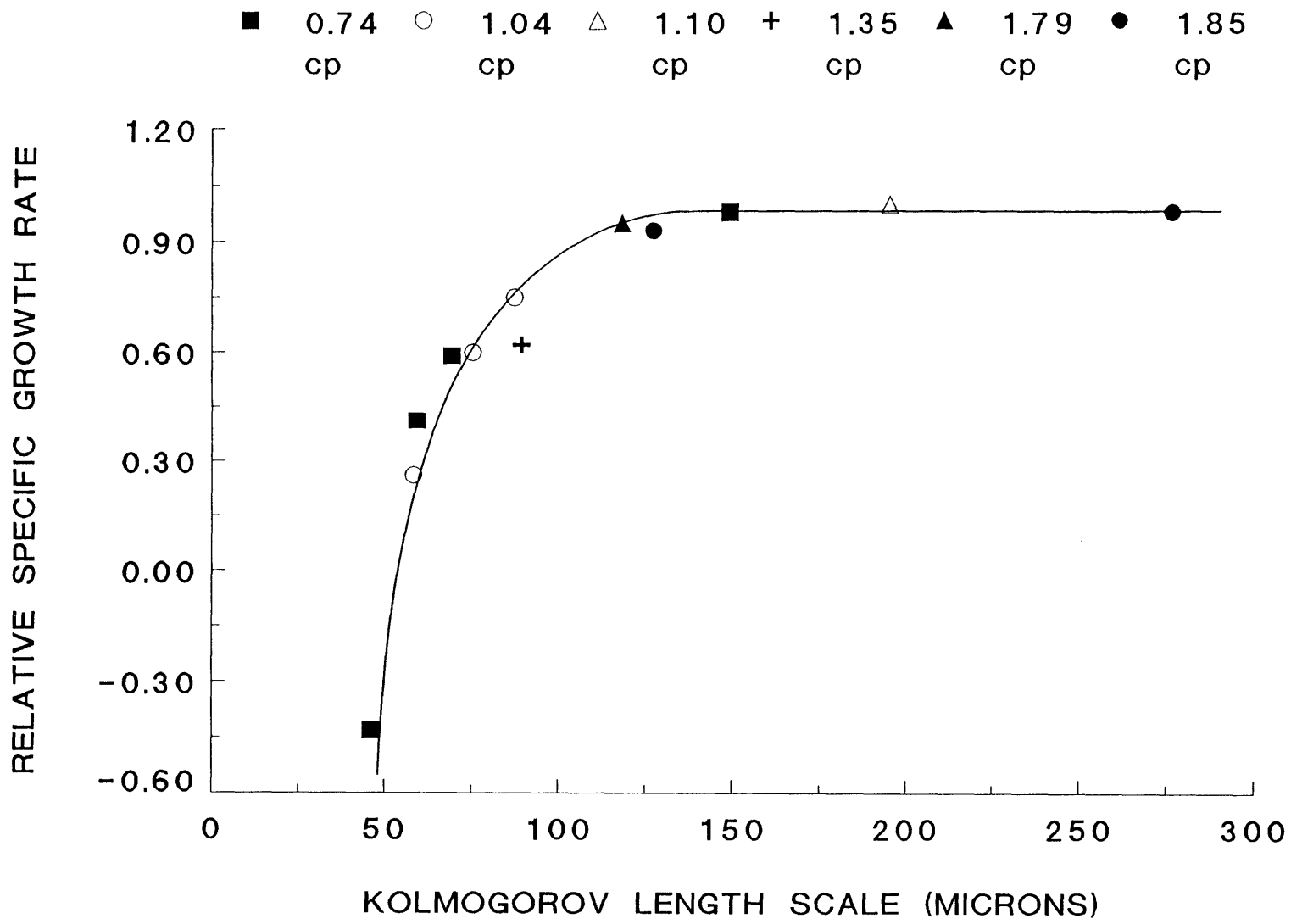

Figure 31. Relative growth rate vs. Kolmogorov eddy length scale for FS-4 cultures with 0.2 g/L microcarriers

viscosity and power as combined in the unique length scale group, $(\nu^3/\epsilon)^{1/4}$. The existence of this correlation provides more evidence that isotropic equilibrium exists at the Kolmogorov scale in overagitated microcarrier cultures.

The results in Figure 31 are not the only data which illustrates the correlation of hydrodynamic death with Kolmogorov length scale. Prior to the experimental work in this thesis, the data presented in Hu (1983) and Sinskey et al (1981) were analyzed. Both researchers studied the effects of agitation on net growth of cells in microcarrier cultures. Experiments were performed on the effect of vessel geometry but not on the effect of fluid viscosity.

Figure 32 shows the correlation of the data of Hu (1983) for FS-4 cells. Relative growth extent, or relative net positive growth after inoculation, is compared to average Kolmogorov eddy length scale. Cell death is indicated by a decrease in the relative growth extent, which is proportional to relative observed growth rate for positive net growth. The data show a similar trend to the results in Figure 31. Cell death from turbulence becomes evident when the average Kolmogorov length scale falls below about 130 microns. Further decreases in Kolmogorov length scale lead to a sharper decline than observed in Figure 31. This would be expected with the higher microcarrier concentrations and the corresponding collision damage. The plateau at very small eddy lengths indicates no net positive growth occurred. It is unclear whether net negative growth might have occured.

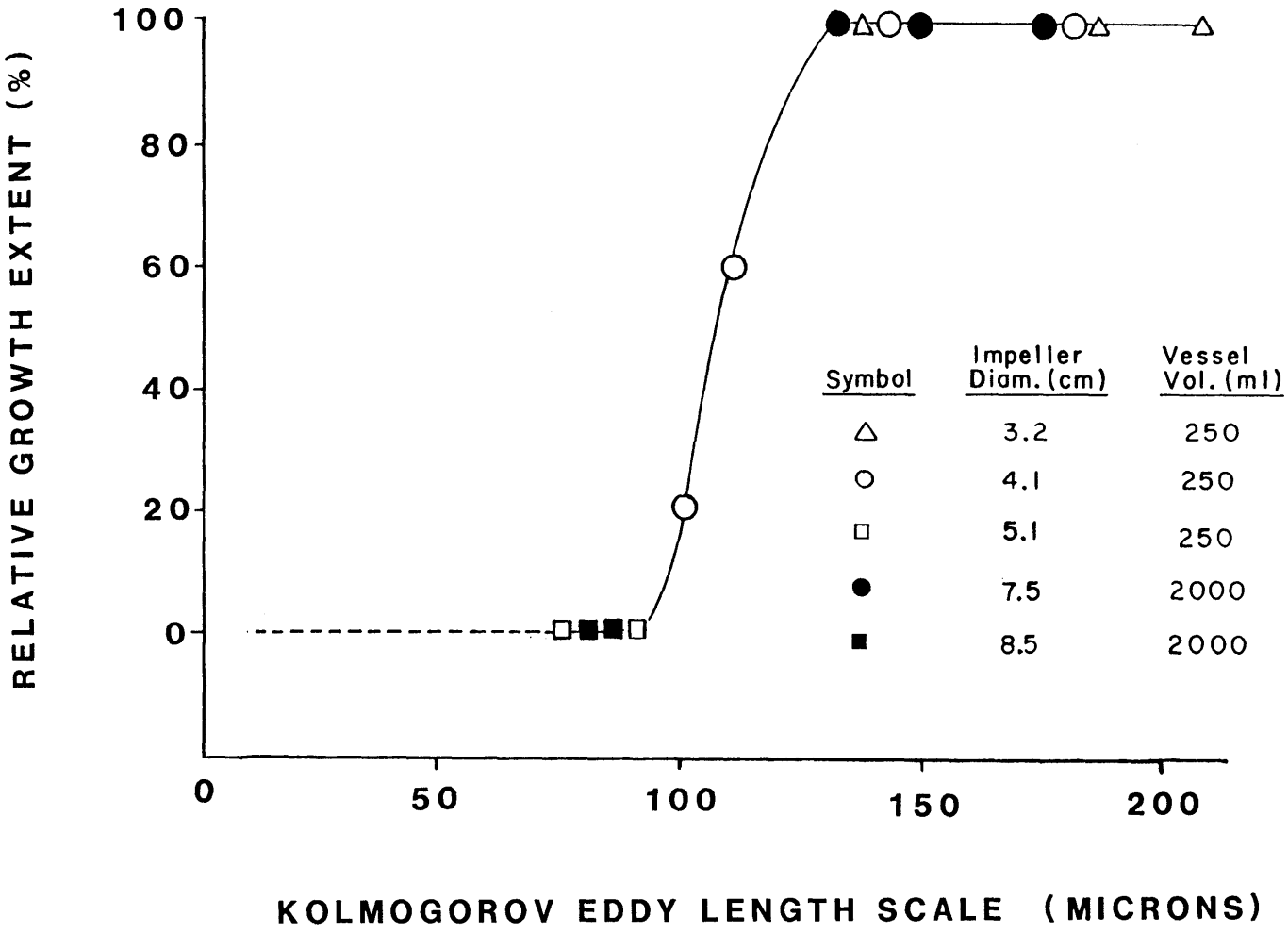

Figure 32. Relative growth rate vs. Kolmogorov eddy length scale for FS-4 cultures with 5 g/L microcarriers (data from Hu, 1983)

In Figure 32, a single correlation describes the data reasonably well for a number of different vessel geometries. This is further indication that cell death arises through eddies in the viscous dissipation regime. Such eddies exist in a state of isotropic equilibrium which depends only on the local power dissipation rate and kinematic viscosity, and not on the vessel geometry. Energy containing eddies, in contrast, are highly dependent on reactor geometry. If cell death arose through the action of the energy-containing eddies, a strong effect of geometry should be observed.

Figure 33 shows the correlation of the data of Sinskey et al (1981) for chicken embryo fibroblasts. Maximum cell concentration is compared to average Kolmogorov length scale. As observed in Figure 32, a single correlation fits the data for a number of different vessel geometries. Hydrodynamic death, as indicated by a decrease in the maximum cell concentration, is evidenced when the length scale falls below 100 microns. The microcarrier diameter was not reported and may have been slightly smaller than 185 microns. Cell growth drops very sharply for eddies smaller than 100 microns; this may indicate a difference between FS-4 cells and chicken embryo fibroblasts. The plateau at very small eddy lengths does not indicate whether net negative growth occurred.

For a number of different data sets, hydrodynamic death in dilute microcarrier cultures correlates well with average Kolmogorov length scale. As expected, cell death occurs when the turbulence generates eddies that are smaller than the microcarriers. In parallel research

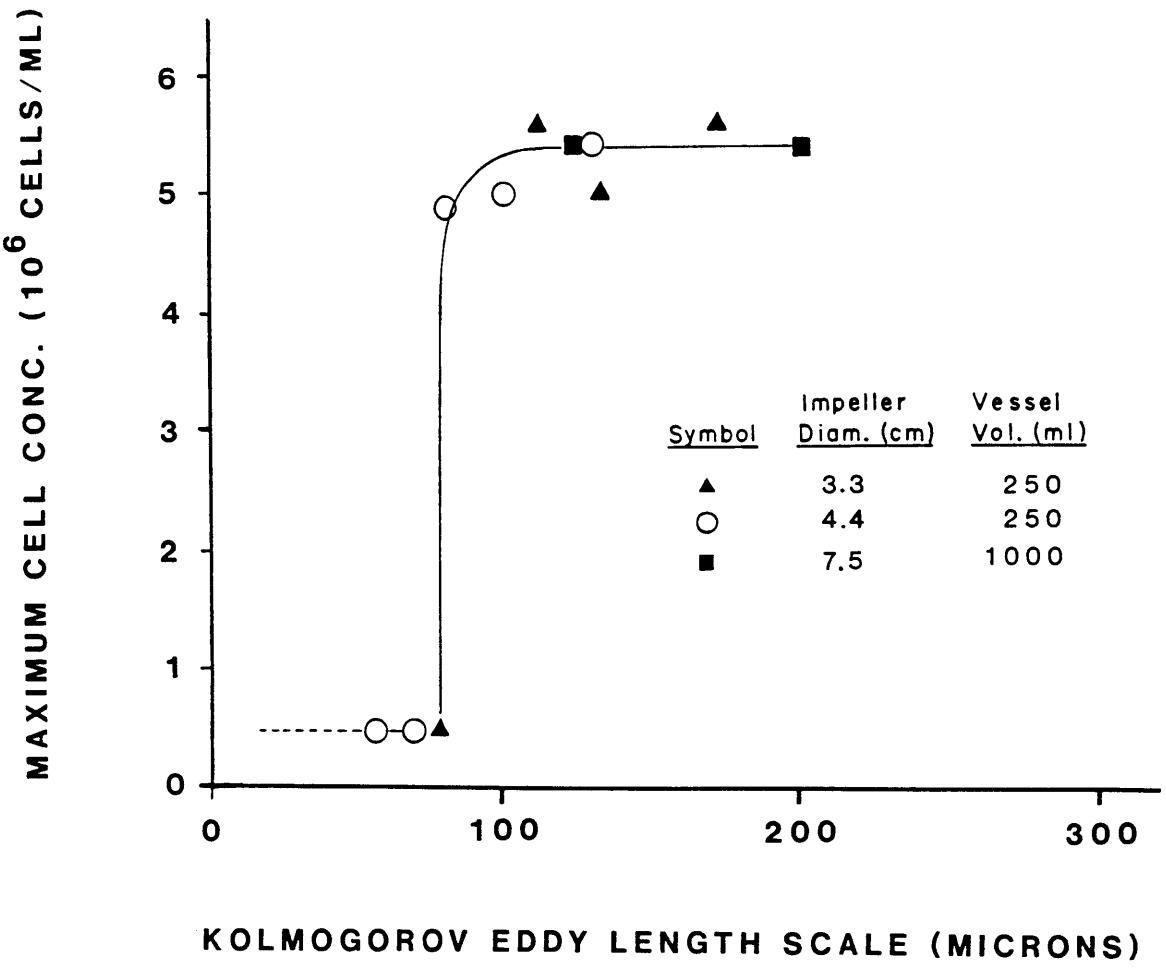

Figure 33. Maximum cell concentration vs. Kolmogorov eddy length scale for chicken embryo fibroblasts on 5 g/L microcarriers (data taken from Sinskey et al., 1981)

with cultures of freely-suspended animal cells, McQueen et al (1987) observed a similar correlation of cell death with Kolmogorov length scale. Cell death occurs when the turbulence generates eddies smaller than about 3.5 microns, or about 1/3 to 1/2 the cell diameter.

4D. Hydrodynamic Forces in Microcarrier-Eddy Interactions

To determine whether the correlation of cell death with eddy length has a fundamental basis, one should determine whether the eddies can produce hydrodynamic forces sufficiently strong to damage cells. Currently, however, there is no thorough description of the complex hydrodynamics near a particle in a turbulent flow field. Accordingly, only very rough estimates of the forces can be made.

If viscous forces predominate, Matsuo and Unno (1981) suggest that the shear stress on the surface of a sphere in a turbulent flow field is given by

$$\tau = 2\eta(2/15)^{1/2} (\epsilon/\nu)^{1/2} \qquad \text{(Eq. 43)}$$

where η is the fluid viscosity. If Reynold's stresses are important, Matsuo and Unno (1981) suggest that

$$\tau = 0.37\rho_f(\epsilon/\nu)d_p^2 \qquad \text{(Eq. 44)}$$

where ρ_f is the fluid density and d_p is the microcarrier diameter.

For the conditions under which cell death was observed, the average power input per unit mass was first used to estimate the shear stresses from equations 43 and 44. From equation 43, shear stress estimates in

the range of 1-3 dyne/cm^2 were obtained. These values are somewhat less than 7 dyne/cm^2, the minimum shear stress for which significant cell damage has been reported (Stathopoulos and Hellums, 1985). From equation 44, shear stress estimates in the range of 2-16 dyne/cm^2 were obtained. The upper range of these values are in the range known to cause cell damage.

The shear stress estimates can alternatively be performed with local instead of average power dissipation rates. In a stirred tank, the power dissipation rates in the impeller discharge stream are much higher than the average dissipation rate. For Rushton turbines, Okamoto et al (1981) and Placek and Tavlarides (1985) report that the power dissipation rates in the impeller discharge stream are approximately 6 fold higher than the average dissipation rates. This ratio was used to estimate the maximum local power dissipation rate and the corresponding maximum shear stress. From equation 43, the maximum shear stress estimates are in the range of 2-6 dyne/cm^2, again still less than the values known to cause damage. From equation 44, the maximum shear stress estimates were in the range of 10-100 dyne/cm2. These values are all within the range known to cause cell death and removal (Crouch et al, 1985; Stathopoulos and Hellums, 1985).

As already mentioned with regard to selectivity of cell removal, cells on microcarriers could be damaged or killed not only by shear stresses, but also by normal forces. Normal forces will be generated by velocity and pressure fluctuations in the turbulent flow field of a

microcarrier culture. In terms of cell death, the critical fluctuations will be those which occur on a scale which is intermediate in size between cells and microcarriers. These flucuations will involve the eddies in the viscous dissipation regime. Thus, the normal force per unit area on the microcarrier surface, F_n, might be estimated from the magnitude of the pressure fluctuations which occur on the scale of the viscous dissipation regime:

$$F_n \sim P'_{vdr} \qquad \text{(Eq. 45)}$$

where P'_{vdr} represents root mean square turbulent pressure fluctuation, or pressure intensity, due to the eddies in the viscous dissipation regime.

Turbulence in the viscous dissipation regime is essentially isotropic and has a characteristic Reynold's number near unity (Hinze, 1975). The pressure fluctuations due to the viscous dissipation eddies might thus be estimated from an extension of the result presented in Hinze (1975) for isotropic turbulence of low Reynold's number:

$$P' = \rho_f u'^2 \qquad \text{(Eq. 46)}$$

where u' and P' represent the velocity and pressure intensity, respectively.

In terms of cell death, the relevant pressure and velocity fluctuations are those which occur on the viscous dissipation scale. The effective velocity intensity might thus be estimated by Kolmogorov velocity scale for the viscous dissipation eddies. The normal force per

unit area on the microcarrier surface, F_n, is then given by

$$F_n = \rho_f (\epsilon\nu)^{1/2} \qquad \text{(Eq. 47)}$$

where ρ_f is the fluid density.

Using average power dissipation rates in equation 47, one can estimate normal forces on the order of 1-4 dyne/cm^2 for the cultures which exhibited hydrodynamic death. If the local power dissipation rates in the impeller stream are used, the normal forces estimates are increased to 2-10 dyne/cm^2. It is unknown whether normal forces of this strength can damage or remove cells from a growth surface. In fact, a literature review indicates no published data with regard to the effects of normal forces on animal cells. Future research will hopefully be performed in this area.

4E. Kinetics of Cell Growth and Death in Dilute Cultures

Although the hydrodynamics near a microcarrier surface must be investigated more thoroughly, the comparison of experimental data with simplified models can help to elucidate the mechanisms of death from excessive agitation. The data in Figures 31-33 indicate that cell death occurs when the turbulence generates eddies which are smaller than the microcarriers. Based upon the correlation of cell death with Kolmogorov length scale, a model was developed to describe the kinetics of hydrodynamic damage in dilute microcarrier cultures. This "eddy-length" model is based upon the following assumptions:

1) hydrodynamic damage occurs through microcarrier-eddy encounters

2) damage will occur only if a microcarrier encounters an eddy smaller than a critical length, L_c, of approximately 130 microns. This assumption is based upon the correlations shown in Figures 31 and 32.

3) cell death and removal, and not growth inhibition, are the only forms of hydrodynamic damage. This assumption is based upon the experimental results previously presented and discussed.

4) a constant fraction of the culture volume is filled with randomly appearing eddies in the Kolmogorov regime. This assumption is implicit in the derivation of the Kolmogorov scales from an energy balance.

Under the fourth assumption, the effective eddy concentration in the Kolmogorov regime is proportional to the inverse of the eddy volume, or $(\bar{\epsilon}/\nu^3)^{3/4}$. Because cell death occurs through cell-eddy encounters, the total rate of cell death is proportional to the product of the cell concentration times the eddy concentration. The specific death rate is therefore proportional to the eddy concentration, or $(\bar{\epsilon}/\nu^3)^{3/4}$. Expressed in mathematical form, the kinetic "eddy-length" model becomes

$$\frac{dC}{dt} = \mu C \qquad L \geq L_c \qquad \text{(Eq. 48)}$$

$$\frac{dC}{dt} = \mu C - q_1 C \qquad L < L_c \qquad \text{(Eq. 49)}$$

$$q_1 = K_e(\bar{\epsilon}/\nu^3)^{3/4} \qquad \text{(Eq. 50)}$$

where μ is the intrinsic specific growth rate and is independent of the

level of agitation, q_1 is the specific death rate due to microcarrier-eddy interactions, $\bar{\epsilon}$ is the average power input per unit mass, ν is the kinematic fluid viscosity, and K_e is a function of the cell and microcarrier properties, and possibly the reactor geometry.

To test the kinetic model presented above, the data for the dilute microcarrier cultures were analyzed. For each culture, the average specific death rate was calculated from the equation:

$$q = \mu_d - \mu_{obs} \qquad \text{(Eq. 51)}$$

where μ_{obs} and μ_d have been defined with equation 42. Figure 34 shows a plot of specific death rate versus eddy concentration group, $(\epsilon/\nu^3)^{3/4}$, for two different vessels with the same impeller. Each set of data shows a linear correlation, as predicted by the eddy length model. The intercept values near zero follow the assumption of insignificant cell death with mild agitation.

For the data from the 500-ml (9.6 cm) vessel, the value of K_e from linear regression is 6.9×10^{-13} cm^3/sec with a 95% confidence interval of $\pm$ 1.7×10^{-13} cm^3/sec. For the data from the 125-ml vessel, the value of K_e from linear regression is 5.4×10^{-13} cm^3/sec with a 95% confidence interval of $\pm$ 1.3×10^{-13} cm^3/sec. The difference between the two values of K_e is not statistically significant within a 95% confidence interval, as determined from the statistical methods presented in Kleinbaum and Kupper (1985). The limited data therefore do not indicate a clear effect of vessel geometry. In fact, a single correlation fits both vessel geometries reasonably well.

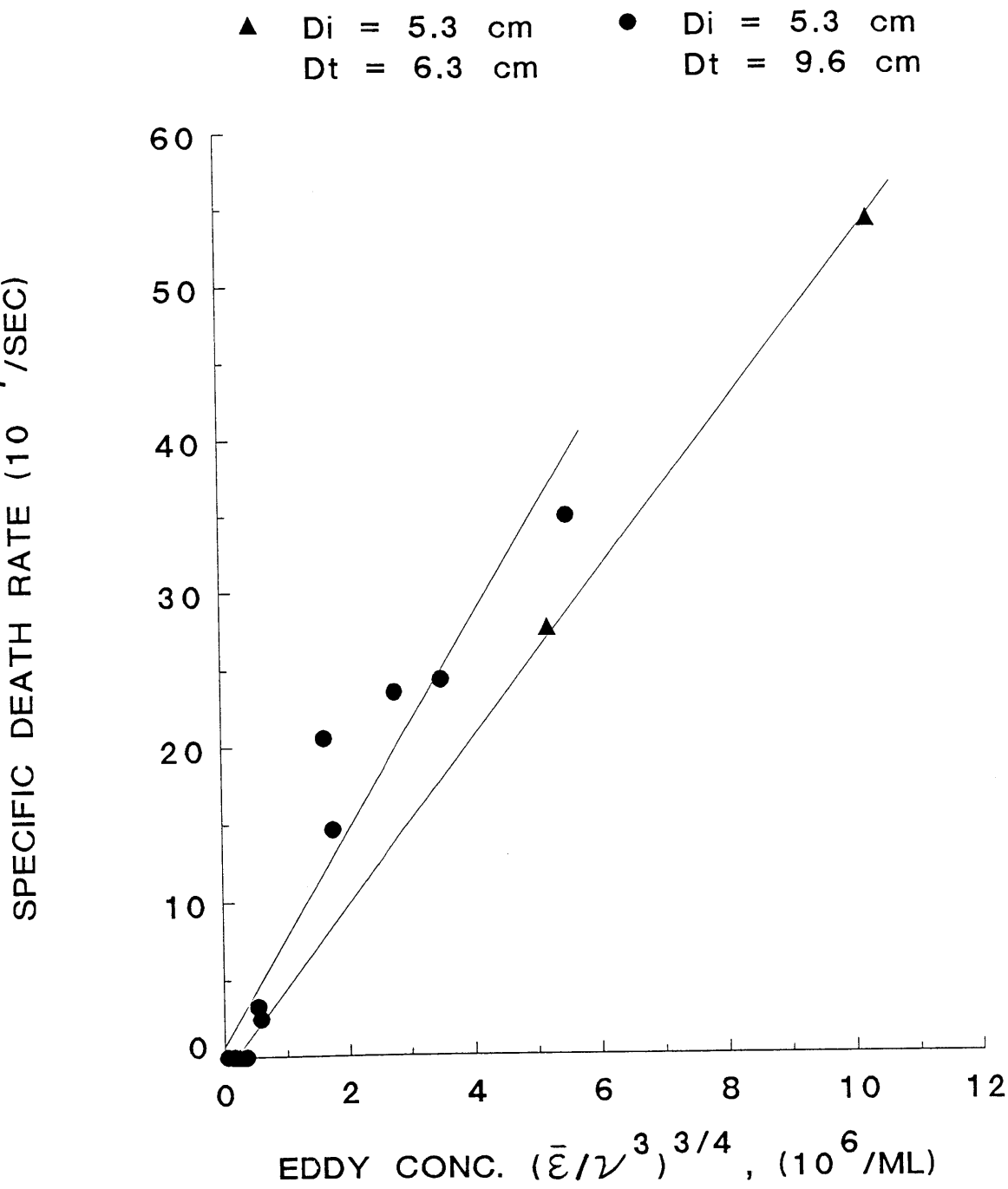

Figure 34. Specific death rate vs. eddy concentration for dilute FS-4 cultures

The data in Figures 31-34 all indicate reasonably good correlations with average power input and do not indicate strong effects of vessel geometry. Because cell death is probabilistic and involve eddies in the viscous dissipation regime, which are also probabilistic, one would not expect a strong effect of geometry. In this thesis, the average value of 6.2×10^{-13} cm^3/sec will be used for K_e in the kinetic expression for cell death from microcarrier-eddy interactions. Future research will hopefully determine and incorporate any effects of vessel geometry in more advanced kinetic expressions.

The hydrodynamic effects in dilute FS-4 cultures followed the predictions of the eddy-length model. To further test the validity of the model, the predictions of the model were also compared to the following sets of results:

1) the effects of agitation on net growth of Vero cells on Cytodex 1 microcarriers, as determined by Hirtenstein and Clark (1981) and shown in Figure 1 of this thesis,
2) the effects of agitation on net growth of FS-4 cells on Cytodex 1 microcarriers, as shown in Figure 24 of this thesis,
3) the effects of agitation on secondary disruption of protozoa in baffled stirred tanks, as determined by Midler and Finn (1966)

For both the Vero and FS-4 cells, the cultures were grown in unbaffled spinner vessels, and the specific death rates were determined from equation 51. The microcarrier concentrations were 3 g/l, or 3% solids by volume, and thus were slightly out of the dilute regime. For

the protozoa, which are shear sensitive and about half the size of microcarriers, the specific death rates were calculated from the slopes of secondary disruption data. The power inputs were determined from the correlations presented in Rushton et al (1950) and Bates et al (1963) with the corrections presented in Bujalski et al (1987).

Figure 35 shows a log-log plot of specific death versus average power input per unit mass for the Vero cells, FS-4 cells, and protozoa. As predicted by the eddy-length model, all three sets of data show a linear correlation with a slope near 0.75. The data indicate that Vero cells are considerably more sensitive to agitation than FS-4 cells. However, the power input calculations for the Vero cells were rough and may have been in error with regard to absolute values. The data for the protozoa was taken over a wide range of tank geometries. The ratios of impeller to tank diameter were varied between 0.24 and 0.71. Over this wide range of geometries, the data can be reasonably described by a single correlation based on average power input. This is more evidence that there are no strong effects of geometry when cell death arises through eddies in the viscous dissipation regime.

For a number of sets of data, the eddy-length model accurately describes that kinetics of cell death in dilute or reasonably dilute cultures. Thus, it appears that cell death truly does arise through random interactions between microcarriers and eddies in the viscous dissipation regime. Such interactions will not lead to cell death, however, if the eddy is larger than the microcarrier.

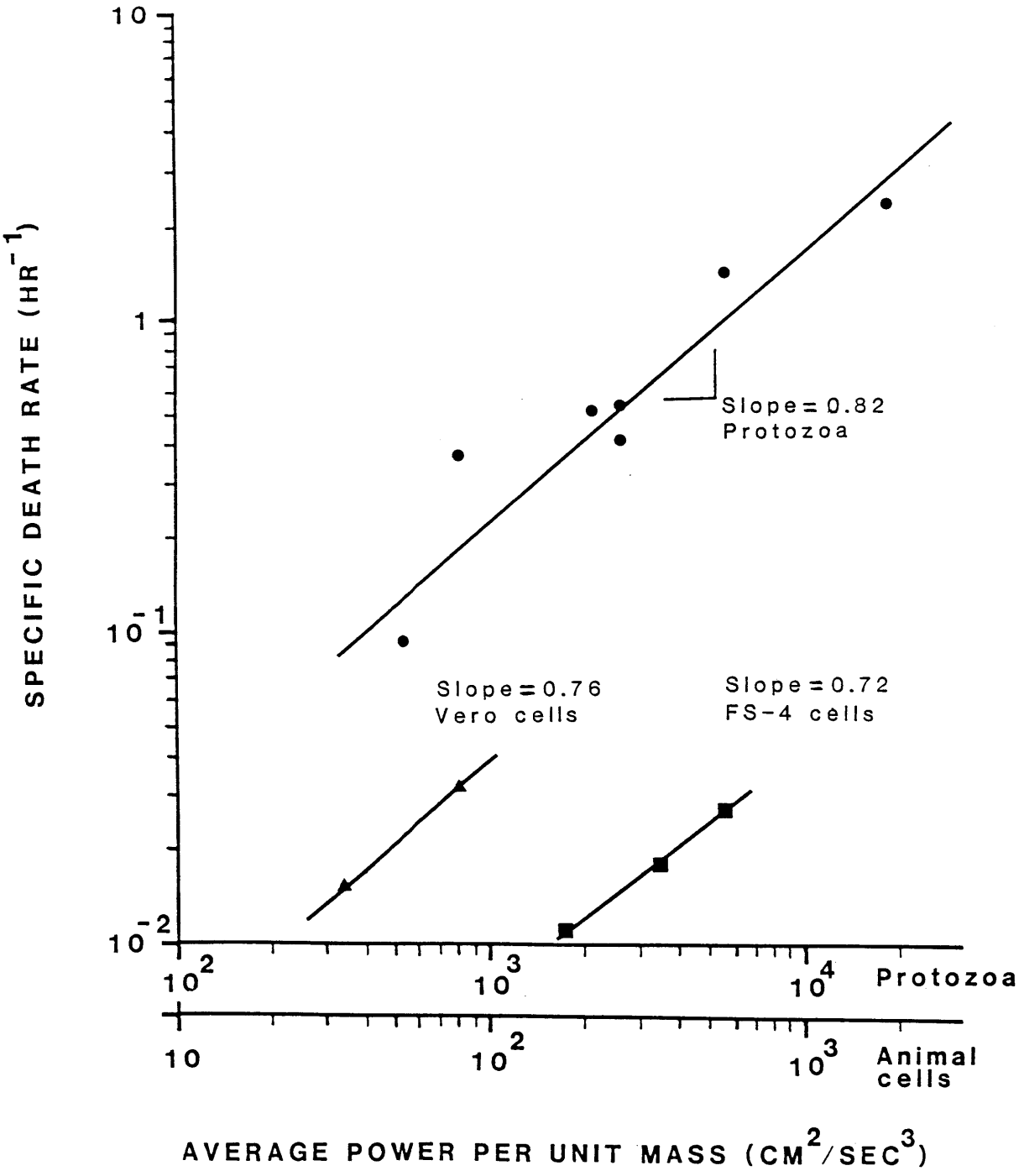

Figure 35. Specific death rate vs. power input per mass for Vero cells, FS-4 cells, and protozoa

4F. Cell Damage from Time-Average Flow Fields

To investigate the conditions under which damage from time-average shear fields might occur, experiments were performed with dilute cultures in the 125-ml vessels with high viscosity increases. In the these vessels, there is a clearance of only 5 mm between the impeller tip and vessel wall. Under high rates of impeller rotation, strong time-average shear rates are generated in the region between the impeller tip and tank wall. For operation at 220 RPM, the maximum time-average shear rate is approximately 160 sec^{-1}, as estimated from equation 16. A viscosity increase to 1.5 cp or higher might therefore induce damage from time-average shear fields, as it will lead to shear stresses greater than 7 $dyne/cm^2$ (equation 14). Shear stresses of this value are the minimum reported to cause cell damage (Stathopoulos and Hellums, 1985). Accordingly, the onset of damage from time-average shear fields was investigated by increasing the fluid viscosity above 1.5 cp in the 125-ml vessels at 220 RPM.

Figure 36 shows the results of this investigation. Growth curves are presented for four conditions in the 125-mL vessels. Because many of the conditions were investigated with duplicate cultures, and because different inocula were used for each set of duplicates, viable cell concentrations are reported relative to initial values at inoculation. The cultures at 35 RPM exhibited the normal cell growth with insignificant hydrodynamic death. The cultures at 220 RPM with no dextran had very low viable cell concentrations and exhibited a great degree of hydrodynamic death. When the viscosity was increased to 1.04

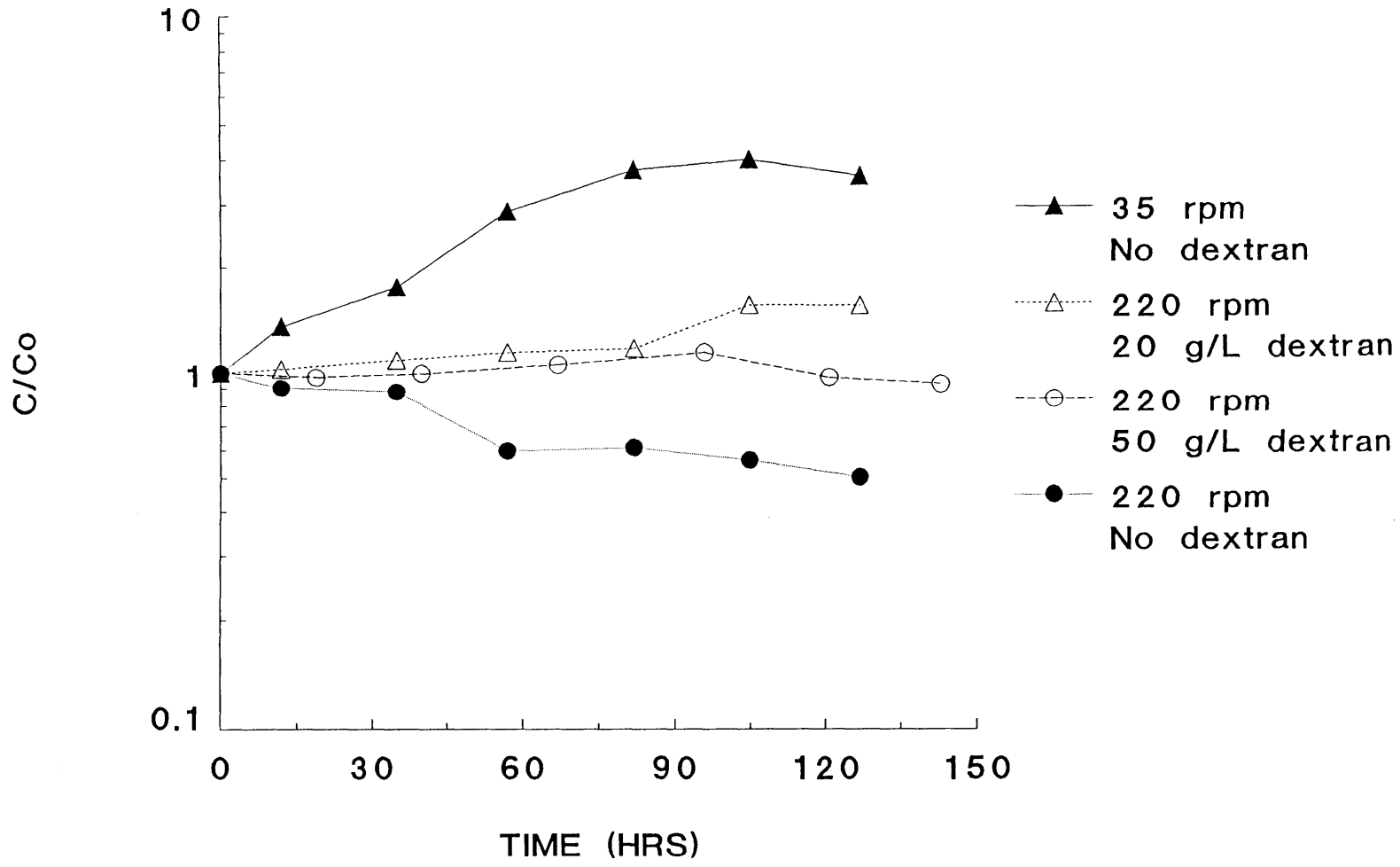

Figure 36. Effect of dextran on net growth in a reactor with strong time-average shear fields

cp with 20 g/l dextran, cell death and removal were strongly reduced. When the viscosity was further increased to 1.85 cp with 50 g/l dextran, cell death was more pronounced than in the 20 g/l cultures.

In the culture at 220 RPM with 50 g/l dextran, the maximum shear stress from time-average flow fields, or T_{max}, was approximately 9 dyne/cm^2. If cell death from time-average flow fields was occuring in this culture, but not in the other cultures, the specific death rate should be higher than would be expected for the given viscosity and power. Figure 37 shows that this hypothesis is correct. The specific death rates from Figure 34, and the best-fit linear correlation, are shown for the cultures with $T_{max} < 5$ dyne/cm^2. The specific death rate for the culture with $T_{max} = 9$ dyne/cm^2 is far above the correlation for the other cultures. The difference is statistically significant within a 99% confidence interval and is indicative of cell damage from time-average shear fields. Thus, it appears that cell damage from time-average shear fields can occur. The onset of such damage can be roughly predicted through fluid-mechanical modelling and through knowledge of a critical shear stress for cell damage. The predictions can be used to purposely avoid cell damage from time-average flow fields, as was done in many of the experiments in this thesis. The predictions can also be used to develop criteria for reactor design and scale-up.

4G. Effects of Cavitation

In the turbulent flow field of a stirred tank, dynamic reductions in pressure will occur as the fluid flows around the impeller. For

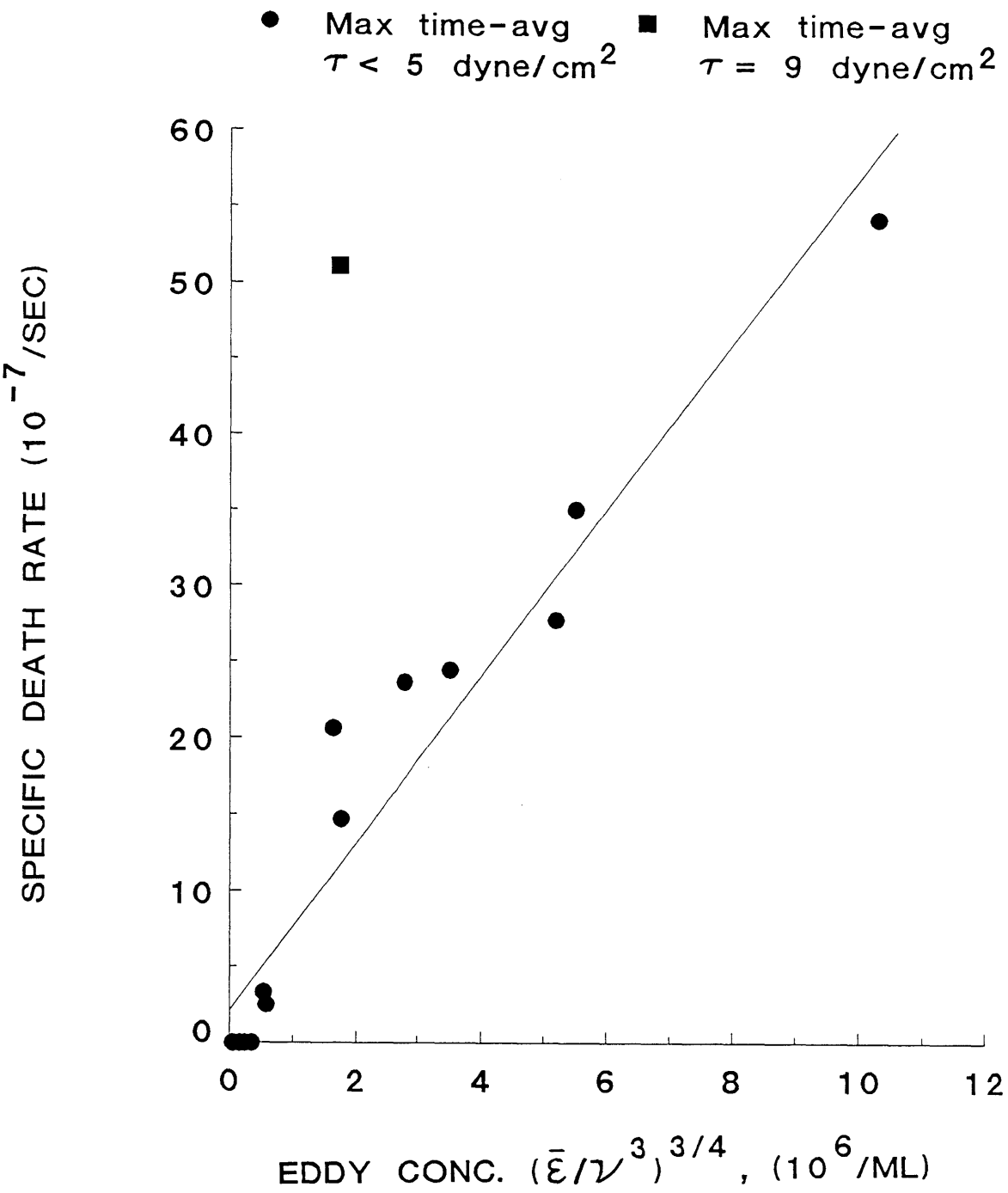

Figure 37. Specific death rate vs. eddy concentration at different levels of maximum shear stress from time-average shear fields

sufficiently strong agitation, the reduction in pressure may lead to the formation of vapor cavities, an explosive phenomena known as *cavitation*. Cavitation will arise only if the local pressure falls below the fluid vapor pressure at the given operating temperature. If cavitation were to occur in a microcarrier bioreactor, it likely would result in cell damage or lysis.

The existence of cavitation can generally be correlated with a cavitation number (Daily and Harleman, 1966). The cavitation number, σ, is given by (Boucher and Alves, 1973)

$$\sigma = \frac{P - P_v}{\rho_f U^2/2} \qquad \text{(Eq. 52)}$$

where P is the static pressure in the undisturbed flow, P_v is the fluid vapor pressure, ρ_f is the fluid density, and U is the free-stream fluid velocity. Cavitation will occur only if the cavitation number falls below a critical value characteristic of the given geometry. These critical values are gnerally in the range of 0.2 to 2.5 (Boucher and Alves, 1973).

For a stirred tank, the minimum cavitation number might be reasonably estimated from the maximum fluid velocity, including both the time-average and turbulent components. For a radial flow impeller, both the maximum time-average fluid velocity and turbulent intensity generally occur in the radial jet off the impeller. The maximum time-average radial velocity, $\overline{U}_{max}$, is proportional to the tip speed of the

impeller, as given by the data presented in Oldshue (1983):

$$\bar{U}_{max} = 0.7 \pi N D_i \qquad \text{(Eq. 53)}$$

In reference to this velocity, the maximum values of relative turbulent intensity are generally on the order of 60% (Placek and Tavlarides, 1985). Thus, an upper limit on the total fluid velocity U_{max} can be estimated by

$$U_{max} = \bar{U}_{max} + u'_{max} = (0.7 \pi N D_i)\ 1.6 \qquad \text{(Eq. 54)}$$

where u'_{max} is the maximum root mean square turbulent velocity fluctuation.

For the microcarrier cultures which exhibited cell death and removal, the maximum total fluid velocities given by equation 54 were less than 72 cm/sec. Thus, with P = 760 mm Hg and P_v = 47.1 mm Hg (Liley and Gambill, 1973), one can estimate a minimum cavitation number of 370. This is over two orders of magnitude greater than the typical maximum values for which cavitation occurs. Thus, it appears that cavitation did not occur in the experiments performed in this thesis.

In general, for the levels of agitation employed in microcarrier cultures, cavitation should not present a problem. Nonetheless, for any given design and set of operating conditions, the cavitation number can be calculated. A minimum value for the cavitation number might be set as one of the design criteria. The critical cavitation number for incipient cavitation, however, appears to depend on the scale of the equipment (Boucher and Alves, 1973).

CHAPTER 5. MECHANISMS OF HYDRODYNAMIC DEATH IN CONCENTRATED CULTURES

5A. Effect of Microcarrier Concentration with High Agitation

For dilute cultures under high agitation, cell death occurs primarily through microcarrier-eddy encounters and, in unusual circumstances, time-average flow fields. For concentrated cultures under high agitation, cell death might also occur through hydrodynamic interactions between microcarriers. As discussed previously, these interactions will be referred to as collisions, even though they may primarily involve the fluid flow between microcarriers which come in close but not actual contact.

To determine whether cell death occurs through microcarrier collisions with high agitation, inert microcarriers were added to microcarrier cultures agitated at 150 RPM in the 125-ml vessels. All cultures contained 1.5 g/l Cytodex 1, 5% (v/v) serum, and no dextran. The inert microcarriers were added to levels of 0, 5, 10, 15, 20, 25, and 30 g/l. A control culture at 35 RPM without inert microcarriers was grown for reference purposes.

Figure 38 shows the attached cell concentrations for various inert microcarrier concentrations. The culture at 150 RPM without inert microcarriers exhibited a moderate amount of cell death and removal. As the inert microcarrier concentration was increased, the attached cell concentrations were progressively reduced. A detrimental effect from adding inert microcarriers was especially apparent during the attachment

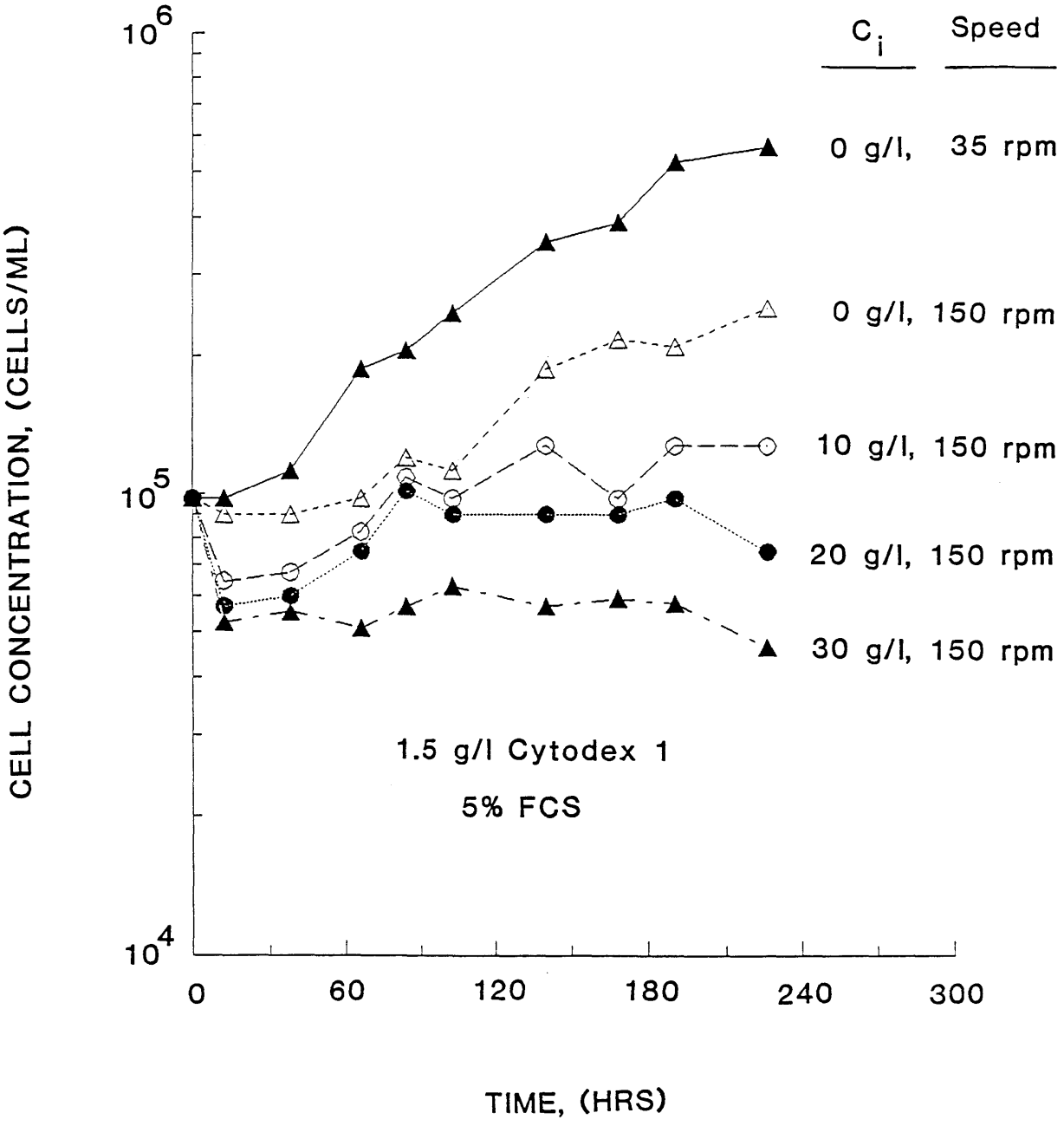

Figure 38. Effect of inert microcarriers on net growth with high agitation

stage. With high inert microcarrier concentrations, cell concentrations dropped precipitously during the first 12 hours. At 30 g/l, only 54% of the inoculum was viably attached. The debri from the unattached cells was clearly evident for up to 30 hours past inoculation.

A detrimental effect of adding inert microcarriers was also apparent during the growth stage. In the absence of inert microcarriers, the culture at 150 RPM grew to 45% of the maximum density observed in the control culture at 35 RPM. As inert microcarriers were added, growth progressively decreased until the culture with 30 g/l exhibited only 8% of the maximum density of the control. At high levels of agitation, the observed growth rates were clearly reduced through the addition of inert microcarriers.

5B. Cell Death through Microcarrier Collisions

Because microcarriers are very small and nearly neutrally buoyant, they will primarily follow fluid streamlines. Almost all relative motion between two neighboring microcarriers will arise from the action of turbulent eddies. The viscous forces or pressure fluctuations from a single eddy might throw two neighboring microcarriers against each other. The volumetric frequency of such collisions, f_c, would be second order in microcarrier concentration, C_m, and would thus be given by:

$$f_c = K_2 C_m^2 \qquad \text{(Eq. 55)}$$

where K_2 is a collision frequency constant. The amount of cell death from each collision will be proportional to the cells per unit surface

area, Ψ, and the effective surface area exposed to each collision, K_3. If a cell in an exposed area had a probability K_4 of death from each collision, the volumetric rate of cell death from collisions, $(dC/dt)_{coll.}$, would be then be given by

$$(dC/dt)_{coll.} = - (K_2 K_3 K_4) \Psi_m C_m^2 = - q_2 C_m C \qquad \text{(Eq. 56)}$$

where C is volumetric cell concentration. The specific death constant, q_2, represents the combined product of the parameters K_2, K_3, and K_4 divided by the total surface area per microcarrier, K_5, or $4\pi r_p^2$.

As all three parameters K_2, K_3, and K_4 will vary with the level of agitation and the strength of the hydrodynamic forces involved with the collision, the combined term q_2 should be a function of the level of agitation and fluid viscosity. For mild agitation, there was no effect of adding inert microcarriers, and thus the value of q_2 was zero. In general, the value of q_2 will depend not only on hydrodynamic variables, but also on the cell and microcarrier properties.

If the eddy-length model is now extended to include cell death from microcarrier collisions, the attached (or viable) cell concentrations should follow the equations

$$\frac{dC}{dt} = \mu C \qquad \text{with mild agitation} \qquad \text{(Eq. 57)}$$

$$\frac{dC}{dt} = \mu C - q_1 C - q_2 C_m C \qquad \text{with strong agitation} \qquad \text{(Eq. 58)}$$

where the criteria for cell death involves the level of agitation and

may not be a simple function of Kolmogorov eddy length. If cell damage occurred from a microcarrier collision, and if one of the microcarriers was an inert microcarrier with no cells, the resulting damage should be, on average, half of that which would occur if both microcarriers had cells. Thus, if inert microcarriers are added at high levels of agitation, equation 58 should be extended to

$$\frac{dC}{dt} = \mu C - q_1 C - q_2 C_m C - (q_2/2) C\, C_i \qquad \text{(Eq. 59)}$$

where C_i is the concentration of inert microcarriers.

To evaluate whether microcarrier collisions are important at high levels of agitation, one can analyze the data shown in Figure 38. If the model presented in equation 59 is correct, the data should follow the relation

$$\mu_{obs} = b - (q_2/2) C_i \qquad \text{(Eq. 60)}$$

where

$$\mu_{obs} = \left(\frac{1}{C} \frac{dC}{dt} \right)_{avg} \qquad \text{(Eq. 61)}$$

and with constant q_1, C_m, and average μ

$$b = \text{constant} = \mu - q_1 - q_2 C_m \qquad \text{(Eq. 62)}$$

If there is a second order damage mechanism, and if all first order mechanisms are relatively independent of microcarrier concentration, the observed growth rate should decrease in a linear fashion with the inert microcarrier concentration. The rate of damage from the second order

mechanism(s) (involving the inert microcarriers) should be proportional to the slope. The rate of damage from the first order mechanism(s) should be proportional to the difference between the intercept, b, and the value of $(\mu - q_2 C_m)$.

Figure 39 shows the average growth rate observed after attachment versus the inert microcarrier concentration. The data follows the predictions of equations 60-62 and clearly indicates that there are at least two distinct death mechanisms. One mechanism is second order in microcarrier concentration and thus involves microcarrier collisions. The other mechanism is first order in microcarrier concentration and involves microcarrier-eddy encounters.

For the cultures at 150 RPM, the bulk kinematic viscosity was increased through the addition of inert microcarriers. According to the power number correlations presented in the Materials and Methods section, the culture with 30 g/l inert microcarriers should have had an average power input 25% higher than the culture with no inert microcarriers at 150 RPM. This would have apparently resulted in a 18% increase in q_1 and an (as yet) undetermined increase in q_2. This effect may have introduced minor errors in the calculations of q_1 and q_2 from equations 60-62.

The linearity of the data in Figure 39 does not strictly prove that the first order mechanism was independent of microcarrier concentration. Nonetheless, the data follows a model which assumes this independence

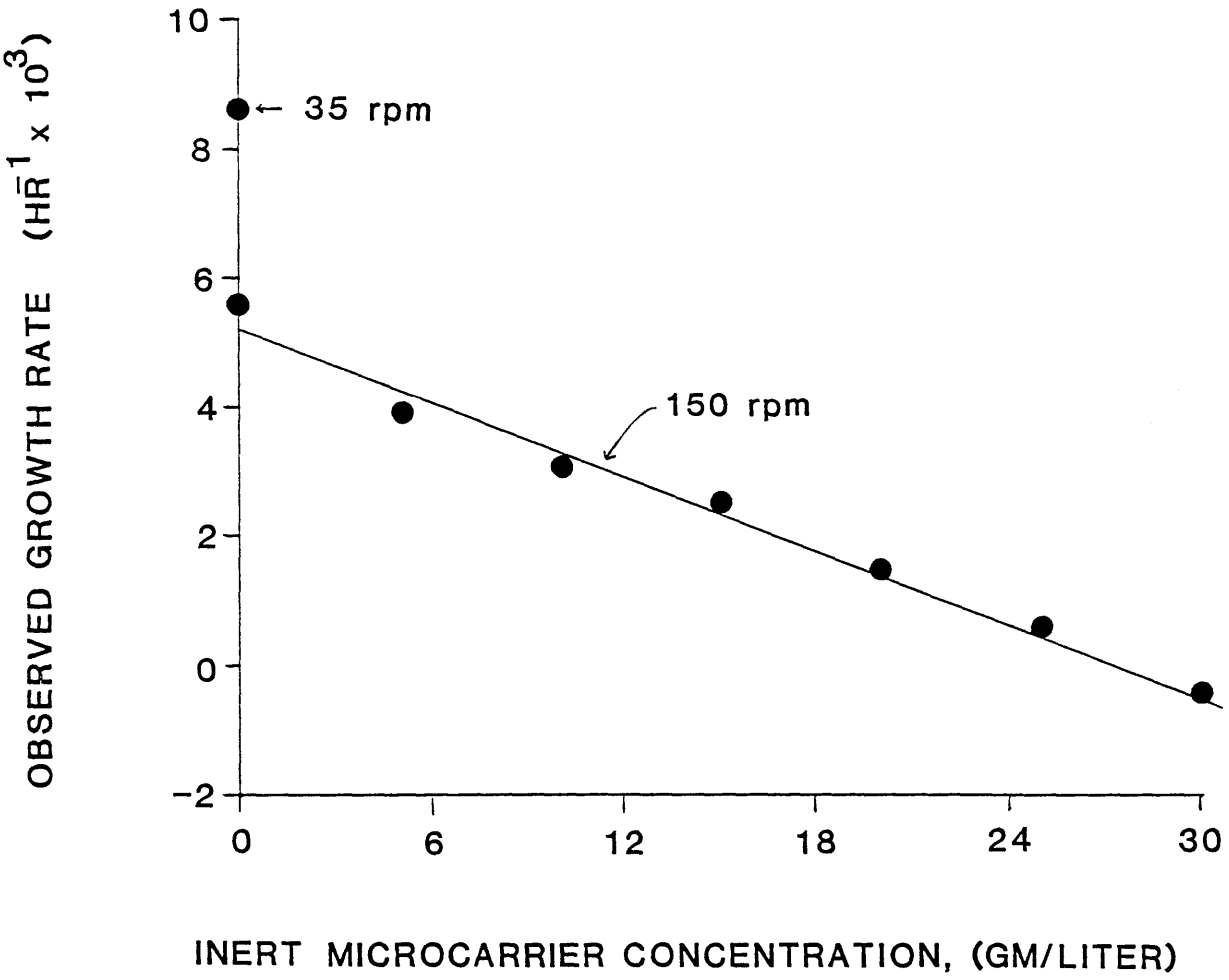

Figure 39. Observed specific growth rate vs. inert microcarrier concentration

over the range of concentrations investigated. The pertinent criteria is the rate of energy dissipation on the microcarrier surface. If microcarriers are added at constant speed, the power draw will go up, but so will the amount of energy dissipated by other microcarriers. The average energy dissipation rate on each microcarrier may remain relatively unchanged. Thus, the increased power draw from increased solids may be offset by the increased dissipation on the other microcarriers. This effect may account for the linearity of the data in Figure 39.

For the cultures at 150 RPM, the average spacing between the microcarrier surfaces ranged from 50 to 380 microns, while the average Kolmogorov length scales ranged from 50 to 60 microns. The average microcarrier spacing was greater than the average Kolmogorov length scale for all but the most concentrated culture.

In order for an eddy-microcarrier mechanism to be independent of microcarrier concentration, one might think that average spacing between the microcarrier surfaces would have to be greater than the smallest eddy diameter, or somewhat loosely, the Kolmogorov length scale. Strictly, however, the Kolmogorov length scale is not defined as an eddy diameter, but rather as the typical distance over which viscous dissipation occurs in the absence of solids. This subtle difference does not invalidate the logic behind the eddy-length model, but it should make one wary of comparing eddy lengths with the distance between microcarriers. For microcarrier-eddy interactions to be independent of

microcarrier concentration, it is not required that the microcarrier spacing is greater than the Kolmogorov length scale, but rather that the microcarrier spacing is greater than the distance over which viscous dissipation occurs when an eddy interacts with a microcarrier. This distance should be somewhat less than the Kolmogorov length scale, as the presence of solids is known to increase power dissipation (Hiemenz, 1977; Monin and Yaglom, 1971).

5C. Effects of Agitation Power on Cell Death from Collisions

To investigate the effects of agitation power on collision damage, cultures with inert microcarriers were grown in the 125-ml vessels. All cultures contained 3 g/l Cytodex 1 microcarriers, 15 g/l inert microcarriers, 5% FCS, and no dextran. All cultures were agitated at 35 RPM for a 44 hour attachment period. The cultures were subsequently agitated at various speeds during the growth period.

The results of the experiment are shown in Figure 40. The cultures at the higher stirring speeds, especially 140 and 200 RPM, exhibited lower viable cell concentrations than the control culture at 35 RPM. Extensive cell death from hydrodynamic forces occurred at the higher stirring speeds. The amount of death increased sharply with stirring speed; the culture at 200 RPM exhibited a strong and continual decrease in attached cell concentration. As shown by a comparison between Figures 29 and 40, the rate of death for the concentrated culture at 200 RPM far exceeded that for a dilute culture at 220 RPM in the same vessel. The difference was due to death from microcarrier collisions.

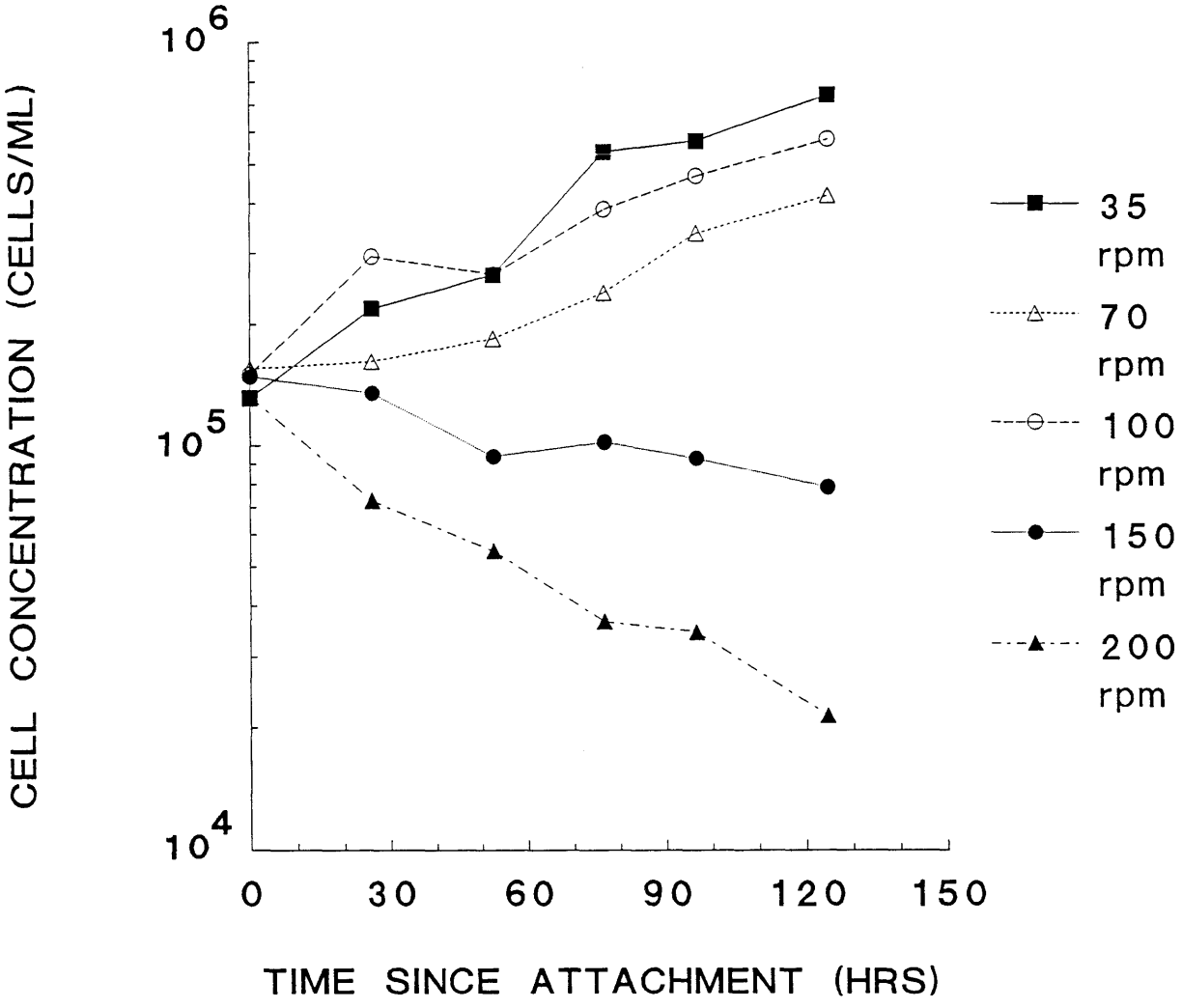

Figure 40. Net growth at different stirring speeds with 15 g/L inert microcarriers

The data in Figure 40 were analyzed to determine the relationship between the second order specific death constant, q_2, and average agitation power per unit mass. For each culture, the observed net growth rate, μ_{obs}, was calculated from a linear regression on the attached cell concentrations. For the cultures at high agitation, the total specific death rate q was calculated from the equation:

$$q = \mu - \mu_{obs} \qquad \text{(Eq. 63)}$$

where μ was the observed growth rate for the control culture at 35 RPM with no hydrodynamic death. The specific death rate due to microcarrier-eddy interactions, q_1, was calculated from the correlation derived for the dilute cultures in the 125-ml (6.3 cm) vessels, as shown in Figure 34. The collision death rate constant, q_2, was then calculated from the equation

$$q_2 = \frac{q - q_1}{C_m + C_i/2} \qquad \text{(Eq. 64)}$$

where the factor of 2 accounts for the lack of cells on the inert microcarriers. For each value of q_2, a 95% confidence interval was calculated according to the statistical methods presented in Walpole and Myers (1972). Because uncertainty in the value of q_2 arises from uncertainity in the values of both q and q_1, the total interval for each q_2 was estimated as the sum of the intervals for each q_t and q_1.

Figure 41 shows the collision death rate constant, q_2, versus the average agitation power per unit mass. The data scatters somewhat but indicates that q_2 increases with the level of agitation. The intercept

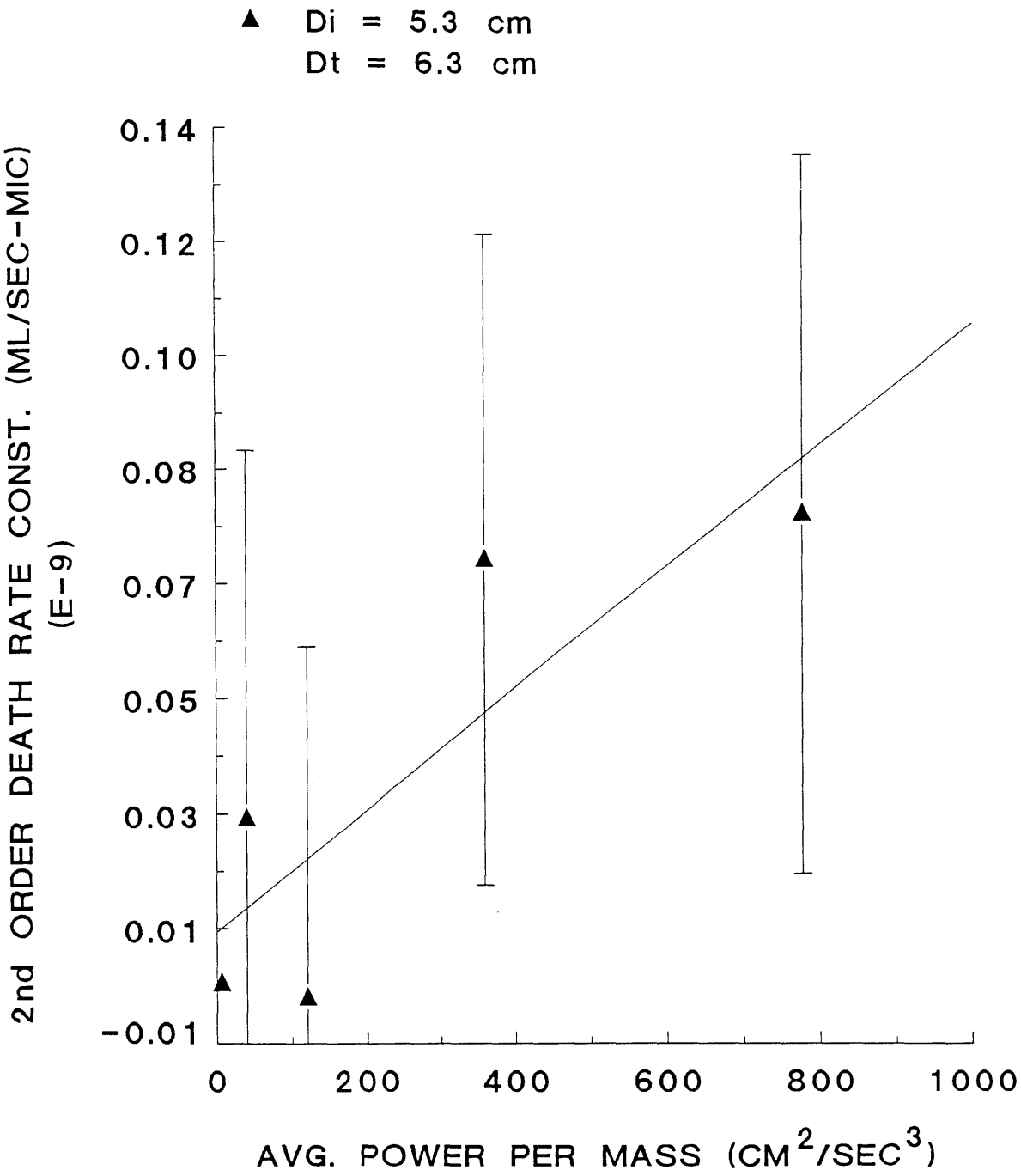

Figure 41. Second order death rate constant q_2 vs. average power input per unit mass

falls close to the value of zero, further verifying the observation of insignificant hydrodynamic death with mild agitation. The error bars represent the 95% confidence intervals for each data point. The combined uncertainty in the calculation of q and q_1 lead to tremendous uncertainty in the calculation of q_2. Almost any mathematical relationship which shows an increase between q_2 and ϵ can be drawn through the confidence intervals. For purposes of simplicity, the data has been graphed on arithmetic coordinates with a simple linear correlation. As determined through regression, the line has a correlation coefficient of 0.85.

5D. Effects of Fluid Viscosity on Cell Death from Collisions

To investigate the effects of fluid viscosity on collision damage, cultures with inert microcarriers were grown with various dextran supplements. To avoid cell damage from time-average flow fields, the 500-ml vessels were used with the 5.3 cm impellers. All five cultures contained 3 g/l Cytodex 1 microcarriers, 15 g/l inert microcarriers, and 5% FCS. All five cultures were grown at 60 RPM with no dextran supplement for a 33 hour attachment period. Four of the cultures were subsequently agitated at 190 RPM while one control culture continued to be agitated at 60 RPM. The four cultures at 190 RPM were supplemented with various levels of 78,500 MW dextran.

The results of the experiment are shown in Figure 42. All four cultures at 190 RPM exhibited lower viable cell concentrations than the control culture at 60 RPM. Extensive hydrodynamic death and removal

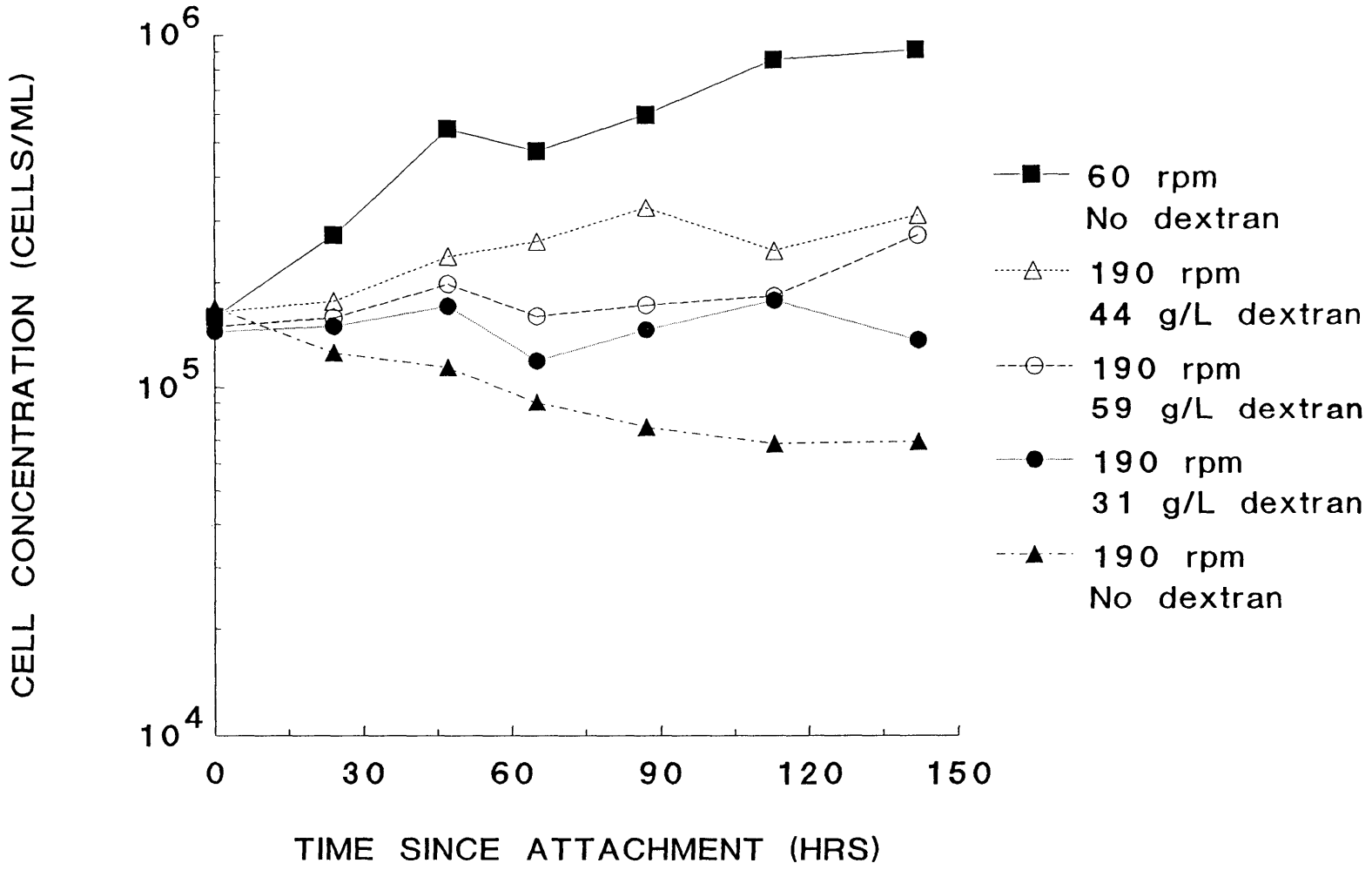

Figure 42. Effect of dextran (78,500 MW) on net growth at different stirring speeds with 15 g/L inert microcarriers

occurred at 190 RPM. The total rate of death was the greatest in the culture with no dextran but was moderately reduced with 31 g/l dextran and strongly reduced with 44 and 59 g/l dextran. As shown by a comparison between Figure 30 and Figure 42, the rate of death in the concentrated culture with no dextran at 190 RPM far exceeded that for the dilute culture with no dextran at 185 RPM in the same vessel. The difference was again due to cell death from microcarrier collisions.

The data in Figure 42 were analyzed to determine the relationship between the collision death rate constant, q_2, and the kinematic fluid viscosity. For each culture, the specific death rate due to microcarrier-eddy interactions, q_1, was calculated from the correlation derived for the dilute cultures in the 500-ml (9.6 cm) vessels, as shown in Figure 34. The collision death rate constant, q_2, was calculated from the methods presented in section 5C. Due to differences in power inputs, the collision death rate constants were normalized by the average agitation power per unit mass.

Figure 43 shows the normalized collision death rate constant, q_2/ϵ, versus kinematic fluid viscosity. The data scatters somewhat but clearly indicates that q_2 decreases with the kinematic fluid viscosity. The error bars represent the 95% confidence intervals for each data point. Again, there was tremendous uncertainty in the calculation of q_2, and almost any mathematical relationship can be drawn through the confidence intervals. For the purpose of simplicity, the data was graphed on arithmetic coordinates with a simple linear regression. As

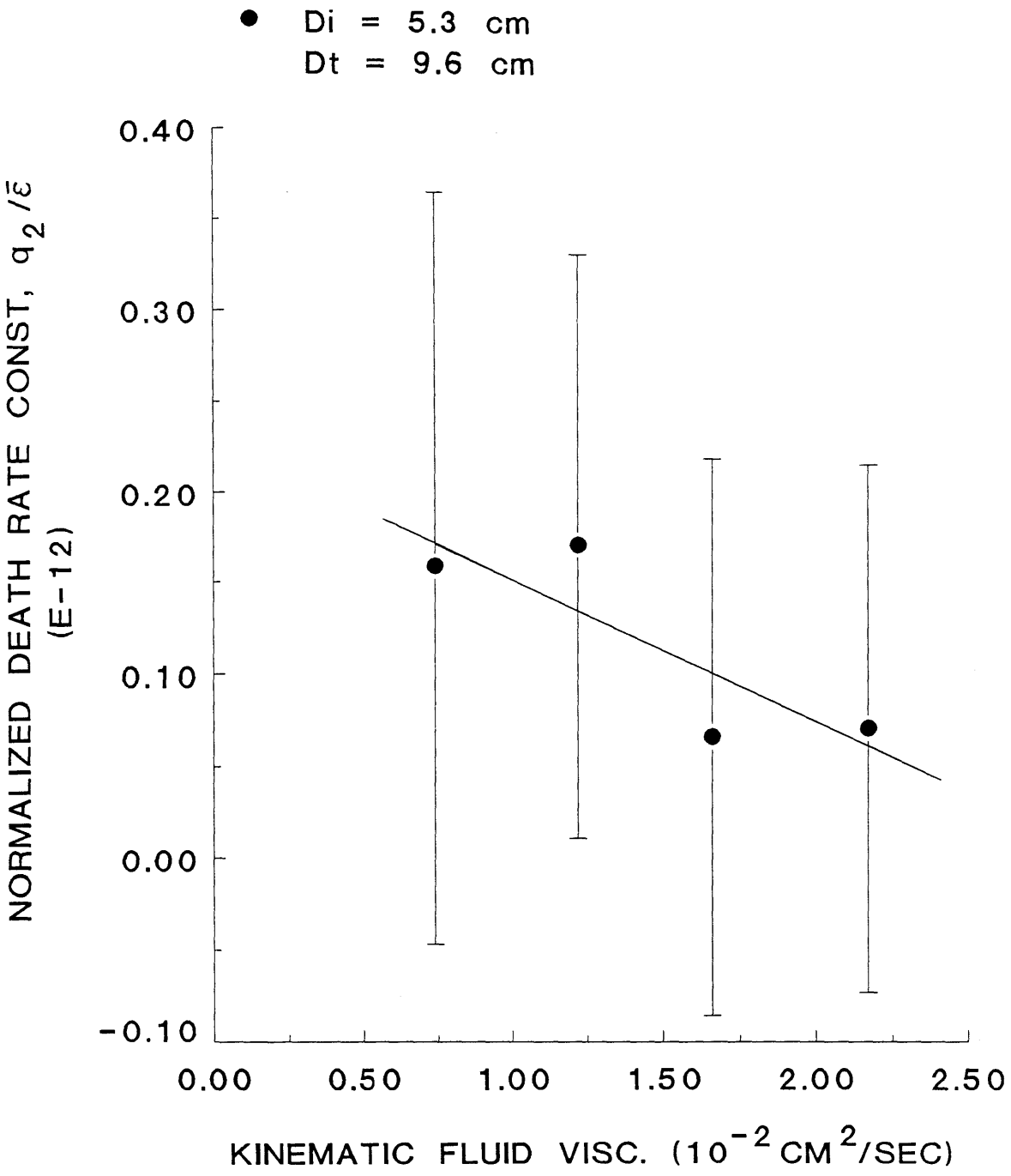

Figure 43. Normalized second-order death rate constant vs. kinematic fluid viscosity

determined through regression, the line has a correlation coefficient of 0.84.

Figure 44 shows the collision death rate constant, q_2, as a function of ϵ/ν for both the 125 and 500-ml vessels with the same impeller. The data scatters but clearly shows that q_2 increases with ϵ/ν. The regressed line has a correlation coefficient of 0.84/1.0. The data do not indicate a significant effect of vessel geometry. The regressed line through all of the data has an intercept near zero, further verifying the observation of insignificant cell death with mild agitation.

The collision death rate constant increased with the power input and decreased with the fluid viscosity. This indicates that microcarrier collisions arise through the action of turbulence in the fluid. The collisions may occur primarily through turbulent eddies which are of a size comparable to spacing between microcarriers. As discussed in Cherry and Papoutsakis (1986a), such eddies may lead to high relative velocities and collisions between neighboring microcarriers.

In microcarrier cultures, the eddies which are in or near the viscous dissipation regime are typically comparable in size to the spacing between microcarriers. It is likely that such high wave number eddies account for most of the cell death from microcarrier collisions. This hypothesis is supported by the lack of geometric effects observed in Figure 44. High wave number eddies exist in states of equilbrium

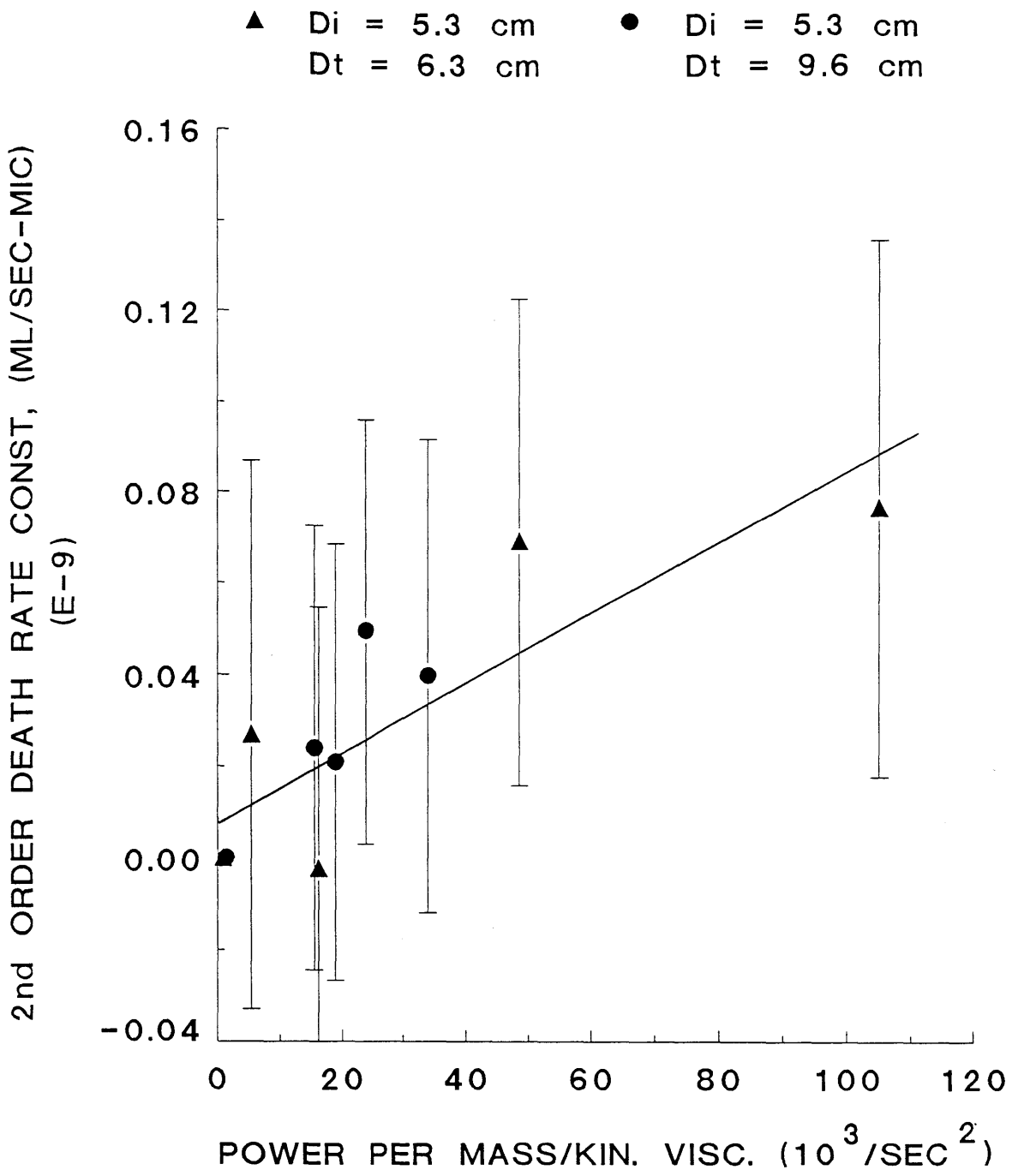

Figure 44. Second-order death rate constant vs. $(\bar{\varepsilon}/\nu)$

which are not strongly dependent on reactor geometry. Low wave number eddies and time-average flow fields are strongly influenced by reactor geometry.

CHAPTER 6. CELL DAMAGE FROM DIRECT SPARGING

6A. Effect of antifoam addition and direct sparging on cell growth

It is frequently stated that direct sparging causes damage to cells on microcarriers (Pharmacia, 1981; Spier and Griffiths, 1984). Nonetheless, no published reports were found which document such damage. Cell damage is known to occur from direct sparging of suspension cultures (Tramper et al, 1986; Handa et al, 1987). It is likely that damage occurs from direct sparging in microcarrier cultures. In fact, the damage may be more extensive in microcarrier cultures, given that the cells are immobilized and are more susceptible to mechanical forces.

The effect of sparging on cell growth was examined for FS-4 microcarrier cultures. As described in the Materials and Methods section, two experimental cultures were grown in 500-ml Bellco spinner flasks equipped with filter sticks for direct sparging. One experimental culture was sparged at a superficial gas velocity of 0.01 cm/sec with a 90:10 air-CO_2 mixture. Foaming was essentially eliminated through the daily addition of 20-40 ppm Medical Emulsion AF antifoam (Dow Corning, Midland, MI). A second experimental culture was grown with antifoam in an identical vessel, complete with filter stick, but with no sparging. A third experimental culture was grown with no antifoam, no filter stick, and no sparging in a 500-ml Corning vessel with a 7.8 cm impeller. All cultures contained 2.0 g/l microcarriers in DMEM with 5% FCS, were replenished with nutrients on the normal interval feeding basis, and were essentially at saturation with the 90:10 air CO_2 gas

mixtures.

Figure 45 shows the results of the experiment. Cell growth in the modified Bellco vessel with antifoam was essentially identical to cell growth in the Corning vessel with no antifoam. This indicates that the modifications to the Bellco vessel, including the presence of the filter stick, had no effect on cell growth. It also indicates that antifoam AF, at levels between 40 and 180 ppm, had no effect on cell growth. For tPA-CHO cells on microcarriers, Aunins et al (1986) similarly found no effect on cell growth from antifoam AF at 100 ppm.

For the culture which was directly sparged, the viable cell concentrations were lower than in the controls. This is evidence of significant cell damage from the sparging. The damage was clearly evident even though the superficial gas velocity was only 0.01 cm/sec and there was no significant foam formation. To my knowledge, this is the first published evidence of cell damage from sparging in microcarrier cultures.

Subsequent to the experiment described above, which covered the growth period up to 180 hours after inoculation, antifoam was no longer added to the sparged culture. A foam layer began to form at a rate of approximately 0.5 cm/day. After four days, nearly all of the microcarriers had collected on the vessel wall above the foam layer. Many microcarriers were spattered through bubble bursts into distant regions of the vessel. If one wishes to keep the microcarriers in the

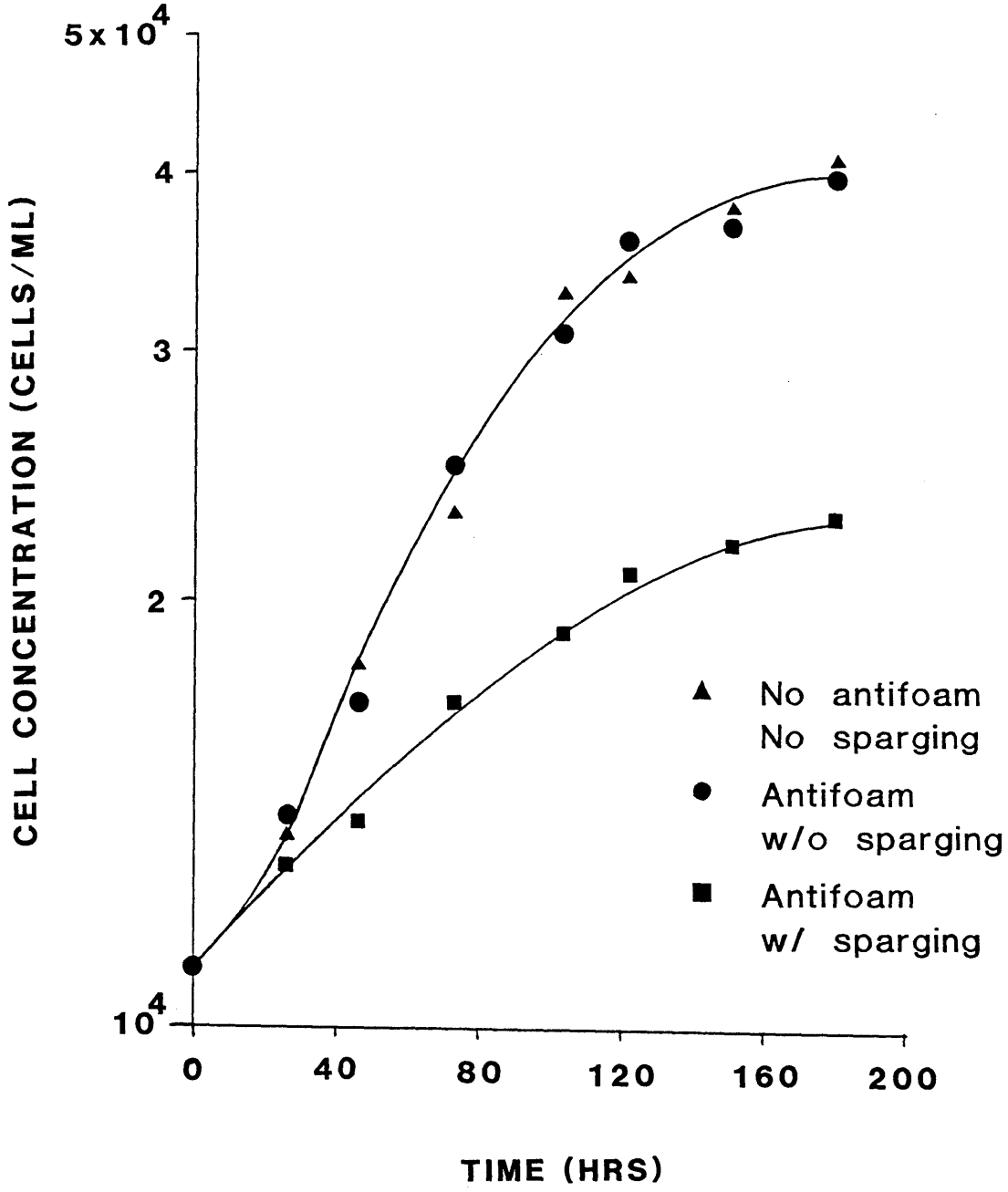

Figure 45. Effect of antifoam and sparging on net cell growth

liquid phase, foam formation must be strictly avoided.

6B. Mechanisms of Cell Damage from Sparging in Microcarrier Cultures

For suspension cultures, there has been considerable amount of research on cell damage from direct sparging. For microcarrier cultures, there has been little investigation. In the absence of foam formation, the mechanism of cell damage from sparging in microcarrier cultures is not clear. The possible mechanisms are listed below along with a review of the results for suspension cells:

1) Nutrient depletion. Required nutrients which are surface active, such as many proteins, could be adsorbed out of the fluid phase onto the bubble interface. These substances could be concurrently denatured or deactivated as they rose with the bubble or as the bubble burst at the culture surface. Aunins et al (1986) have shown that significant medium degradation can occur through direct sparging over a week long period. Such degradation may arise through protein denaturation at the liquid-gas interface.

2) Interfacial forces. Upon cell contact with a moving bubble interface, the cell membrane could spread and lyse, or non-integral membrane proteins, such as fibronectin, could be removed. If cell lysis did not occur upon initial contact, the cell may still adhere to the bubble and then lyse when the bubble bursts at the culture surface. Kilburn and Webb (1968) and Handa et al (1987) have found that damage of suspension cells from sparging is significantly reduced by adding surface active agents, such as Pluronic F-68. In general, surface active agents may form a shield between the cell

and bubble, and thus eliminate cell lysis or entrainment. It appears, however, that protection comes only from surface-active agents which are high in molecular weight (Kilburn and Webb, 1968).

3) Bubble bursts. Cells could be killed or damaged if they are directly exposed to the bubble bursts at the culture surface. Evidence for this mechanism has been given by Tramper et al (1986) and Handa et al (1987) for suspension cells. Tramper et al (1986) showed that cells caught in a bubble burst at the end of a pipette were damaged. For bubble columns, both Handa et al (1987) and Tramper and Vlak (1987) found that the volumetric rate of damage from sparging of suspension cells decreased with an increase in the height-to-diameter ratio. This is indicative of cell damage from bubble disengagement at the culture surface (Handa et al, 1987; Tramper and Vlak, 1987) or at the injector nozzle (Tramper and Vlak, 1987).

4) Hydrodynamic forces. Cells could be killed or damaged by hydrodynamic forces in the fluid adjacent to a rising or bursting bubble. This effect should increase with volumetric gas flow rate, but should decrease with fluid viscosity. An increase in viscosity should slow the bubble rise and dampen the turbulence in the fluid adjacent to the bubble.

For suspension cells, cell damage from sparging appears to be essentially unaffected by increase in fluid viscosity through dextran supplementation (Handa et al, 1987). Although the data is limited and not conclusive, it appears that damage of suspension cells from sparging

may not be hydrodynamic in nature. This is not surprising, as suspension cells are more than two orders of magnitude smaller than most bubbles and are relatively resistant to damage from hydrodynamic forces (Augenstein et al, 1972; Dodge and Hu, 1986; McQueen et al, 1987; Smith et al, 1987).

Cells on microcarriers, however, are much more sensitive to damage from hydrodynamic forces. A simple calculation readily illustrates that the damage observed from sparging in Figure 45 could have been hydrodynamic in nature. In the sparged culture, the bubbles rose in a column which occupied approximately 10% of the culture volume. As discussed in Aunins et al (1986), the power input to the liquid near bubbles may be approximated by the power required to match the buoyancy forces. Thus, for the sparged column region, the power input from sparging per unit mass of fluid, ϵ_s, may be roughly calculated by:

$$\epsilon_s = \frac{Q (\rho_f - \rho_b) g H}{\rho_f (H (\pi D_t^2/4) 0.1 - H_o)} \qquad \text{(Eq. 65)}$$

where ρ_b is the gas density, Q is the volumetric flow rate of gas in ml/sec, g is the gravitational acceleration, H is the reactor height, and H_o is the gas hold-up in the sparged region. The gas hold-up was estimated to be 20 ml from the increase in culture volume upon sparging.

Equation 65 was used to estimate a value of 100 cm^2/sec^3 for the local power input per unit mass in the sparged region. This is well into the range for which death occurs from impeller-generated power,

even with the mild viscosity increase brought about by the antifoam supplementation. Thus, the damage from sparging could have been due, at least in part, to power dissipation in the fluid adjacent to rising bubbles. Future research will hopefully elucidate the mechanisms and kinetics of cell damage from sparging in microcarrier cultures.

CHAPTER 7. BIOREACTOR DESIGN AND OPTIMIZATION

7A. Mass Transfer Requirements

In microcarrier cultures, agitation is required for cell-liquid mass transfer, gas-liquid mass transfer (oxygenation), and liquid phase mixing. As previously discussed, cell-liquid mass transfer can be approached with a Sherwood number analysis. For each chemical species which is consumed or produced by cells on microcarriers, the normalized gradient between the chemical concentration in the bulk medium, X_b, and the concentration at the cell surface, X_c, is given by

$$\frac{X_b - X_c}{X_b} = \frac{\Psi R_c d_p}{D_f X_b Sh_c} \qquad \text{(Eq. 66)}$$

where Ψ is the surface coverage in cells per unit area, D_f is the diffusion coefficient for the given chemical species, and R_c is the uptake rate per cell for the given chemical species. The Sherwood number for cell-liquid mass transport, Sh_c, is given by (Sano et al, 1974; Chaudhari and Ramachandran, 1980)

$$Sh_c = 2 + 0.4(\bar{\epsilon}\, d_p^4/D_f\, \nu^2)^{1/3} \qquad \text{(Eq. 67)}$$

where $\bar{\epsilon}$ is the average power input per unit mass and d_p is the microcarrier diameter.

In the design of a reactor, one might specify the chemical concentrations at the cell surface, or the acceptable gradients between the cell surface and bulk media. In general, as long as the

microcarriers are suspended (Sh_c = 2) and the viscosity has not been greatly increased, the gradients will be negligible.

Given negligible gradients between the cells and bulk fluid, one should also consider the requirements for adequate mixing in the liquid phase. Mixing is required to maintain appropriate chemical concentrations throughout the liquid phase in the reactor. In regions where chemicals are transferred into the liquid phase, mixing should be adequate to to eliminate cell damage from locally high concentrations. If acid or bases are directly added for pH control, mixing should be adequate to minimize the pH excursion and any corresponding cell damage. If pure oxygen is used for oxygenation, mixing should be adequate to limit the local concentration of dissolved oxygen, as dissolved oxygen levels in excess of normal air saturation are frequently toxic (Kilburn and Webb, 1968; Balin et al, 1976).

In general, the fluid should be circulated among the regions of nutrient supply and nutrient uptake. Adequate circulation is required not only to minimize the transients in regions where chemicals are added, but also to ensure that adequate nutrient levels are maintained in distant regions of the reactor. Oxygen is often the nutrient most susceptible to depletion. As oxygen is toxic in excess of air saturation, which represents a very low molar concentration, the oxygen content of the medium must be limited in the region where oxygen is supplied. For sufficiently high cell concentrations and low mixing rates, the limited oxygen content may be completely consumed before the

medium recirculates back to the region of oxygen supply.

Liquid phase mixing requirements are frequently analyzed in terms of mixing times. The mixing time represents the time required for a chemical to reach a homogeneous concentration throughout the reactor after it has been added at a single position. For many reactors in the fully-turbulent regime, the mixing time, M_t, for the fluid phase can be estimated from (McCabe et al, 1985):

$$M_t = \alpha 1 \, (H/D_i) \, (D_t/D_i)^2/N \qquad \text{(Eq. 68)}$$

where H is the liquid height, N is the impeller rotation rate, and $\alpha 1$ is a constant which is characteristic of the reactor and impeller geometry.

The mixing time generally represents the time required for about five complete circulations of the tank contents (McCabe et al, 1985). Thus, the time required for fluid element to circulate once around a reactor can be estimated as one-fifth of the mixing time given by equation 68. From this circulation time and the volumetric oxygen consumption rate, the variation in dissolved oxygen level between the oxygen supply and uptake regions of the reactor, ΔD_o, can be roughly estimated

$$\Delta D_o = \frac{R_o \, C \, M_t}{5} \qquad \text{(Eq. 69)}$$

where M_t is the mixing time given by equation 68, C is the viable cell concentration, and R_o is the specific oxygen uptake rate per cell. In

the design of a microcarrier reactor, one might specify the maximum ΔD_o based on the cell metabolism and any gradients in oxygen concentration between the cells and local medium. The agitation should then be sufficient to provide a ΔD_o less than the specified maximum.

Given adequate cell-liquid transport and liquid-phase mixing, one should also consider the overall transfer of nutrients and waste products into and out of the bulk fluid. Oxygen is generally the most difficult nutrient to supply, as it is consumed at a considerable rate by the cells and yet is only sparingly soluble in cell culture medium. Nearly all other nutrients and waste products are highly soluble in aqueous solution; adequate levels can be easily maintained through perfusion (Nahapetian, 1986) or medium exchange. Oxygen can also be supplied through continuous perfusion and recycle through an external oxygenator, also this technique requires high recirculation rates and cell immobilization. For normal microcarrier cultures in a stirred tank, the perfusion techique is not a viable means of supplying oxygen.

Oxygen is generally supplied through continuous mass transfer between the bulk fluid and a gas phase. The volumetric rate of oxygen transfer, N_o, is generally described by an equation of the form:

$$N_o = K_L a \, (D_o^* - D_o) \qquad \text{(Eq. 70)}$$

where K_L is the overall oxygen transfer coefficient, a is the interfacial gas-liquid surface area per unit culture volume, D_o^* is the dissolved oxygen concentration in equilibrium with the gas phase, and D_o

is the average dissolved oxygen concentration in the bulk media. At steady state, the volumetric oxygen transfer rate will equal the volumetric oxygen consumption rate, and thus

$$R_o C = K_L a (D_o^* - D_o) \qquad \text{(Eq. 71)}$$

where R_o is the specific oxygen uptake rate per cell and C is the viable cell concentration.

In the design of a microcarrier bioreactor, one might specify the maximum partial pressure of oxygen in the gas phase and the average concentration of dissolved oxygen in the bulk medium. The partial pressure of oxygen in the gas phase, P_o, will specify the equilibrium value D_o^* in the liquid from the typical Henry's Law relation

$$D_o^* = P_o \beta \qquad \text{(Eq. 72)}$$

where β is the Henry's Law coefficient. In setting the gas phase composition or equilbrium value D_o^*, one should consider the level of mixing near the gas phase and the toxic effects of dissolved oxygen levels above air saturation. In setting the average concentration of dissolved oxygen in the bulk medium, one should consider the desired concentration at the cell surface, the variation in dissolved oxygen between different regions of the vessel, and gradient in dissolved oxygen between the cells and local fluid.

Specification of D_o and D_o^* sets the driving force for oxygen transfer. The maximum cell concentration is then determined by the

values of R_o and K_La. If surface aeration is employed, the value of K_La is generally given by equations of the form (Aunins et al, 1987; Oldshue, 1983):

$$K_L a = K_s a_s = (Sh_s D_{f,o}/D_t)(1/H) \qquad \text{(Eq. 73)}$$

where $$Sh_s = \alpha 2\ (Re)^{\delta 1}(Sc)^{\delta 2}(Fr)^{\delta 3} \qquad \text{(Eq. 74)}$$

$$Re = N D_i^2/\nu_b \qquad \text{(Eq. 75)}$$

$$Sc = \nu/D_{f,o} \qquad \text{(Eq. 76)}$$

$$Fr = N^2 D_i/g \qquad \text{(Eq. 77)}$$

where $\alpha 2$, $\delta 1$, $\delta 2$, and $\delta 3$ are empirical constants, Sh_s is the Sherwood number for surface aeration, K_s is the oxygen transfer coefficient for surface aeration, a_s is the gas-liquid surface area per unit culture volume as given by the reciprocal of the liquid height H for surface aeration, Re is the impeller Reynold's number, Sc is the Schmidt number, Fr is the Froude number, $D_{f,o}$ is the diffusion coefficient for oxygen, D_i is the impeller diameter, D_t is the tank diameter, N is the impeller rotation rate, ν is the kinematic fluid viscosity, ν_b is the kinematic suspension viscosity, and g is the acceleration due to gravity. If the tank is fully baffled, the effect of Froude number becomes negligible and $\delta 3$ is essentially zero.

Aunins et al (1986) have investigated surface aeration in baffled cell culture reactors containing medium with 10% serum and no thickening

agents. From their results, one can determine a value of 0.61 for $\alpha 2$ and 0.73 for $\delta 1$. The value of $\delta 2$ is generally considered to be 0.33 (Aunins et al, 1986).

If oxygen is supplied through both silicone tubing and surface aeration, the value of $K_L a$ is determined by the sum:

$$K_L a = K_s a_s + K_t a_t \qquad \text{(Eq. 78)}$$

where $K_s a_s$ represents the contribution from surface aeration, as given by equation 73-77, and $K_t a_t$ represents the contribution from silicone tubing aeration, as determined by the tubing mass transfer coefficient, K_t, and the tubing surface area per unit culture volume, a_t. For baffled cell culture reactors which are geometrically similar, the tubing mass transfer coefficient is given by an equation of the form (Aunins et al,1986):

$$1/K_t = c + \alpha 3 \, (d_t/D_{f,o}) \, (Re)^{-\delta 4} (d_t/D_t)^{-\delta 5} (Sc)^{-\delta 6} \qquad \text{(Eq. 79)}$$

where $\alpha 3$, $\delta 4$, $\delta 5$, and $\delta 6$ are empirical constants, c is the conduction resistance through the tubing wall, d_t is the tubing diameter, D_t is the tank diameter, $D_{f,o}$ is the diffusion coefficient for oxygen in the medium, Re is the impeller Reynold's number as given by equation 75, and Sc is the Schmidt number as given by equation 76. Aunins et al (1986) have found values of 0.055 for $\alpha 3$ and 0.69 for $\delta 4$, and have estimated values of 0.53 for $\delta 5$ and 0.33 for $\delta 6$. For 0.03 cm silastic silicone tubing, the value of c was estimated to be 140 sec/cm.

7B. Basic Principles in Bioreactor Design and Optimization

The design of bioreactors is a classic chemical engineering optimization problem. Upon scale-up, the maximum cell concentration will be determined by the effects of several independent variables, such as the microcarrier concentration, fluid viscosity, level of agitation, and sparging rate. An increase in microcarrier concentration will provide more surface area for growth; however, it may also lead to more cell death from collisions. An increase in fluid viscosity will reduce hydrodynamic death, but will also reduce mass transfer. An increase in agitation will increase mass transfer, but may also increase hydrodynamic death. An increase in sparging rate will increase mass transfer, but may also lead to more cell death. In general, there will be a trade-off between mass transfer and hydrodynamic death.

To accurately incorporate these trade-offs in bioreactor design, one needs quantitative expressions for the rates of mass transfer and hydrodynamic death. In the previous section of this chapter, quantitative expressions for the rates of mass transfer were reviewed. In this thesis, quantitative expressions for the rates of hydrodynamic death in microcarrier cultures have been derived for the first time. The cell population kinetics have been found to follow the expression:

$$\frac{dC}{dt} = \mu C - q_1 C - q_2 C_m C \qquad \text{(Eq. 80)}$$

$$q_1 = 6.2 \times 10^{-13} \left(\bar{\epsilon}/\nu^3\right)^{3/4} \qquad \text{(Eq. 81)}$$

$$q_2 = 7.6 \times 10^{-16} \left(\bar{\epsilon}/\nu\right) \qquad \text{(Eq. 82)}$$

where μ is the inherent growth rate and is independent of the level of agitation, q_1 is the first-order specific death rate in sec^{-1}, and q_2 is the collision death rate constant in micro/ml-sec. For low levels of agitation, hydrodynamic death is essentially insignificant, and the values of q_1 and q_2 are generally negligible.

Equations 81 and 82 describe the kinetics of cell death from microcarrier-eddy interactions and microcarrier collisions. These processes appear to involve high wave number eddies and appear to be relatively independent of reactor geometry. In contrast, cell damage from time-average flow fields is highly dependent on reactor geometry. Such damage appears to occur when the maximum shear stress on the microcarrier surface from time-average flow fields, τ_{max}, exceeds approximately 5-9 dyne/cm^2. This fact can be used as a criterion for the avoidence of cell damage from time-average flow fields.

Kinetic expressions for the rates of mass transfer and hydrodynamic death can be used to optimize the reactor performance according to many different objectives. The objective may be to minimize hydrodynamic death, maximize the yield of a given product on a given set of nutrients, or maximize the cell concentration and volumetric reactor productivity. In the most general sense, the overall objective will be to minimize the cost of production. As economies of scale will generally be significant, the kinetic expressions may find their greatest use in the design of large scale units.

To illustrate the use of the kinetic expressions, one might consider the problem of maximizing the cell concentration in a large scale bioreactor. In such bioreactors, the maximum cell concentration is frequently limited by the rate of oxygen transfer (Aunins et al, 1986). The oxygen limitation will occur as the cells grow and the dissolved oxygen level drops below a critical or minimally acceptable value. Specification of this minimum value, $D_{o,min}$, and the gas phase composition will specify the maximum driving force for oxygen transfer. Specification of the reactor geometry, agitation power input, and fluid viscosity will specify the value of K_La. At the point of maximum oxygen transfer, an oxygen balance gives:

$$R_o C_{max} = K_L a (D_o^* - D_{o,min}) \qquad \text{(Eq. 83)}$$

where R_o is the specific oxygen uptake rate and C_{max} is the maximum cell concentration which can be adequately supplied with oxygen.

For many cells, oxygen uptake is both growth and maintenance associated (Tyo and Wang, 1980; Goldstein, 1986). The specific oxygen uptake rate can generally be described by an equation of the form (Pirt, 1975):

$$R_o = \frac{\mu}{Y_{n/o}} + M_o \qquad \text{(Eq. 84)}$$

where $Y_{n/o}$ is the growth yield of cells on oxygen and M_o is the oxygen maintainence coefficient, or the specific oxygen uptake rate under no growth.

If the oxygen transfer capabilites of a reactor are utilized to their fullest extent, the maximum cell concentration given by the limitations of oxygen transfer will equal the maximum cell concentration given by the limitations of hydrodynamic death. This maximum cell concentration will be reached as the cells grow toward confluence and become contact inhibited. When the specific growth rate drops to a value equal to the total specific death rate, the rate of change in cell concentration will be zero, and the cells will have reached the maximum cell concentration:

$$\frac{dC}{dt} = 0 = \mu C - q_1 C - q_2 C_m C \qquad \text{(Eq. 85)}$$

or

$$\mu = q_1 + q_2 C_m \qquad \text{(Eq. 86)}$$

Substituting between equations 83, 84, and 86, one arrives at the result:

$$C_{max} = \frac{Y_{n/o} \; K_L a \; (D_o^* - D_{o,min})}{Y_{n/o} \; M_o + q_1 + q_2 \; C_m} \qquad \text{(Eq. 87)}$$

where C_{max} is the maximum cell concentration as determined by the rate of oxygen transfer and hydrodynamic death.

Equation 87 quantitatively sets forth the trade-off between oxygen transfer and hydrodynamic death. It specifies a quantitative relation for maximixing cell concentration. Through information on the rates of oxygen transfer and hydrodynamic cell death, equation 87 can be used to determine which reactor geometry, fluid viscosity, microcarrier

concentration, and level of agitation lead to the maximum cell concentration. These calculations must be performed, however, with consideration for the other mass transfer requirements. The agitation must be sufficient to suspend the microcarriers and provide adequate liquid-phase mixing.

As shown in Equation 87, an increase in oxygen transfer without a concurrent increase in hydrodynamic death will lead to a higher maximum cell concentration. For microcarrier cultures, hydrodynamic damage appears to involve only the smallest eddies, which are not strongly dependent on geometry. In contrast, mass transfer involves not only small eddies, but also large eddies, which are strongly dependent on geometry. By manipulating the effects of geometry on the large eddies, significant increases in mass transfer should be attainable without concurrent increases in hydrodynamic damage.

7C. Illustration of Optimization Calculations

To fully illustrate how bioreactor design can be approached as an optimization problem involving quantitative rate expressions, optimization calculations are described below for an FS-4 microcarrier culture. The optimum combination of agitation, microcarrier concentration, and fluid viscosity were determined for a given reactor. The objective was to maximize the maximum cell concentration. In general, such an optimization might be performed for a number of different reactor geometries. The geometry which leads to the highest maximum cell concentration would be chosen as the best.

The geometry of the reactor for this optimization is shown in Figure 46 and in Table 3. The reactor has a liquid volume of 100-liters and is equipped with baffles, a pitched-blade turbine (PBT), and a flat-blade turbine (FBT). The reactor is geometrically similar to the reactors which have been extensively studied by Aunins et al (1986). For this optimization, it was assumed that oxygen transfer came solely through surface aeration. The oxygen transfer coefficient is then given by equations 73-77 with $\alpha 2 = 0.61$, $\delta 1 = 0.73$, $\delta 2 = 0.33$, and $\delta 3 = 0$ (Aunins et al, 1986).

From the results of Bates et al (1963) and Rushton et al (1950), one can estimate a power number of 1 for the pitched-blade turbine and a power number of 4 for the flat-blade turbine, with both turbines in the fully-turbulent regime. The spacing between the turbines is less than 60% of their diameter. As such, the impellers may not operate independently. From the results in Richards (1963), one could estimate that the power draw would be only 80% of the value for independent operation. Thus, for operation in the complete turbulent regime, as required for microcarrier suspension, the average power input per unit mass, $\bar{\epsilon}$, was estimated by:

$$\bar{\epsilon} = 0.8\, N_p\, N^3\, D_i^5 / V_c \qquad \text{(Eq. 88)}$$

where N_p is the combined power number with an estimated value of five, V_c is the culture volume, and N is the impeller rotation rate, with all terms in cgs units.

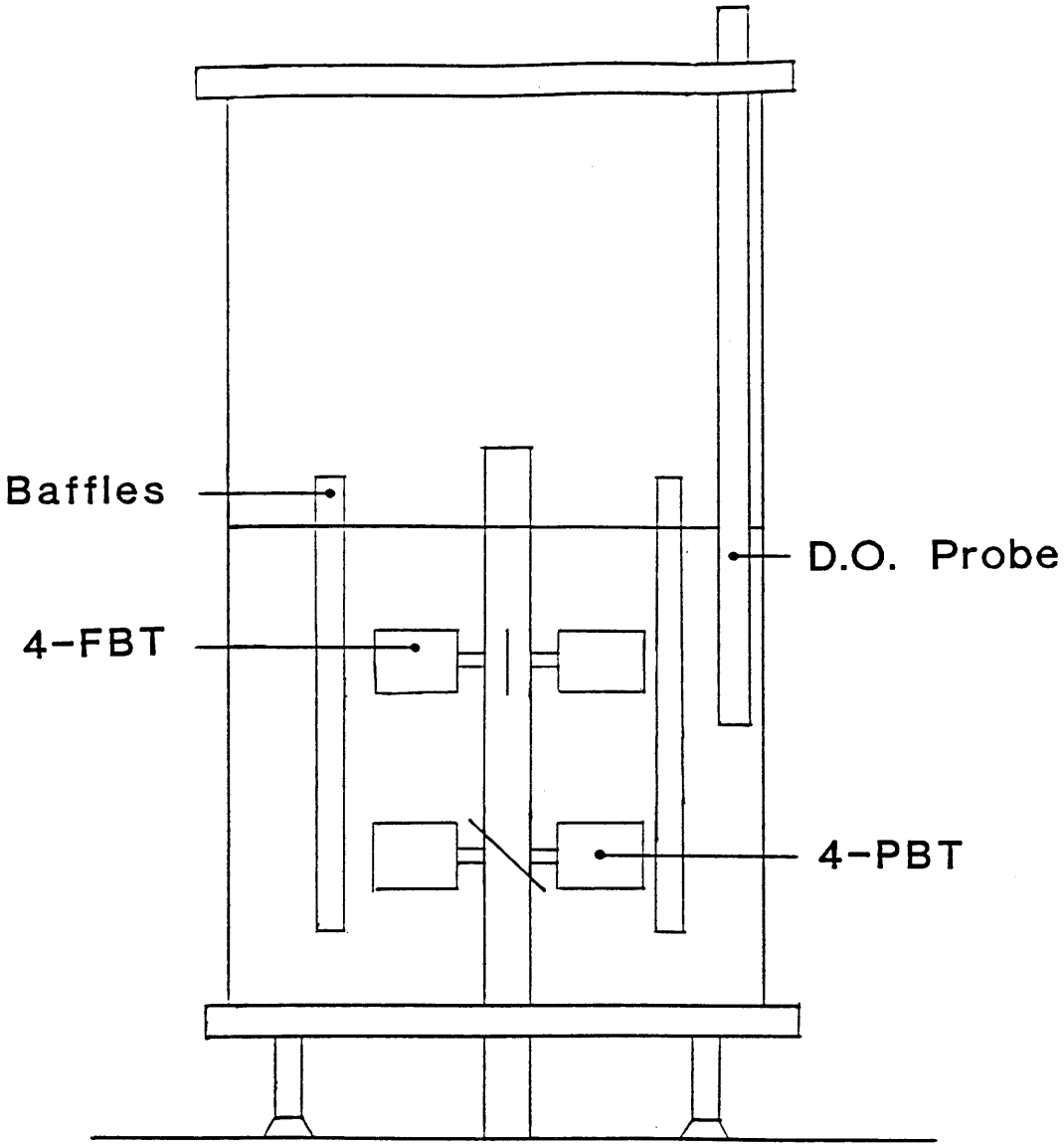

Figure 46. 100-Liter reactor with 4-bladed flat-blade turbine (4-FBT) and pitched-blade turbine (4-PBT)

TABLE 3. GEOMETRY OF 100-LITER BIOREACTOR

Dimension	Size (cm)
Tank diameter	53.3
Liquid height	44.8
Impeller diameter	26.7
Baffle width	6.1
Radius to baffle inner edge	15.6
Impeller blade width	8.0
Height of center of pitched-blade turbine	15.0
Height of center of flat-blade turbine	30.0

For the 10-liter reactor investigated by Aunins et al (1986), the minimum speed for complete microcarrier suspension was approximately 30 RPM (Goldstein, 1986) for medium with 10% serum, 10 g/l microcarriers, and no thickening agents. This correponds to an estimated value of 16 cm^2/sec^3 for the average power input per unit mass. Upon scale up to the geometrically-similar 100-liter reactor, the agitation power per unit mass required for suspension should be reduced according to the equation (Nienow, 1985):

$$(\bar{\epsilon}_1/\bar{\epsilon}_2) = (D_{i,2}/D_{i,1})^{0.28} \qquad \text{(Eq. 89)}$$

where $\bar{\epsilon}_1$ is the average power input per unit mass required for microcarrier suspension in the 10-liter reactor, $\bar{\epsilon}_2$ is the average power per unit mass required for microcarrier suspension in the 100-liter reactor, $D_{i,1}$ is the impeller diameter for the 10-liter reactor, and $D_{i,2}$ is the impeller diameter for the 100-liter reactor. From equation 89, one can estimate a minimum power per unit mass of 13 cm^2/sec^3 for complete microcarrier suspension in the 100-liter vessel with unthickened medium. From the results of Zweitering (1958), one can incorporate the minor effects of fluid viscosity and volume fraction solids on the power required for microcarrier suspension.

This optimization was performed under the criteria of adequate liquid-phase mixing and cell-liquid transport. The liquid phase mixing was considered adequate if the estimated variation in dissolved oxygen content, as determined from equation 69, was less than 2% of saturation with air. The cell-liquid transport was considered adequate if the

estimated normalized gradient in oxygen between the cells and local fluid, as determined from equation 66, was less than 0.10. The viscosity increase was limited so as to not introduce cell-mass transport limitations at a Sherwood number of two, or the minimum value for complete suspension.

Cell damage from time-average flow fields was easily avoided by limiting the viscosity increase. For all conditions investigated, the maximum shear stress on the microcarrier surface from time-average flow fields was less than 1 dyne/cm^2.

This optimization requires knowledge of the mathematical dependence of specific growth rate on cell and microcarrier concentration. For FS-4 cells, the mathematical dependence involves both the effects of contact inhibition and cell-derived growth inhibitors. The effect of contact inhibition on growth was incorporated with the following empirical equations which fit the data presented in Hu et al (1985) for FS-4 cells:

$$\mu = \mu_{max} \ (100 - Z)/60 \qquad \text{for } Z > 40 \qquad \text{(Eq. 90)}$$

$$\mu = \mu_{max} \qquad \text{for } Z \leq 40 \qquad \text{(Eq. 91)}$$

where Z is the percent confluence. The growth rate free of contact inhibition, μ_{max}, and the maximum surface coverage depend weakly on the volumetric cell concentration, as shown in Chapter 1. Because FS-4 cells are inoculated at a roughly constant number of cells per microcarrier, the weak dependence on volumetric cell concentration can

be roughly described by a empirical dependence on microcarrier concentration. For this optimization, the relevant range of microcarrier concentrations is between 5 and 15 g/l. For this range, the data in Figures 12-14 for 5% serum can be described by the empirical relations:

$$\mu_{max} = 4.3 \times 10^{-5} / C_m^{0.262} \qquad \text{(Eq. 92)}$$

$$Z = \frac{100\ C}{500\ (C_m)^{0.80}} \qquad \text{(Eq. 93)}$$

where C_m is the microcarrier concentration in microcarriers/ml, C is the cell concentration in cells/ml, μ_{max} is the maximum growth rate in sec^{-1}, and Z is the percent confluence.

This optimization was performed under the following assumptions:

1) the headspace gas contained a 90:10 air-CO_2 mixture,
2) the medium was supplemented with 5% (v/v) fetal calf serum
3) the diffusion coefficient for oxygen in unthickened medium with 5% serum was 2.5×10^{-5} cm^2/sec, as given in Reid et al (1977) for oxygen diffusion in water and corrected for minor temperature effects from the correlation of Wilke and Chang (1955)
4) the diffusion coefficent for oxygen was inversely proportional to fluid viscosity, as given by Wilke and Chang (1955)
5) the Henry's law coefficient for oxygen was 0.86 mM/L-atm (Fleischaker and Sinskey, 1981)
6) the minimum acceptable level of average dissolved oxygen in the

fluid was 10% of saturation with air. Below this value, oxygen can become growth-limiting (Miller et al, 1987; Balin et al, 1976).

7) the growth yield of cells on oxygen, $Y_{n/o}$, was 3.8×10^8 cells/mmole and the maintenance coefficient on oxygen, M_o, was 1.3×10^{-11} mmole/cell-hr. The estimation of these values is described in Appendix 2.

After making the assumptions listed above, one has reduced the number of independent variables to two: fluid viscosity and average power input per unit. The optimization involves calculation of the maximum cell concentration for each combination of fluid viscosity and average power input. The combination which gives the highest maximum cell concentration would be chosen as the optimum.

For each combination of fluid viscosity and agitation power, calculation of the maximum cell concentration and the corresponding microcarrier concentration involved an iterative procedure. At the maximum cell concentration, the specific growth rate, μ, should equal the total specific death rate, $q_1 + q_2 C_m$. For each value of fluid viscosity and agitation power, the values of q_1 and q_2 were calculated from equations 81 and 82. If one then guesses a value for the microcarrier concentration, the maximum cell concentration can be determined from equation 87, and the corresponding specific growth rate can be determined from equations 90-93. This procedure can be repeated until the specific growth rate given by equations 90-93 is equal to the total specific death rate, $q_1 + q_2 C_m$. The corresponding maximum cell

concentration represents the solution to the iteration.

After having calculated the maximum cell concentration and microcarrier concentration, one can determine whether the criteria of adequate liquid mixing and cell-liquid transport were fulfilled. If they were not, the agitation power should be increased until the criteria are fulfilled. For this optimization, the calculations were extended into a range of power levels far above the minimum values for adequate liquid mixing and cell-liquid transport.

Figure 47 shows the results of the optimization calculations. Maximum cell concentration is plotted against power input per unit mass. Calculations are shown for three different viscosities: normal medium (0.74 cp), and medium slightly thickened (0.92 and 1.09 cp). Maximum cell concentrations are shown only for power levels which are equal to or greater than the minimum power for complete microcarrier suspension. For this particular optimization, the agitation required for microcarrier suspension more than fulfilled the requirements for liquid mixing and cell-liquid transport.

The results in Figure 47 show some interesting trends. For all three viscosities, the maximum cell concentration initially rises as the agitation is increased above the minimum level for microcarrier suspension. These increases are due to increased oxygen transfer capabilities. The highest cell concentration is obtained with the lowest viscosity, again due to oxygen transfer capabilities. If the

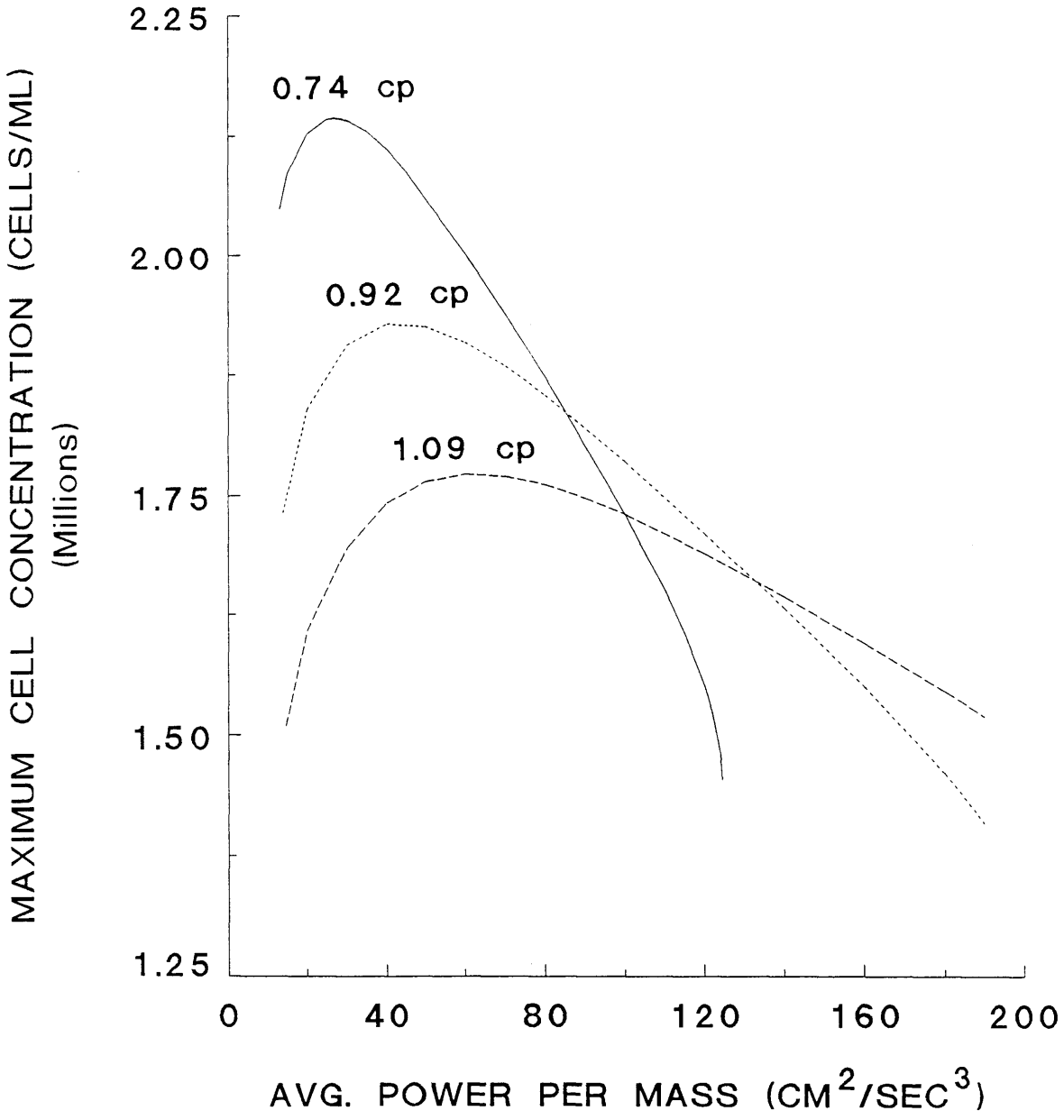

Figure 47. Estimated maximum cell concentration vs. average power input per unit mass at different fluid viscosities

agitation is increased above the optimum at the lowest viscosity, the maximum cell concentrations drop sharply. This is due to cell death from excessive agitation. Eventually, at a power input of approximately 125 cm^2/sec^3 for the viscosity of 0.74 cp, the specific death rate is greater than the maximum growth rate of the cells. The attached cell concentrations will decrease from the time of inoculation.

If the viscosity is increased above 0.74 cp, the curves become flatter and less sensitive to agitation. In general, an increase in viscosity leads to a reduction in both oxygen transfer and hydrodynamic death. For any given power input in a given reactor, there is an optimum viscosity. As the power input increases, the optimum viscosity increases. Higher viscosities allow for operation at higher power inputs.

For this particular optimization, the highest cell concentration was obtained with lowest viscosity. If this optimization was performed for a different reactor, or a different cell line, the highest cell concentration might be obtained with a slightly increased viscosity. The trends shown in Figure 47, however, would still be present. There would still be a trade-off between mass transfer and hydrodynamic death.

Protection through Polymer Adsorption and Viscoelasticity

As previously discussed in the Literature Review section, many investigators have used polymers to protect cells from fluid-mechanical disruption. The mechanism of this protective effect was not previously

identified. In light of the results presented in this thesis, it appears that the polymers may protect cells from turbulent damage by increasing the medium viscosity. Although viscous reduction of turbulent damage most likely does account for some of the protection, it does not appear to fully account for all the results presented in the literature.

In many instances, a great degree of protection is observed, qualitatively, with very low polymer concentrations or viscosity increases. For instance, serum supplementation apparently provides a great deal of protection and yet increases the viscosity only a few percent. Methylcellulose supplementation, at a typical concentration of approximately 1 g/l and with a typical molecular weight of approximately 15000, also apparently provides a great deal of protection (Kuchler et al, 1960; Bryant, 1966; Holmstrom, 1968; Birch and Pirt, 1969) and yet leads to a viscosity increase of only 18%. For a dilute microcarrier culture, an 18% viscosity increase would provide only a 31% reduction in hydrodynamic death. It is difficult to say whether a 31% reduction accurately represents the qualitative results presented in the literature. It appears, however, that the protection provided by some polymers is more than would be expected through only viscous reduction of turbulent damage.

The mechanism of the protective effect is therefore open to more investigation. Kuchler et al (1960), Bryant (1966), and Mizrahi (1984) have hypothesized that the polymers adsorb onto the cells and form a

protective shell. This adsorption would occur along with a concurrent reduction in polymer concentration in the culture supernatant. For methylcellulose, Bryant (1966) observed a steady decrease in the culture viscosity, potentially indicating polymer attachment onto the cells. For carboxymethylcellulose, hydroxyethyl starch, and pluronic polyols, Mizrahi (1984) found a clear protective effect even though over 99% of the added polymer remained in the supernatant. To my knowledge, no one has directly measured whether there is any adsorption of the polymers onto the cells. From the data currently available, the protective shell hypothesis is neither directly supported nor refuted.

Another mechanism of protection may involve viscoelastic interactions between the polymers and the turbulent flow fields. As discussed in the Materials and Methods section, these interactions can occur even with very low polymer concentrations. In the experiments presented in this thesis, low molecular weight dextrans were used as the thickening agents. Viscoelastic interactions were purposefully avoided to isolate the effects of viscosity. For some of the protective polymers, such as methylcellulose and carboxymethylcellulose, viscoelastic behavior has been reported (Amari and Nakamura, 1973, 1974; Hoyt, 1985).

There is great potential behind the use of viscoelasticity to protect cells from turbulent damage. For microcarrier cultures, hydrodynamic damage appears to involve only the smallest eddies while mass transfer involves both small and large eddies. If viscoelastic

polymers are added that interfere with the small eddies but not the large eddies, a strong decrease in hydrodynamic damage may be attainable without a concurrently strong decrease in mass transfer. The viscoelastic polymers should have a characteristic relaxation time equivalent to the burst duration for the smallest eddies. Such polymers might not strongly interfere with the mass transfer processes, as indicated by the results of Quraishi et al (1977). New experiments should be performed to investigate the use of viscoelasticity in protecting cells from turbulent damage.

SUMMARY AND CONCLUSIONS

In this thesis, a fundamental and quantitative approach has been initiated toward the design of microcarrier bioreactors. The effects of hydrodynamic forces on cell growth and death were studied under conditions of both mild and high agitation. With mild agitation, there was no significant hydrodynamic death. Growth was not affected by changes in fluid viscosity, inert microcarrier concentration, or level of agitation, and thus appeared to be unaffected by the hydrodynamic environment per se. With high agitation, a reduction in net growth was observed and was found to be entirely due to cell death and removal and not growth inhibition. Cell growth was still unaffected by the hydrodynamic enviroment per se.

For FS-4 cultures, cell removal from excessive agitation was irreversible and lethal. Secondary growth did not occur over areas from which cells had been previously removed. In γ-CHO cultures, cell removal from excessive agitation was frequently reversible and not lethal. Secondary growth readily occurred over areas from which cells had been previously removed. In fact, cell growth was stimulated as areas were left void through hydrodynamic cell removal. For a moderate level of agitation, the secondary growth was fast enough to overcome any reduction in attached cell concentrations from hydrodynamic death or removal. Secondary growth can clearly lead to reduced hydrodynamic sensitivity.

The mechanisms of hydrodynamic damage were investigated with FS-4 cultures. Through experiments on the effects of fluid viscosity, microcarrier concentration, and agitation power, cell death in microcarrier bioreactors was found to occur through microcarrier-eddy interactions, microcarrier collisions, and, in unusual circumstances, time-average flow fields. Microcarrier-eddy interactions were predominant in dilute cultures and led to cell death when the turbulence generated eddies which were smaller than the microcarriers. For dilute cultures, the specific death rate was found to be proportional to the concentration of eddies in the viscous dissipation regime. For both dilute and concentrated cultures, cell death was found to increase with agitation power and decrease with fluid viscosity.

A quantitative expression was derived which related the cell population kinetics to the microcarrier concentration, kinematic viscosity, and agitation power. The expression included the contributions from cell growth, which was not a function of hydrodynamic environment, and cell death from both microcarrier-eddy interactions and microcarrier collisions. The kinetic expression was used to quantify the trade-off between hydrodynamic cell death and oxygen transfer upon scale-up. An illustration was presented to show how bioreactor design can be approached as an optimization problem involving quantitative rate expressions.

RECOMMENDATIONS FOR FUTURE RESEARCH

The results in this thesis point to several interesting areas for future research. The topics have been discussed throughout the thesis and include:

1) Effects of normal forces on animal cells.

In many cell culture bioreactors, the flow field is turbulent. The cells are exposed not only to shear forces, but also to normal forces. To optimize bioreactor designs, it is important to understand the effects of normal forces on cells. A literature survey indicates that the effects of well-defined normal forces on animal cells have not been investigated. The undiscovered role of normal forces may account for the typically poor agreement between shear effects in laminar flow fields and global hydrodynamic effects in turbulent stirred tanks, such as reported by Rosenberg et al (1987). For cell removal from microcarriers, the observed lack of selectivity for mitotic cells may indicate that cell removal occurs primarily through normal forces.

2) Effects of reactor geometry on the kinetics of hydrodynamic death.

In this thesis, hydrodynamic phenomena were correlated with average power input per unit mass. The results did not indicate a strong effect of reactor geometry on the kinetics of hydrodynamic cell death, although a limited number of reactor geometries was investigated. Future

research should investigate a wider range of reactor geometries and should incorporate quantitative information on local rates of power dissipation. The kinetics of mass transfer should be considered along with the kinetics of hydrodynamic death. For microcarrier cultures, hydrodynamic death appears to involve only the smallest eddies, which are not strongly dependent on geometry. In constrast, mass transfer involves not only small eddies, but also large eddies, which are strongly dependent on geometry. Suspension of the microcarrier also involves large eddies and is again strongly dependent on reactor geometry (Nienow, 1985). If the effects of geometry on the large eddies are manipulated, high rates of mass transfer should be obtainable without high rates of hydrodynamic death.

3) Microscopic fluid flow fields.

In this thesis, the hydrodynamic forces experienced by the cells in microcarrier cultures were calculated in only an approximate manner. Future research should more precisely determine the magnitude and direction of the forces experienced by the cells. This will require extensive modelling of the microscopic flow fields which arise in microcarrier-eddy interactions and microcarrier collisions. The most thorough models might incorporate the protrusion of the cells into the flow field along with the mechanics of cell deformation. The results of these models will allow for more a more precise and thorough approach to bioreactor design and optimization.

4) Reversible cell removal and secondary growth.

For γ-CHO cultures, cell removal from excessive agitation was frequently reversible and non-lethal. Secondary growth readily occurred over areas from which cells had been previously removed. For FS-4 cultures, in contrast, cell removal was irreversible and lethal, and secondary growth did not occur. At a moderate level of agitation, the secondary growth in the γ-CHO cultures was fast enough to overcome any reduction in attached cell concentrations from hydrodynamic death and removal. Secondary growth thus led to reduced hydrodynamic sensitivity and may have occured because the cells were removed whole. Such reversible removal may have been related to the attachment properties of the aneuploid γ-CHO cells. Future research should be performed to more thoroughly elucidate the nature of cell removal and its relation to secondary growth.

5) Hydrodynamic effects on cell metabolism.

Industrial animal cell culture will frequently be used for the production of proteins. The performance of these industrial processes will depend not only on the cell concentration and growth rate, but also on the cell metabolism. It is therefore important to understand the hydrodynamic effects on both cell metabolism and cell growth. In this thesis, the hydrodynamic effects on cell growth were investigated. The growth of the cells appeared to be neither inhibited nor enhanced by hydrodynamic forces. The metabolic events required for growth were therefore not significantly altered by agitation. Nonetheless, all

metabolic events which were not growth associated could have been influenced by agitation. In fact, the specific glucose uptake rate was not growth associated and was significantly reduced at high levels of agitation. There are numerous other limited but interesting results regarding hydrodynamic effects on cell metabolism, as discussed in the Literature Review section. Future research will hopefully extend the current information on the hydrodynamic effects of cell metabolism.

6) Mechanisms of cell damage from direct sparging.

For microcarrier cultures, and for many suspension cultures, direct sparging can often lead to extensive cell damage. One should not, however, prematurely rule out the potential usefulness of direct sparging. Direct sparging potentially represents a simple and inexpensive method for oxygenation of large-scale cell culture reactors. If the mechanisms of cell damage from sparging are elucidated, a viable sparging technique may become apparent. In general, the use of sparging should be considered in light of the trade-off between oxygen transfer and cell death. The kinetics of cell damage from sparging should be quantitatively described along the kinetics of oxygen transfer. The kinetic expressions can be used to determine the sparging conditions and reactor design which lead to optimum performance. If cell damage from bubbles involves turbulence, the use of thickening agents or viscoelastic polymers may reduce the amount of damage.

7) Viscoelastic reduction of hydrodynamic death.

Polymers are frequently added to cell culture medium to protect cells from fluid-mechanical disruption. The mechanism of protection may involve viscoelastic interactions between the polymers and turbulent flow fields. In general, there is great potential behind the use of viscoelastic agents for the reduction of hydrodynamic death from turbulence. Hydrodynamic damage appears to involve only the smallest turbulent eddies, while mass transfer involves both the small and large eddies. If viscoelastic polymers are added that interfere with the small eddies but not the large eddies, a strong decrease in hydrodynamic death should be attainable without a concurrently strong decrease in mass transfer.

NOMENCLATURE

Roman

a	gas-liquid interfacial area per unit culture volume, cm^{-1}
a_s	culture surface area per unit culture volume, cm^{-1}
a_t	silicone tubing surface area per unit culture volume, cm^{-1}
A	parameter in power number correlation, dimensionless
b	intercept value in equation 60, sec^{-1}
B	parameter in power number correlation, dimensionless
c	conduction resistance through silicone tubing, sec/cm
C	volumetric concentration of attached cells, cells/cm^3
C_{max}	maximum volumetric concentration of attached cells, cells/cm^3
C_1	vol. concentration of attached cells at time t_1, cells/cm^3
$C_{1,35}$	C_1 for culture at 35 RPM, cells/cm^3
$C_{1,150}$	C_1 for culture at 150 RPM, cells/cm^3
C_2	vol. concentration of attached cells at time t_2, cells/cm^3
$C_{2,35}$	C_2 for culture at 35 RPM, cells/cm^3
$C_{2,150}$	C_2 for culture at 150 RPM, cells/cm^3
C_i	inert microcarrier concentration, microcarriers/cm^3
C_m	microcarrier concentration, microcarriers/cm^3
D	concentration of DNA in culture fluid, diploid equiv./cm^3
D_1	D at time t_1 in 150 RPM culture, diploid equivalents/cm^3
D_2	D at time t_2 in 150 RPM culture, diploid equivalents/cm^3
D_f	diffusion coefficient, cm^2/sec
$D_{f,o}$	diffusion coefficient for oxygen in culture medium, cm^2/sec
D_i	impeller diameter, cm

$D_{i,1}$	impeller diameter for reactor one, cm
$D_{i,2}$	impeller diameter for reactor two, cm
D_t	inner diameter of vessel, cm
D_o	dissolved oxygen concentration in liquid, mmoles/cm^3
$D_{o,min}$	minimum acceptable D_o, mmoles/cm^3
D_o^*	D_o at saturation with gas phase, mmoles/cm^3
d_p	microcarrier diameter, cm
d_t	silicone tubing diameter, cm
E	number of hemacytometer squares scored
f_c	frequency of microcarrier collisions, #collision/cm^3-sec
f(t)	distribution function of cell age, t, since mitosis
F	ratio of initial to final sample volume for nuclei counts
F_n	normal force per unit area on microcarrier surface, dyne/cm^2
Fr	Froude number, dimensionless
g	acceleration due to gravity, 980 cm/sec^2
G	glucose concentration, g/liter
G_1	glucose concentration at time t_1, g/liter
G_2	glucose concentration at time t_2, g/liter
h	cell height above growth surface, cm
H	liquid height in reactor, cm
H_o	gas hold-up in reactor, cm^3
I_L	interval length between exchanges of medium, sec
I_{Go}	fraction of cell population in G_o resting state, dmsnless.
I_M	fraction of cell population in mitotic phase, dimensionless
ISF	integrated shear factor, sec^{-1}
ITS	impeller tip speed, cm/sec

J_w	specific rate of whole cell removal, sec^{-1}
K_1	ratio of time-average shear rate to impeller tip speed, cm^{-1}
K_2	collision frequency constant, #collisions-cm^3/micro.^{2}-sec
K_3	average effective surface area exposed to each collision, cm^2
K_4	probability of death for a cell in the collision-exposed area
K_5	total surface area per microcarrier ($= 4\pi r_p^2$), cm^2/micro.
K_6	specific fluorescence of FS-4 DNA, fluor./(dip. equiv./cm^3)
K_e	first-order specific death rate constant, cm^3/sec
K_L	overall oxygen transfer coefficient, cm/sec
K_s	oxygen transfer coefficient for surface aeration, cm/sec
K_t	oxygen transfer coefficient for tubing aeration, cm/sec
L	length scale for eddies in viscous dissipation regime, cm
L_c	critical eddy length scale for cell death, cm
M_o	specific oxygen uptake rate with no growth, mmoles/cell-sec
M_t	mixing time for fluid phase in reactor, sec
M_w	molecular weight of polymer, daltons
N	rotation rate of impeller or viscometer, rotations/sec
N_o	volumetric rate of oxygen transfer into liquid, mmole/cm^3-sec
N_p	power number for impeller, dimensionless
Nu	Nusselt number for cell-liquid heat transport, dimensionless
p	parameter in power number correlation, dimensionless
P	static pressure in undisturbed flow, dyne/cm^2
P_v	vapor pressure of fluid, dyne/cm^2
P′	intensity of turbulent pressure fluctuation, dyne/cm^2
P'_{vdr}	P′ due solely to eddies in viscous diss. regime, dyne/cm^2
q	total specific death rate, sec^{-1}

q_1	specific death rate due to micro.-eddy interactions, sec^{-1}
q_2	second-order death rate constant, cm^3/microcarrier-sec
Q	flow rate of gas for sparging, cm^3/sec
r_i	radius of inner viscometer cylinder, cm
r_o	radius of outer viscometer cylinder, cm
r_p	microcarrier radius, cm
R	ideal gas constant, 8.31×10^7 g-cm^2/mole-°K-sec^2
R_c	specific uptake rate of a given chemical, mmole/cell-sec
Re	Reynolds number for flow, dimensionless
R_g	specific glucose uptake rate, g/cell-sec
R_o	specific oxygen uptake rate, mmole/cell-sec
S_a	average DNA content of cell population, diploid equiv./cell
S_r	average DNA content of cells removed, diploid equiv./cell
Sc	Schmidt number, dimensionless
Sh_c	Sherwood number for cell-liquid mass transport, dimensionless
Sh_s	Sherwood number for surface aeration, dimensionless
T	temperature, degrees Kelvin
t_1	time at beginning of interval, sec
t_2	time at end of interval, sec
T_c	total time of cell cycle with constant T_{G1}, sec
T_d	doubling time of cell population, sec
T_{G2}	duration of G2 phase, sec
T_M	duration of mitotic phase, sec
T_S	duration of DNA synthesis (S) phase, sec
S_a	average DNA content per cell, diploid equivalents/cell
u'	root mean square turbulent velocity component, cm/sec

u'_{max}	maximum root mean square turbulent velocity component, cm/sec
$\bar{U}$	time-average fluid velocity component, cm/sec
U	total fluid velocity component, cm/sec
U_{max}	maximum total fluid velocity component, cm/sec
$\bar{U}_{max}$	maximum time-average fluid velocity component, cm/sec
v	velocity scale for eddies in viscous diss. regime, cm/sec
V_c	average culture volume, cm^3
w	impeller width, cm
W	volumetric concentration of unattached whole cells, cells/cm^3
x	polymer concentration, g/cm^3
X_b	concentration of given nutrient in bulk liquid, mmole/cm^3
X_c	concentration of given nutrient at cell surface, mmole/cm^3
Y	shear rate in flow field undisturbed by microcarrier, sec^{-1}
$Y_{n/o}$	growth yield of cells on oxygen, cells/mmole oxygen
Z	percent confluence, dimensionless

Greek

$\alpha 1$	parameter in fluid mixing-time relation, dimensionless
$\alpha 2$	parameter in gas-liquid mass transfer relation, dimsnlss.
$\alpha 3$	parameter in tubing-liquid mass transfer relation, dimsnlss.
β	Henry's law coefficient for oxygen solubility, mmole/cm^3-atm
Γ	shear rate at surface of inner viscometer cylinder, sec^{-1}
$\delta 1$	exponent on Reynolds number for surface aeration, dimsnlss.
$\delta 2$	exponent on Schmidt number for surface aeration, dimsnlss.
$\delta 3$	exponent on Froude number for surface aeration, dimsnlss.
$\delta 4$	exponent on Reynolds number for tubing aeration, dimsnlss.

$\delta 5$	exponent on diameter ratio for tubing aeration, dimensionless
$\delta 6$	exponent on Schmidt number for tubing aeration, dimensionless
ΔD_o	spatial variation in dissolved oxygen level, mmole/cm^3
ϵ	power input or dissipation per unit mass, cm^2/sec^3
$\bar{\epsilon}$	average power input or dissipation per unit mass, cm^2/sec^3
$\bar{\epsilon}_1$	average power input per unit mass in reactor 1, cm^2/sec^3
$\bar{\epsilon}_2$	average power input per unit mass in reactor 2, cm^2/sec^3
ϵ_{max}	maximum local power dissipation per unit mass, cm^2/sec^3
ϵ_s	power input from sparging per unit mass of fluid, cm^2/sec^3
Λ	response time of polymer molecule, sec
η	viscosity of fluid, gm/cm-sec
λ	Hoechst-dye fluorescence of culture fluid, fluor. units
$\lambda_{1,35}$	λ for 35 RPM culture at time t_1, fluorescence units
$\lambda_{1,150}$	λ for 150 RPM culture at time t_1, fluorescence units
$\lambda_{2,35}$	λ for 35 RPM culture at time t_2, fluorescence units
$\lambda_{2,150}$	λ for 150 RPM culture at time t_2, fluorescence units
η_s	viscosity of solvent, gm/cm-sec
η_{sp}	specific viscosity, dimensionless
$[\eta]$	intrinsic viscosity, cm^3/gm
θ	time scale for eddies in viscous dissipation regime, sec
μ	specific growth rate, sec^{-1}
μ_d	μ under mild agitation for a given dextran conc., sec^{-1}
μ_{max}	maximum growth rate with no contact inhibition, sec^{-1}
μ_{obs}	difference between actual growth rate and death rate, sec^{-1}
μ_r	relative observed specific growth rate, dimensionless
ν	kinematic viscosity of fluid, cm^2/sec

ν_b	kinematic viscosity of suspension, cm^2/sec
ξ	number of nuclei counted in hemacytometer
ρ_b	density of bubbles, gm/cm^3
ρ_f	density of fluid, gm/cm^3
ρ_m	density of hydrated microcarriers, gm/cm^3
σ	cavitation number, dimensionless
τ	shear stress on microcarrier surface, $dyne/cm^2$
T_{max}	maximum shear stress from time-average flow fields, $dyne/cm^2$
ϕ	volume fraction of solids, dimensionless
Ψ	surface coverage of microcarriers or T-flasks, $cell/cm^2$
ζ_1	correction factor for DNA release calculations, dimsnlss.
ζ_2	correction factor for DNA release calculations, dimsnlss.

REFERENCES

Aherne, W.A., Camplejohn, R.S., and Wright, N.A., 1977. An Introduction to Cell Population Kinetics (Edward Arnold, London, 1977) p. 58

Alberts, B., Bray, D., Lewis, J., Raff, M., Roberts, K., Watson, J.D., 1983. Molecular Biology of the Cell (Garland Publishing, NY), pp. 611-621

Amari, T., and Nakamura, M., 1973. *Viscoelastic properties of aqueous solution of methylcellulose.* J. Applied Polymer Sci., 17, 589-603

Amari, T., and Nakamura, M., 1974. *Viscoelastic properties of dilute aqueous solution of methylcellulose at ultrasonic frequencies.* J. Applied Polymer Sci., 18, 3329-3344

Augenstein, D.C., Sinskey, A.J., and Wang, D.I.C., 1971. *Effect of shear on the death of two strains of mammalian tissue cells.* Biotech. Bioeng., 13, 409-418

Aunins, J.G., Croughan, M.S., Wang, D.I.C., and Goldstein, J.M., 1986. *Engineering developments in the homogeneous culture of animal cells: oxygenation of reactors and scale-up.* Biotech. Bioeng. Symp. Series, No 17, 699-723

Balin, A.K., Goodman, D.B., Rasmussen, H., Christofalo, V.J., 1976. *The effect of oxygen tension on the growth and metabolism of WI-38 cells.* J. Cell Physiol., 89, 235-250.

Baserga, R., 1976. Multiplication and Division of Mammalian Cells (Marcel Dekker, NY) pp. 27, 35, 50

Bates, R.L, Fondy, P.L, and Corpstein, R.R., 1963. *An examination of some geometric parameters of impeller power.* I & EC Proc. Design Dev., 2, 310-314

Birch, J.R., and Pirt, S.J., 1969. *The choline and serum protein requirements of mouse fibroblast cells (strain LS) in culture.* J. Cell Science, 5, 135-142

Bohmer, F-D., Lehmann, W., Noll, F., Samtleben, R., Langen, P., and Grosse, R., 1985. *Specific neutralizing antiserum against a polypeptide growth inhibitor for mammary cells purified from bovine mammary gland.* Biochemica et Biophysica Acta, 846, 145-154

Boraston, R., Thompson, P.W., Garland, S., and Birch, J.R., 1984. *Growth and oxygen requirements of antibody producing mouse hybridoma cells in suspension culture.* Devel. Biol. Stand., 55, 103-111

Boucher, D.F. and Alves, G.E., 1973. *Fluid and particle mechanics*, in Chemical Engineers' Handbook, Perry, R.H. and Chilton, C.H., Eds., (McGraw-Hill, NY) p 5-59

Brunk, C.F., Jones, K.C., and James, T.W., 1979. *Assay for nanogram quantities of DNA in cellular homogenates.* Anal. Biochem., 92, 497-500

Bryant, J.C., 1966. *Mammalian cells in chemically defined media in suspension cultures.* Annals NY Acad. Sci., 139, 143-161

Bryant, J.C., 1969. *Methylcellulose effect on cell proliferation and glucose utilization in chemically defined medium in large stationary cultures.* Biotech. Bioeng., 11, 155-179

Bujalski, W., Nienow, A.W., Chatwin, S., and Cooke, M., 1987. *The dependency on scale of power numbers of Rushton disc turbines.* Chem. Eng. Sci., 42, 317-326

Butler, M., 1986. *Serum-free media,* in Mammalian Cell Technology Thilly, W.G., Ed., (Butterworths, Boston, MA) pp. 91-104

Chaudhari, R.V., and Ramachandran, P.A., 1980. *Three phase slurry reactors.* AIChE J., 26, 177-201

Cheng, L.Y., 1987. *Deformation analyses in cell and developmental biology. Part 1 - formal methodology, Part 2 - mechanical experiments on cells.* J. Biomech. Eng., 109, 10-24

Cherry, R.S. and Papoutsakis, E.T., 1986a. *Hydrodynamic effects on cells in agitated tissue culture reactors.* Bioprocess Engineering, 1, 29-41

Cherry, R.S. and Papoutsakis, E.T., 1986b. *Physical mechanisms of cell damage in microcarrier cell culture bioreactors.* Presented at the 1986 National Meeting of the American Chemical Society, Anaheim, CA, accepted for publication in Biotechnology and Bioengineering

Clark, J.M. and Hirtenstein, M.D., 1981. *Optimizing culture conditions for the production of animal cells in microcarrier culture.* Ann. N.Y. Acad. Sci., 369, 33-46

Crouch, C.F., Fowler, H.W., and Spier, R.E., 1985. *The adhesion of animal cells to surfaces: the measurement of critical surface shear stress permitting attachment or causing detachment.* J. Chem. Tech. Biotechnol., 35B, 273-281

Croughan, M.S., Hamel, J-F., and Wang, D.I.C., 1987. *Hydrodynamic effects on animals grown in mircocarrier cultures.* Biotech. Bioeng., 29, 130-141

Daily, J.W. and Harleman, D.R.F., 1966. Fluid Dynamics (Addison-Wesley, Reading, MA) pp 395-401

Darnell, J., Lodish, H., and Baltimore, D., 1986. Molecular Cell Biology (Scientific American Books, W.H. Freeman, NY), pp. 147, 148, 1035-1046

Defendi, V. and Manson, L.A., 1963. *Analysis of the life-cycle in mammalian cells.* Nature, 198, 359-361

DeForrest, J.M. and Hollis, T.M., 1980. *Relationship between low intensity shear stress, aortic histamine formation, and aortic albumin uptake.* Exp. Molecular Path., 32, 217-225

Denn, M.M., 1980. Process Fluid Mechanics (Prentice Hall, Englewood Cliffs, NJ) pp 358-363

Dewey, C.F., Bussolari, S.R., Gimbrone, M.A., and Davies, P.F., 1981. *The dynamic response of vascular endothelial cells to fluid shear stress.* J. Biomech. Eng., 103, 177-185

Dodge, T.C. and Hu, W.S., 1986. *Growth of hybridoma cells under different agitation conditions.* Biotech. Lett., 8, 683-686

Dow, 1985. *Handbook on Methocel.* Technical literature, Dow Chemical Company, Midland, MI

Dunn, G.A. and Ireland, G.W., 1984. *New evidence that growth in 3T3 cell cultures is a diffusion-limited process.* Nature, 312, 63-65

Evans, E.A., 1983. *Binding elastic modulus of red blood cell membrane derived from bucking instability in micropipet aspiration tests.* Biophys. J., 43, 27-30

Feder, J. and Tolbert, W.R., 1983. *The large-scale cultivation of mammalian cells.* Sci. Amer., 248, 36-43

Fleischaker, R.J., 1982. *An experimental study in the use of instrumentation to analyze metabolism and product formation in cell culture.* Doctoral thesis, Dept. Applied Biol. Sci., M.I.T., Cambridge, MA

Fleischaker, R.J. and Sinskey, A.J., 1981. Eur. J. Appl. Microb. Biotech., 12, 193

Frangos, J.A., Eskin, S.G., McIntire, L.V., and Ives, C.L., 1985. *Flow effects on prostacyclin production by cultured human endothelial cells.* Science, 227, 1477-1479

Freshney, R.I., 1983. Culture of Animal Cells (Alan R. Liss, NY) pp. 168, 245

Fry, D.L., 1968. *Acute vascular endothelial changes associated with increased blood velocity gradients.* Circ. Res., 22, 165-197

Giard, D.J., Loeb, D.H., Thilly, W.G., Wang, D.I.C., and Levine, D.W., 1979. *Human interferon production with diploid fibroblast cells grown on microcarriers.* Biotech. Bioeng., 21, 433-442

Goldstein, J.M., 1986. *Scale-up of membrane oxygenated recombinant animal cell bioreactors.* Masters thesis, Dept. Applied Biol. Sci., M.I.T., Cambridge, MA

Handa, A., Emery, A.N., and Spier, R.E., 1987. *Detrimental effects of sparger aeration on suspended mammalian cell cultures - and their prevention.* Proc. 4th European Congress on Biotech., 3, 601-604

Heisenberg, W., 1948. Z. Phys., 124, 168

Hiemenz, P.C., 1977. Principles of Colloid and Surface Chemistry (Marcel Dekker, NY) pp. 62-80

Hinze, J.O., 1975. Turbulence (McGraw-Hill, NY) pp. 222-227, 309-310

Hirtenstein, M. and Clark, J., 1980. Tissue Culture in Medical Research, R. Richards and K. Rajan, Eds. (Pergamon, Oxford, England) p. 97

Hochmuth, R.M. and Mohandas, N., 1972. *Uniaxial loading of the red-cell membrane.* J. Biomechanics, 5, 501-509

Hochmuth, R.M., Mohandas, N., and Blackshear, P.L., 1973. *Measurement of the elastic modulus for the red cell membrane using a fluid-mechanical technique.* Biophys. J., 13, 747-762

Hollis, T.M. and Ferrone, R.A., 1974. *Effects of shearing stress on aortic histamine synthesis.* Exp. and Molec. Path., 20, 1-10

Holmstrom, B., 1968. *Continuous flow cultures of a HeLa cell line as a basis for a steady supply of Rubella virus.* Biotech. Bioeng., 10, 373-384

Hoyt, J.W., 1985. *Drag reduction in polysaccharide solutions.* Trends in Biotechnology, 3, 17-21

Hsu, Y-M. and Wang, J.L., 1986. *Growth control in cultured 3T3 fibroblasts v. purification of an M_r 13,000 polypeptide responsible for growth inhibitory activity.* J. Cell Biol., 102, 362-369

Hu, W.S., 1983. *Quantitative and mechanistic analysis of mammalian cell cultivation on microcarriers.* Doctoral dissertation, Dep. Appl. Biol. Sci., M.I.T., Cambridge, MA, pp. 204-211

Hu, W.S., Meier, J., and Wang, D.I.C., 1985. *A mechanistic analysis of the inoculum requirement for the cultivation of mammalian cells on microcarriers.* Biotech. Bioeng., 27, 585-595

Hyman, W.A., 1972a. *Shear flow over a protrusion from a plane wall.* J. Biomechanics, 5, 45-48

Hyman, W.A., 1972b. *Shear flow over a protrusion from a plane wall: addendum.* J. Biomechanics, 5, 643

Johnson, H.A., 1961. *Some problems associated with the histological study of cell proliferation kinetics.* Cytologia, 26, 32-41

Kilburn, D.G., and Webb, F.C., 1968. *The cultivation of animal cells at controlled dissolved oxygen partial pressure.* Biotech. Bioeng., 10, 801-814

Kleinbaum, D.G. and Kupper, L.L., 1985. Applied Regression Analysis and Other Multivariable Methods (Duxbury Press, North Scituate, MA) pp 95-106

Komasawa, I., Kuboi, R., and Otake, T., 1974. *Fluid and particle motion in turbulent dispersion: Measurement of turbulence of liquid by continual pursuit of tracer particle motion.* Chem. Eng. Sci., 29, 641-650.

Kuboi, R., Komasawa, I., Otake, T., 1974. *Fluid and particle motion in turbulent dispersion: Influence of turbulence of liquid on the motion of suspended particles.* Chem. Eng. Sci., 29, 651-657.

Kuchler, R.J., Marlowe, M.L, and Merchant, D.J., 1960. *The mechanism of cell binding and cell sheet formation in L strain fibroblasts.* Experimental Cell Res., 20, 428-437

Landry, J., Freyer, J.P., and Sutherland, R.M., 1981. J. Cell Phys., 106, 23-32

Lee, T-S., 1966. *Turbulent flow of dilute polymer solutions - studies in couette flow.* Doctoral dissertation, Dept. Chem. Eng., M.I.T., Cambridge, MA, pp. 39-51

Levesque, M.J. and Nerem, R.M., 1985. *The Elongation and Orientation of Cultured Endothelial Cells in Response to Shear Stress.* J. Biomechanical Eng., 107, 341-347

Liley, P.E. and Gambill, W.R., 1973. *Physical and chemical data*, in Chemical Engineers' Handbook, Perry, R.H. and Chilton, C.H., Eds., (McGraw-Hill, NY) p 3-45

Lin, C-J., Peery, J.H., Schowalter, W.R., 1970. *Simple shear flow round a rigid sphere: inertial effects and suspension rheology.* J. Fluid Mech., 44, 1-17

Macieira-Coelho, A., Ponten, J., and Philipson, L., 1966. *The division cycle and RNA-synthesis in diploid human cells at different passage levels in vitro.* Exp. Cell Res., 42, 673-684

Margaritas, A. and Pace, G.W., 1984. *Microbial polysaccharides*, in Comprehensive Biotechnology, Volume 3, Blanch, H.W., Drew, S., and Wang, D.I.C., Eds., (Pergamon Press, New York), p. 1015

Maroudas, N.G., 1974. *Short-range diffusion gradients.* Cell, 3, 217-219

Matsuo, T., and Unno, H., 1981. *Forces acting on a floc and strength of floc.* J. Environ. Eng. Div., ASCE, 107, 527-545

McCabe, W.L., Smith, J.C., and Harriot, P., 1985. Unit Operations of Chemical Engineering (McGraw-Hill, NY) p. 229-231

McMahon, J.B., Farrelly, J.G., Iype, P.T., 1982. *Purification and properties of a rat liver protein that specifically inhibits the proliferation of nonmalignant epithelial cells from rat liver.* Proc. Natl. Acad. Sci. USA, 79, 456-460

McQueen, A., Meilhoc, E., and Bailey, J., 1987. *Flow effects on the viability and lysis of suspended mammalian cells.* Biotech. Lett., 9, 831-836

Mered, B., Albrecht, P., and Hopps, H.E., 1980. *Cell growth optimization in microcarrier culture.* In Vitro, 16, 859-865

Midler, M. and Finn, R.K., 1966. *A model system for evaluating shear in the design of stirred fermentors.* Biotech. Bioeng., 8, 71-84

Miller, W.M., Wilke, C.R., and Blanch, H.W., 1987. *The effects of dissolved oxygen concentration on hybridoma growth and metabolism in continuous culture.* Submitted to J. Cellular Physiol.

Mitchell, K.J., and Wray, W., 1979. *Mitotic cell populations obtained from a micro-carrier culturing system.* Exp. Cell Res., 123, 452-455

Mizrahi, A., 1984. *Oxygen in human lymphoblastoid cell line cultures and effect of polymers in agitated and aerated cultures.* Devel. Biol. Standard., 55, 93-102

Monin, A.S., and Yaglom, A.M., 1971. Statistical Fluid Mechanics: Mechanics of Turbulence, Volume 1 (MIT Press, Cambridge, MA) pp. 412-415

Nagata, S., 1975. Mixing: Principles and Applications (Wiley, NY) pp. 24-32, 126-129, 149-163

Nahapetian, A.T., 1986. *Growth and Maintenance of Anchorage-Dependent Mammalian Cells in Perfused Systems and Metabolism of Nutrients*, in Mammalian Cell Technology, Thilly, W.G., Ed., (Butterworth, Stoneham, MA), pp. 151-165

Ng, J.J.Y., Crespi, C.L., and Thilly, W.G., 1980. *Selection of mitotic chinese hamster ovary cells from microcarriers.* Anal. Biochem., 109, 231-238

Nicodemo, L., Nicolais, L. and Landel, R.F., 1974. *Shear rate dependent viscosity of suspensions in Newtonian and non-Newtonian liquids.* Chem. Eng. Sci., 29, 729-735

Nienow, A.W., 1985. *The dispersion of solids in liquids,* in Mixing of Liquids by Mechanical Agitation, Ulbrecht, J.J. and Patterson, G.K., Eds., (Gordon and Breach Science Publishers, NY) p 273-307

Okamoto, Y., Nishikawa, M., and Hashimoto, K., 1981. *Energy dissipation rate distribution in mixing vessels and its effects on liquid-liquid mass transfer.* Int. Chem. Eng., 21, 88-96

Oldshue, J.Y., 1983. Fluid Mixing Technology (McGraw-Hill, NY) pp. 27-31, 170, 198, 213

Pardee, A.B., Dubrow, R., Hamlin, J.L., and Kletzein, R.F., 1978. *Animal cell cycle.* Ann. Rev. Biochem., 47, 715-750

Perry, S.D., 1987. *Packed fiber bed reactor design for animal cell culture.* Masters thesis, Depart. Chem. Eng., M.I.T., Cambridge, MA

Pharmacia, 1981. *Microcarrier cell culture - principles and methods.* Technical literature, Pharmacia Fine Chemicals, Uppsala, Sweden.

Pirt, S.J., 1975. Principles of Microbe and Cell Cultivation (Blackwell Scientific Publications, London)

Placek, J. and Tavlarides, L.L., 1985. *Turbulent flow in stirred tanks, Part 1: Turbulent flow in the turbine impeller region.* AIChE J., 31, 1113-1120

Prescott, D.M., 1976. Reproduction of Eukaryotic Cells (Academic Press, NY) pp. 24, 25, 37, 38

Quraishi, A.Q., Mashelkar, R.A., and Ulbrecht, J.J., 1977. *Influence of drag reducing additives on mixing and dispersing in agitated vessels.* AIChE J., 23, 487-492

Reid, R.C., Prausnitz, J.M., and Sherwood, T.K., 1977. The Properties of Gases and Liquids (McGraw-Hill, NY) p 577

Richards, J.W., 1963. *Power input to fermentors and similar vessels.* British Chem. Eng., 8, 158-163

Rodriquez, F., 1982. Principles of Polymer Systems (McGraw-Hill, NY) p. 162

Rosenberg, M.Z., Kargi, F., and Dunlop, E.H., 1987. *Biological responses of plant cells to hydrodynamic shear stress.* Presented at the Annual Conference of the American Chemical Society, New Orleans, LA

Rosen, L.A., Hollis, T.M., and Sharma, M.G., 1974. *Alterations in bovine endothelial histidine decarboxylase activity following exposure to shearing stress.* Exp. Molecular Path., 20, 329-343

Runyan, W.S. and Geyer, R.P., 1963. *Growth of L cell suspensions on a Warburg apparatus.* Proc. Soc. Exp. Biol. Med., 112, 1027-1030

Rushton, J.H., Costick, E.W., and Everett, H.J., 1950. *Power characteristics of mixing impellers; part 2.* Chem. Eng. Prog., 46, 467-476

Sano, Y., Yagamuchi, N., and Adachi, T., 1974. *Mass transfer coefficients for suspended particles in agitated vessels and bubble columns.* J. Chem. Eng. Japan, 7, 255-261

Sato, Y., Horie, Y., Kamiwano, M., Yamamoto, K., and Ishii, K., 1967. *Turbulent flow in a stirred vessel.* Kagaku-Kogaku, 31, 275-281

Sato, M., Levesque, M.J., and Nerem, R.M., 1987. *An application of the micropipette technique to the measurement of the mechanical properties of cultured bovine aortic endothelial cells.* J. Biomech. Eng., 109, 27-34

Sato, M., Levesque, M., and Nerem, R.M., 1987. *Micropipette aspiration of culutured bovine aortic endothelial cells exposed to shear stress.* Arteriosclerosis, 7, 276-286

Schulz, R., Krafft, H., and Lehmann, J., 1986. *Experiences with a new type of microcarrier.* Biotech. Lett., 8, 557-560

Shiigi, S.M. and Mishell, R.I., 1975. *Sera and the in vitro induction of immune responses, Part 1: Bacterial contamination and the generation of good fetal bovine sera.* J. Immun., 115, 741-744

Shoemaker, D.P., Garland, C.W., Steinfeld, J.I., and Nibler, J.W. 1981. Experiments in Physical Chemistry (McGraw-Hill, NY) pp. 32-38

Sinskey, A.J., Fleischaker, R.J., Tyo M.A., Giard, D.J., and Wang, D.I.C., 1981. *Production of cell-derived products: virus and interferon.* Ann. N.Y. Acad. Sci., 369, 47-59

Smith, C.G., Greenfield, P.F., and Randerson, D.H., 1987. *A technique for determining the shear sensitivity of mammalian cells in suspension culture.* Biotech. Techniques, 1, 39-44

Spier, R.E., and Griffiths, B., 1984. *An examination of the data and concepts germane to the oxygenation of cultured animal cells.* Devel. Biol. Stand., 55, 81-92

Sprague, E.A., Steinbach, B.L., Nerem, R.M., and Schwartz, C.J., 1987. *Influence of a laminar steady-state fluid-imposed wall shear stress on the binding, internalization, and degradation of low-density lipoproteins by cultured arterial endothelium.* Circulation, 76, 648-656

Stathopoulos, N.A. and Hellums, J.D., 1985. *Shear stress effects on human embryonic kidney cells in vitro.* Biotech. Bioeng., 27, 1021-1026

Stoker, M.G.P., 1973. *Role of diffusion boundary layer in contact inhibition of growth.* Nature, 246, 200-203

Stoker, M. and Piggott, D., 1974. *Shaking 3T3 cells: further studies on diffusion boundary effects.* Cell, 3, 207-215

Swim, H.F., and Parker, R.F., 1960. *Effect of Pluronic F68 on growth of fibroblasts in suspension on rotary shaker.* Proc. Soc. Exp. Biol. Med., 103, 252-254

Tennekes, H. and Lumley, J.L., 1985. A First Course in Turbulence (M.I.T. Press, Cambridge, MA) pp 19-20, 262-264

Terasima, T., and Tolmach, L.J., 1962. *Growth and nucleic acid synthesis in synchronously dividing populations of HeLa cells.* Exp. Cell Res., 30, 344-362

Thomas, J.A. and Johnson, M.J., 1967. *Trace-metal requirements of NCTC clone 929 strain L cells.* J. Natl. Cancer Inst., 39, 337-345

Tramper, J., and Vlak, J.M., 1987. *Bioreactor design for growth of shear-sensitive mammalian and insect cells.* Advances in Biotechnological Processes, in press

Tramper, J., Williams, J.B., and Joustra, D., 1986. *Shear sensitivity of insect cells in suspension.* Enzyme Microb. Tech., 8, 33-36

Tyo, M. and Wang, D.I.C., 1980. *Engineering characterization of animal cell and virus production using controlled charge microcarriers,* in Advances in Biotechnology, Volume 1: Scientific and Engineering Principles, Moo-Young, M., Ed., (Pergamon Press, NY) pp 141-146

Vaishnav, R.N., Patel, D.J., Atabek, H.B., Deshpande, M.D., Plowman, F., and Vossoughi, J., 1983. J. Biomech. Eng., 105, 77-83

van Wezel, A.L., 1967. *Growth of cell-strains and primary cells on micro-carriers in homogeneous culture.* Nature, 216, 64-65 (1967)

Viggers, R.F., Wechezak, A.R., and Sauvage, L.R., 1986. *An apparatus to study the response of cultured endothelium to shear stress.* J. Biomech. Eng., 108, 332-337

Virk, P.S., 1975. *Drag reduction fundamentals.* AIChE Journal, 21, 625-656

Wadia, P.H., 1975. Doctoral dissertation, Department of Chem. Eng., M.I.T., Cambridge, MA

Walpole, R.E. and Myers, R.H., 1978. Probability and Statistics for Scientists and Engineers (MacMillan, NY) pp 280-308, 514

Wilke, C.R., and Chang, P., 1955. AIChE J., 1, 264

Wolf, A.V., Brown, M.G., and Prentiss, P.B., 1979. *Concentrative properties of aqueous solutions: conversion tables*, in CRC Handbook of Chemistry and Physics, Eds. R.C. Weast and M.J. Astle (CRC Press, Boca Raton, FA) p. D-235

Zimm, B.H., 1956. *Dynamics of polymer molecules in dilute solutions: viscoelasticity, flow birefringence and dielectric loss.* J. Chem. Phys., 24, 269

Zwietering, T.N., 1958. *Suspending of solid particles in liquid by agitators.* Chem. Eng. Sci., 8, 244-253

APPENDIX 1

CALCULATION OF THE RELATIVE DNA RELEASE UNDER HIGH AGITATION

As described in Chapter 2, an experiment was performed to investigate the release of DNA into the culture fluid under high agitation. Cultures of FS-4 cells were grown on 5 g/l microcarriers in two 500-ml vessels with 7.8 cm impellers. The cultures were operated at 45 RPM to eliminate microcarrier agglomeration. When nearly confluent, the microcarriers were pooled, concentrated to 15 g/l, and transferred to two identical 125-ml vessels. One of these 15 g/l cultures was agitated at 35 RPM while the other was agitated at 150 RPM. The attached cell concentrations were shown in Figure 21.

Figure 48 shows the cumulative change in Hoechst-dye fluorescence for samples taken from the culture fluid of the 15 g/L cultures. In the culture at 150 RPM, there was extensive cell death and removal of cells into suspension. The data show a strong increase in Hoechst-dye fluorescence, or DNA content, in the culture fluid. In the culture at 35 RPM, there was very little removal of cells into suspension. The data show a moderate decrease in Hoechst-dye fluorescence.

The cause of the decrease in fluorescence for the 35 RPM culture was not determined. The culture medium contained approximately 1 μg/ml DNA from the 5% (v/v) serum supplement. The background fluorescence from this DNA may have decreased over time. This decrease could have come

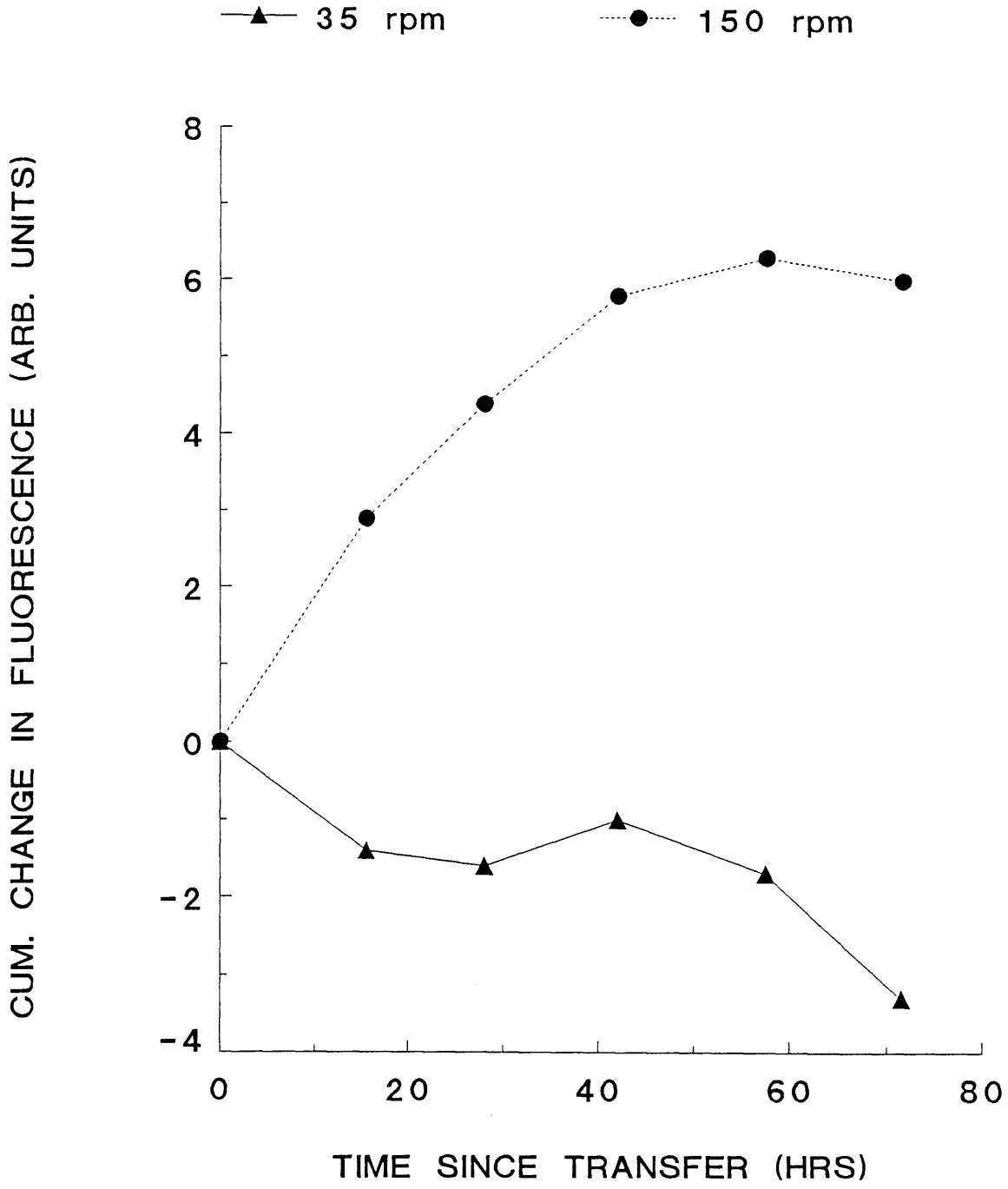

Figure 48. Cumulative change in Hoechst-dye fluorescence for culture fluid from 15 g/L cultures

about through:

1) cellular uptake of DNA polymers (unlikely)
2) cellular production of a substance which reduced the specific fluorescence of the DNA-Hoechst dye complexes
3) cellular uptake of a substance which otherwise enhanced the specific fluorescence of the DNA-Hoechst dye complexes
4) degradation of the DNA into smaller molecules or single chains with a concurrent reduction of the specific fluorescence

To calculate the absolute release of DNA into the culture fluid at 150 RPM, one must correct for the decrease in the control at 35 RPM. There are at least three reasonable methods to perform this correction:

1) Absolute correction. This represents the simplest correction. The change in fluorescence at 35 RPM is simply subtraced from the change in fluorescence at 150 RPM. For each time interval t_1 to t_2, the absolute release of DNA into the culture fluid at 150 RPM, $D_2 - D_1$, is given by:

$$D_2 - D_1 = \frac{(\lambda_{2,150} - \lambda_{1,150}) - (\lambda_{2,35} - \lambda_{1,35})}{K_6} \qquad \text{(Eq. 94)}$$

where K_6 represents the specific fluorescence of FS-4 cellular DNA, $\lambda_{1,150}$ and $\lambda_{2,150}$ represent the fluorescence in the samples from the 150 RPM culture at times t_1 and t_2, respectively, and $\lambda_{1,35}$ and $\lambda_{2,35}$ represent the fluorescence in the samples from the 35 RPM culture at times t_1 and t_2, respectively.

2) Correction proportional to volumetric cell concentration. This method of correction would be appropriate if the fluorescence decrease at 35 RPM was due to: a) cellular production of a substance which reduced the specific fluorescence, b) cellular uptake of a subtance which otherwise increased the specific fluorescence, or c) cellular uptake of DNA. If one corrects for the decrease in fluorescence due to one of these cellular processes, the absolute release of DNA into the culture fluid at 150 RPM, $D_2 - D_1$, is given by:

$$D_2 - D_1 = \frac{(\lambda_{2,150} - \lambda_{1,150}) - \zeta_1(\lambda_{2,35} - \lambda_{1,35})}{K_6} \qquad \text{(Eq. 95)}$$

where ζ_1 is a correction factor roughly given by:

$$\zeta_1 = \frac{C_{1,150} + C_{2,150}}{C_{1,35} + C_{2,35}} \qquad \text{(Eq. 96)}$$

where $C_{1,150}$ and $C_{2,150}$ represent the attached, or viable, cell concentrations in the 150 RPM culture at times t_1 and t_2, respectively, and $C_{1,35}$ and $C_{2,35}$ represent the attached, or viable, cell concentrations in the 35 RPM culture at times t_1 and t_2, respectively.

3) Correction proportional to DNA concentration. This method of correction would be appropriate if the fluorescence decrease at 35 RPM was due to degradation and breakdown of the DNA. This would likely be a first order process. The amount of DNA breakdown would be proportional to the amount of DNA present. If one corrects for this breakdown, the

absolute release of DNA into the culture fluid at 150 RPM, $D_2 - D_1$, is given by:

$$D_2 - D_1 = \frac{(\lambda_{2,150} - \lambda_{1,150}) - \zeta_2(\lambda_{2,35} - \lambda_{1,35})}{K_6} \qquad \text{(Eq. 97)}$$

where ζ_2 is a correction factor roughly given by:

$$\zeta_2 = \frac{\lambda_{1,150} + \lambda_{2,150}}{\lambda_{1,35} + \lambda_{2,35}} \qquad \text{(Eq. 98)}$$

Figure 49 shows the cumulative release of DNA into the culture fluid at 150 RPM. Data is shown for the three different methods of calculation. The correction proportional to cell concentration (Method 2) gives the lowest release while the correction proportional to DNA concentration (Method 3) gives the highest release. Nonetheless, there is not a large difference in the results from the three different methods of calculation. For the purposes of this thesis, the average value of three methods is used and is plotted in Figures 22 and 23 in Chapter 2. The error bars in Figures 22 and 23 cover the range of results from the three different methods of calculation. The error bars are given by the range of results plus twice the standard deviation of the assay.

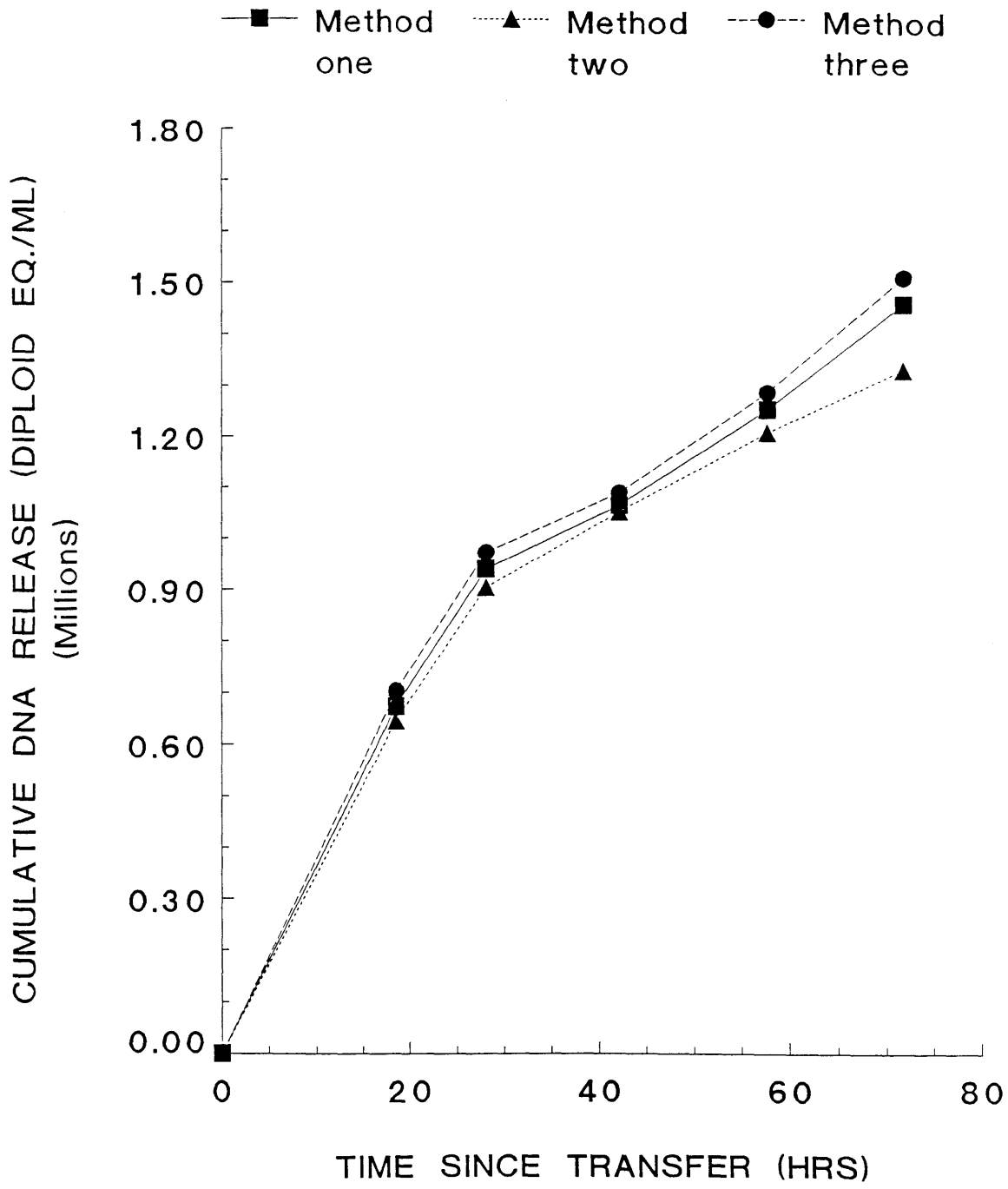

Figure 49. Cumulative release of DNA into suspension for 15 g/L culture at 150 RPM. Data is shown for 3 different methods of calculation.

APPENDIX 2.

ESTIMATION OF THE GROWTH YIELD AND MAINTENANCE COEFFICIENT FOR OXYGEN

For FS-4 cells, the growth yield of cells on oxygen was estimated from the results of Balin et al (1976) for oxygen-limited growth of WI-38 cells. These cells are human diploid fibroblasts and are similar to FS-4 cells. At a dissolved oxygen level equivalent to 7.8 mm Hg O_2, the WI-38 cells had a specific growth rate, μ, of 0.032 hr^{-1}, a total specific oxygen uptake rate, R_o, of 1.3×10^{-10} mmole/cell-hr, and a maintenance-associated oxygen uptake rate, M_o, of 2.8×10^{-11} mmole/cell-hr, as estimated through interpolation. The growth yield of cells on oxygen, $Y_{n/o}$, was then calculated from the equation

$$Y_{n/o} = \mu / (R_o - M_o) \qquad \text{(Eq. 99)}$$

and was thus estimated to be 3×10^8 cell/mmole. This yield was used for the optimization calculations in Chapter 7.

The results from Fleischaker and Sinskey (1981) were used to estimate the maintainence coefficient on oxygen, M_o, for FS-4 cells. At a specific growth rate of approximately 0.011 hr^{-1}, the FS-4 cells had a specific oxygen uptake rate, R_o, of 5×10^{-11} mmole/cell-hr. Using equation 99 and the yield of 3×10^8 cells/mmole estimate above, one can calculate a value of 1.3×10^{-11} mmole/cell-hr for the maintenance coefficient on oxygen, M_o. This maintenance coefficient was used for the optimization calculations in Chapter 7.